Numerical Determination of Permeability in Unsaturated Cementitious Materials

Li, Kai

DOI
10.4233/uuid:4634305a-ac8f-4193-aef7-15927da1c272

Publication date
2017

Document Version
Final published version

Citation (APA)
Li, K. (2017). *Numerical Determination of Permeability in Unsaturated Cementitious Materials*. [Dissertation (TU Delft), Delft University of Technology]. https://doi.org/10.4233/uuid:4634305a-ac8f-4193-aef7-15927da1c272

Important note
To cite this publication, please use the final published version (if applicable).
Please check the document version above.

Numerical Determination of Permeability in Unsaturated Cementitious Materials

Kai Li

Numerical Determination of Permeability in Unsaturated Cementitious Materials

Proefschrift

ter verkrijging van de graad van doctor
aan de Technische Universiteit Delft,
op gezag van de Rector Magnificus prof. ir. K.C.A.M. Luyben,
voorzitter van het College voor Promoties,
in het openbaar te verdedigen op
dinsdag 12 september 2017 om 15:00 uur

door

Kai LI

Master of Engineering aan de Wuhan University of Technology, P.R. China
geboren te Honghu, Hubei Province, P.R. China

This dissertation has been approved by
promotor: Prof.dr.ir. L.J. Sluys
copromotor: Dr. ir. M. Stroeven

Composition of the doctoral committee:

Rector Magnificus	chairman
Prof.dr.ir. L.J. Sluys	Delft University of Technology, promotor
Dr.ir. M. Stroeven	Delft University of Technology, copromotor

Independent members:

Prof.dr. K.L. Scrivener	EPFL, Switzerland
Prof.dr. Z.H. Shui	Wuhan University of Technology, China
Prof.dr.ir. S. Luding	University of Twente
Prof.dr.ir. H.E.J.G. Schlangen	Delft University of Technology
Prof.dr.ir. K. van Breugel	Delft University of Technology, reserve member

Other members:

Prof.dr.ir. P. Stroeven	Delft University of Technology Professor: Beijing Jiaotong University, China

This research was funded by the China Scholarship Council (No.201206950005).

Printed by: Gildeprint

ISBN number: 978-94-6186-839-8

Front image: Illustration of partly saturated cement paste

An electronic version of this dissertation is available at http://repository.tudelft.nl/.

To my parents, wife and lovely daughter

献给我的父母，妻子和可爱的女儿

Summary

To assess durability of cement-based materials, permeability is commonly considered as an important indicator. It is defined as the rate of movement of an agent (liquid or gas) through the porous medium under an applied pressure. Although permeability can be directly measured in laboratories, these experimental tests generally require specialized equipment and long periods of time to be completed, so they are laborious and expensive. For economic and ecological interests, numerical models are considered as an attractive alternative. Up until now, however, permeability of virtual cement seems to exceed experimental data by several orders of magnitude. Full saturation however, as generally assumed in numerical evaluations, does not realistically represent the experiments. Modelling fluid flow through unsaturated cement-based materials constitutes the focal point of this thesis. It is shown that the saturation degree has a significant effect on the permeability.

To numerically determine the permeability of a partially saturated cement paste, a comprehensive computational methodology has been developed, consisting of the following stages:

- Creation of an initial particle packing representing fresh cement;
- Simulation of the chemical hydration process, using the initial packing structure as a starting point;
- Evaluation of pore characteristics of any hydrated specimen;
- Blocking empty (dried-out) pores;
- Evaluation of the permeability using a tube network modelling constructed in the pore space.

Significant for this method is that no discretization is performed in any of the stages. Each individual module has been separately validated. Spherical particles representing fresh cement are initially distributed at a low density in a large cubical container. This container is then gradually decreased in size while the particles move around and interact to ultimately reach a densified structure at the desired dimension of the specimen. By setting the initial density of the particles at the calculated (but still low) value, any possible density can be achieved at an apriori given size of the container. Discrete element modelling is used for the modelling of motion and interactions of the particles. The so obtained densified structure is used as input for hydration simulation by assigning each particle with a mixture of chemical components, thereby influencing its hydration behaviour. The hydration simulation is realized by the vector-based XIPKM (Extended Integrated Particle Kinetics Model). The four major components of cement clinker, i.e., tricalcium silicate (C3S), dicalcium silicate (C2S), tricalcium aluminate (C3A) and tetracalcium aluminoferrite (C4AF), are taken into account. At any stage during the hydration simulation, the pore-structure can be evaluated using the DRaMuTS (Double Random Multiple-Tree Structuring) approach and the star volume method. Since the specimens in practice are seldom at fully saturated state, air pockets existing in the material actually block the transport of water in a similar way as solid material would do. Therefore, a blocking algorithm is developed to numerically generate solid particles in pore space simulating empty pores. This method allows to simulate all degrees of saturation between 0 and 100. In the case of fluid permeability, the algorithm starts to empty the largest pores first in accordance with the Kelvin-Laplace equation. The remaining pores are assumed

fully filled by water so that Darcy's law can still be applied to calculate the permeability of partially saturated cement paste. Using the water-filled pores only, a tube network can be established representing the fluid transport paths. Based on this network, the permeability can be calculated by solving the equations of flow. Using the developed computational methodology, permeability of partially saturated cement pastes can be numerically determined. A satisfactory agreement between the simulation results and experimental data regarding permeability is found.

The effects of technological parameters (*i.e.*, hydration time, water/cement ratio and particle size range) on permeability have also been investigated. It is found that the obtained simulation results are in accordance with the effects of these material parameters on the permeability of cementitious materials observed by experimentalists. Although the presented (multi-stage) approach is faster than experimental approaches, the numerical calculation of the permeability still takes a few hours to complete. A direct mathematical method for permeability estimation was also developed on the basis of the numerical parameter study mentioned above. Numerical studies show that water permeability of cement paste can be directly linked to water-filled porosity. Thus, a simple mathematical formula is proposed to quickly estimate permeability and it is found that the obtained results from the proposed model show a satisfactory agreement with the literature data.

Cement paste is selected in the first part of this work because of its simple structure, however, concrete is more popular in the engineering field. Concrete on meso-level is generally considered a three-phase material composed of aggregate particles, cement matrix and a (cement-paste) region close to the aggregate particle surface called interface transition zone (ITZ). This region reveals significant compositional differences as compared to those in the bulk paste. In general, the ITZ contains larger pores and it has a higher porosity, resulting potentially in a higher permeability in contrast to that in the bulk phase. As a consequence, it is expected that permeability goes up with an increasing aggregate fraction. This is verified by experiments, however, the opposite effect is observed as well. These controversial experimental observations are studied in this thesis using the developed methodology to see if these differences can be explained. An aggregate surface is introduced in the model by making one of the sides (two actually) rigid instead of periodic. A flat plane to represent the aggregate surface is assumed realistic since the size of an aggregate is orders larger than the size of cement particles. The effect of the rigid side automatically leads to the formation of an ITZ during the packing simulation. By "cutting of" the ITZ region from the bulk part and treating it as a separate sample for which the permeability is determined, the contributions from the ITZ and from the bulk matrix to the permeability of concrete can be determined individually. The results indicate that for partially saturated samples, it is not likely that the permeability will increase with an increasing density of the aggregates.

The presented computational methodology in this thesis can be utilized by engineers or researchers to estimate the permeability and thus assess durability of cementitious materials. The present-day powerful computational resources make realistic simulations possible, which can therefore be considered an attractive alternative as compared to laborious experimental work. To approach more realistic situations, further extension of this work would include considering gel pores inside C-S-H (calcium silicate hydrate), and developing a multi-scale method to link cement paste and concrete to specimens that also have micro-cracks.

Samenvatting

Doorlatendheid wordt gewoonlijk als een belangrijke indicator gezien voor de duurzaamheid van cementgebonden materialen. Het wordt gedefinieerd als de snelheid waarmee een vloeistof of gas zich onder een aangebrachte drukspanning door het poreuze medium beweegt. Doorlatendheid kan direct in laboratoria worden gemeten, maar deze proeven vragen in het algemeen specialistische apparatuur en veel tijd. Ze zijn dus bewerkelijk en kostbaar. Omdat ze tevens destructief zijn, vormen numerieke modellen een aantrekkelijk alternatief. De voorspelde doorlatendheid van het numeriek gemodelleerde cement lijkt vooralsnog echter de experimentele waarnemingen een paar ordes van grootte te overtreffen. De verzadigingsgraad lijkt een belangrijke factor om dit verschil te verklaren. Dit onderzoek focust zich daarom op het modelleren van het vocht- en gas-transport door cementgebonden materialen die niet volledig verzadigd zijn. De numerieke aanpak in dit onderzoek laat inderdaad een dominant effect zien van de verzadigingsgraad op de doorlatendheid.

Een veelomvattende numerieke methodologie is daarom ontwikkeld teneinde de doorlatendheid van gedeeltelijk verzadigde cementsteen te kunnen bepalen. Deze bestaat uit de volgende onderdelen:

- Het maken van een numerieke deeltjespakking als beginpakking van vers cement;
- Het gebruiken van deze pakking voor het simuleren van cement-hydratatie;
- Het meten van porie-eigenschappen van het gehydrateerde cement;
- Het blokkeren van geselecteerde poriën voor het nabootsen van een lage verzadigingsgraad.
- Modelleren van een poriënnetwerk en het bepalen van de doorlatendheid van het gehydrateerde numerieke cement.

Deze methodologie maakt nergens gebruik van discretisering. Ieder van de bovenstaande onderdelen van de methodologie is apart gevalideerd. Bolvormige deeltjes, die de verse cementkorrels representeren, worden aanvankelijk met lage dichtheid verdeeld in een grote kubische container. Het containervolume wordt daarop geleidelijk verminderd. Door de beweging en interactie van de deeltjes verdicht de structuur steeds verder totdat de gewenste grootte van de container is bereikt. Door de initiële dichtheid te regelen kan iedere mogelijke dichtheid worden bereikt bij een van te voren opgelegde eind-grootte van de container. De discrete elementen methode wordt gebruikt voor het afhandelen van de deeltjesdynamica en interactie. De zo verkregen deeltjesstructuur is input voor de hydratatiesimulatie, gerealiseerd met behulp van de op geometrie gebaseerde XIPKM (eXtended Integrated Particle Kinetics Method). Deeltjes krijgen nu een chemische samenstelling toegewezen en daarmee een hydratatiegedrag wat geometrisch gesproken leidt tot het tegen elkaar aan groeien van de deeltjes. De vier hoofdbestanddelen van de cementklinker, met name tricalciumsilicaat (C3S), dicalciumsilicaat (C2S), tricalcium aluminaat (C3A) en tetracalciumaluminoferrite (C3AF) zijn in het hydratatieproces opgenomen. Op ieder gewenst moment tijdens de hydratatie kunnen de poriën gekarakteriseerd worden en kan de doorlatendheid worden bepaald. Karakterisatie van de poriën gebeurt met behulp van DRaMuTS (Double Random Multiple Tree Structuring) en SVM (Star Volume Measuring) waarmee naast porositeit, de poriëngrootte en de continuïteit van de poriën in het netwerk kunnen worden bepaald. Aangezien in de praktijk proefstukken zelden volledig verzadigd zullen zijn, komen er

luchtbellen in het poriënnetwerk voor die het water-transport zullen blokkeren op gelijke wijze als een vaste stof dat zou doen. Daarom is een blokkeeralgoritme ontwikkeld dat vaste deeltjes in het poriënnetwerk genereert om verschillende graden van verzadiging te kunnen simuleren. Op deze wijze kan een lage verzadigingsgraad worden nagebootst. Bij het meten van vloeistofdoorlatendheid start het opdroog-proces (en dus blokkeer-proces) bij de grootste poriën, in overeenstemming met de Kelvin-Laplace wetmatigheid. Het restant van de poriën wordt verondersteld volledig verzadigd te zijn met vloeistof, zodat Darcy's wet kan worden gebruikt om de doorlatendheid in gedeeltelijk verzadigde cementsteen vast te kunnen stellen. Daarbij wordt gebruik gemaakt van een geschematiseerd poriënnetwerk.

Bij vergelijking met experimentele waarden wordt een goede mate van overeenkomst vastgesteld. Daarnaast zijn de effecten van verschillende technologische karakteristieken (hydratatieduur, water/cement verhouding en korrelgrootteverdeling) op de doorlatendheid onderzocht. Ook hier blijken de verkregen resultaten in lijn met bekende effecten van dergelijke materiaalparameters, hetgeen een verdere validatie betekent van de methodologie. Hoewel sneller dan experimentele bepaling, vraagt de numerieke vaststelling van doorlatendheid nog steeds een aantal uren. Een verkorte methode is daarom ontwikkeld binnen de geschetste methodologie. Numerieke studies hebben laten zien dat de doorlatendheid van cementsteen direct gerelateerd kan worden aan de porositeit van verzadigde poriën. Een eenvoudige wiskundige formule wordt daarom voorgesteld, gebaseerd op dit concept, waarmee waterdoorlatendheid snel kan worden vastgesteld; de resultaten tonen een goede mate van overeenkomst met relevante gegevens uit de literatuur.

Cementsteen is in deze numerieke studie onderzocht vanwege zijn eenvoudige structuur, hoewel in het algemeen beton wordt gebruik voor constructies. Beton wordt op mesoniveau in het algemeen beschouwd als een drie-fase materiaal dat bestaat uit toeslagkorrels, een cementmatrix, en het cement dat zich rondom de toeslagkorrels bevind. Deze cement zone rondom de toeslagkorrel (ITZ) bezit afwijkende eigenschappen van die van de rest van de cementsteen. De ITZ bevat relatief grote poriën en een hoge porositeit, waardoor een grotere waterdoorlaatbaarheid verwacht kan worden. Evenzo zou de doorlaatbaarheid groter moeten worden bij een toenemende toeslagfractie. Experimenteel onderzoek bevestigt dit, maar ook tegengestelde effecten zijn waargenomen. De hierboven omschreven methodologie wordt in dit onderzoek gebruikt om te zien of deze controversiële waarnemingen kunnen worden verklaard. Voor de simulatie van de grenslaag wordt aangenomen dat een van de zijden van de kubus het oppervlak van toeslagkorrels representeert, terwijl de andere zijden periodiek zijn. Door het grote verschil in afmeting van een toeslagkorrel en een cementkorrel kan een plat vlak als grens realistisch worden beschouwd. Op deze manier ontstaat er bij de pakkingssimulatie vanzelf een grenslaag (ITZ) dichtbij de rigide zijde van de kubus die andere eigenschappen zal hebben als die in bulk. Door deze twee te scheiden kan de doorlaatbaarheid van de ITZ en de bulkzone apart worden bepaald en daarmede de bijdragen aan de waterdoorlatendheid van beton. Dit onderzoek laat zien dat het niet waarschijnlijk is dat bij gedeeltelijke verzadiging van beton, de ITZ de transporteigenschappen van normaal beton zal bevorderen, wat zoveel betekent als dat de waterdoorlatendheid niet verhoogd zal worden wanneer de toeslagfractie vergroot wordt.

De in deze dissertatie beschreven numerieke methodologie kan door ingenieurs en onderzoekers gebruikt worden om de doorlaatbaarheid van cementgebonden materialen te

bepalen en daarmede hun duurzaamheid te beoordelen. De huidige krachtige rekenfaciliteiten maken een realistische simulatie mogelijk, zodat dit als een aantrekkelijk alternatief kan worden gezien voor het bewerkelijke experimentele onderzoek. Teneinde het realistisch gehalte nog te vergroten kan voor toekomstige uitbreidingen van de huidige methodiek gedacht worden aan het opnemen van gelporiën in C-S-H (calcium silicate hydrate) en het ontwikkelen van een meerschalige benadering waarbij de cementsteen en beton met microscheuren kunnen worden gerelateerd.

Table of contents

Chapter 1 Introduction

Permeability is commonly considered as an important indicator for durability assessment of cementitious materials. Although it can be measured in laboratories, experimental measurements are generally time-consuming, laborious and destructive. As a consequence, the modelling approach can be considered an attractive alternative. However, various studies have shown that the permeability of cement paste obtained by numerical modelling exceeds experimental data by several orders of magnitude. Saturation degree is found to be an important factor in explaining this discrepancy. Numerical samples generally assume fully saturated conditions while in practice, even though full saturation is aimed for, this is seldomly achieved. In this thesis, a numerical methodology that allows to vary material parameters (*i.e.*, water/cement ratio, particle size range, water saturation degree) has been developed for determining the permeability of unsaturated cementitious materials. In this chapter, some background information of this research work (*i.e.*, materials, properties and existing techniques) is first provided in Sections 1.1 and 1.2. Then in Section 1.3, it is discussed how the mismatch between simulations and experiments (in terms of permeability) can be bridged by water saturation degree. Finally, the objectives of this work and a condensed overview of this thesis are given at the end of this chapter.

1.1 Background: concrete, durability and permeability

Concrete is a common construction material and widely used for building and infrastructural applications. Due to its significant contributions to global CO_2 emissions in the world, it is of great ecological interest to develop environmentally friendly concretes and to enhance the durability of modern concrete. The latter problem has received the attention of many researchers in the past and also this study aims contributing to this important issue. In fact, concrete durability is to a large extent dependent on its resistance to the ingress of aggressive agents, such as chloride, sulphates and carbon dioxide, which results in serious degradation and rebar corrosion of concrete structures (Zhang and Zhang, 2014). Most degradation mechanisms relevant for concrete durability can be attributed to water transport that makes the migration of the abovementioned aggressive agents possible (Zalzale, 2014). Permeability is therefore considered as an important indicator for durability assessment of concrete. Most commonly, permeability is measured by laboratorial experiments. Unfortunately, direct permeability measurements require in general specialized equipment and long periods of time

to complete (Nokken and Hooton, 2008). In some cases, the experimental results show a large unexplained scatter and anomalous behavior. An experimental parameter study, whereby the influence of a number of practical parameters on the permeability is evaluated, would require a very long time. For those types of studies, computer models seem to provide powerful alternatives. The main focus in this work is on cement paste rather than on concrete, because of its simpler structure. It forms the framework for the development and application of the computational methodology described in Chapters 2-4. Nevertheless, a first step to concrete as the major construction material is made in Chapter 5.

1.2 Permeability of cementitious materials

1.2.1 Definition of permeability

Permeability is defined as the movement of an agent (liquid or gas) through a fully saturated porous medium under an applied pressure load (Banthia *et al.*, 2005). Note that two different permeabilities are distinguished in this work, *i.e.*, intrinsic permeability and non-intrinsic permeability (also called hydraulic conductivity). The intrinsic permeability is fluid-independent and only determined by the pore structure of the material. So, it is the intrinsic permeability that is selected in this work for characterizing the transport properties and denoted as permeability in the rest of this thesis. The intrinsic permeability can be obtained by multiplying the hydraulic conductivity by a factor $\mu/\rho g$ where μ, ρ, g represent the fluid viscosity, the fluid density and the gravitational acceleration, respectively. For water at room temperature, this factor is approximately equal to 10^{-7} m·s. A standard procedure for measurement of the intrinsic permeability involves application of a pressure gradient in one spatial direction of a fully saturated specimen, measuring the fluid inflow and outflow at a steady state, and calculating the permeability using Darcy's law (Zalzale, 2014) given in the next section.

1.2.2 Darcy's law for permeability measurement

Darcy's law is the common way to calculate the permeability of cementitious materials. An illustration of Darcy's law is given in Figure 1.1. It can be written in the form:

$$\kappa = \frac{L}{A}\frac{Q\,\mu}{\Delta P} \tag{1.1}$$

where κ = intrinsic permeability (m^2), L (m) and A (m^2) are the length and cross sectional area of a test sample under the pressure gradient ΔP. Q (m^3/s) is the measured fluid flow ($Q = Q_{in} = Q_{out}$ at a stable flow state). μ denotes the dynamic viscosity of the intruding fluid (Pa·s). Basically, all the input parameters required by Darcy's equation can be determined experimentally or numerically. Once these parameters are known, permeability can easily be

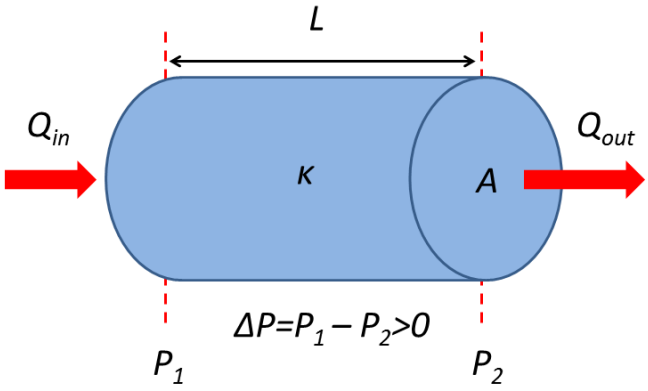

Figure 1.1 Schematic illustration of Darcy's law (Darcy, 1856). Permeability is measured once the fluid flow through the specimen is stable ($Q_{in} = Q_{out}$).

obtained using Eq. (1.1). A brief outline of experimental methods and numerical techniques to measure permeability will be given in the next two sections.

1.2.3 Experimental methods

Cementitious materials are generally characterized by their low porosity and high pore tortuosity, which make the standard permeability measurements time-consuming and laborious (Nyame and Illston, 1981; Banthia and Mindess, 1989; Ye, 2005). In particular, it is not easy to force a measurable fluid flow through such a material and reach a steady state as required by Darcy's law. The completion of the whole procedure usually requires a long period of time. As an alternative, indirect measurement methods such as beam-bending (Vichit-Vadakan and Scherer, 2003) can be employed. Although the experimental tests can be expected to provide direct and reliable data, the reported experimental results are in a very wide range (10^{-16}–10^{-22} m^2) and they reveal a large (unexpected) scatter. In theory, the intrinsic permeability is a property of the medium and should be independent of the penetrating fluid or applied pressure (Zalzale, 2014). However, this is not the case in practice since the reported values of air permeability are considerably different from typical values of water permeability. The differences may be affected by the following factors:

(1) The specimens chosen for the different experiments have not the same water/cement ratio, cement composition, hydration time and curing conditions;

(2) Micro-cracks introduced by the sample drying process prior to gas permeability measurements (Wong *et al.* 2009);

(3) Continuous hydration due to the supplementary water during water permeability measurements;

(4) The real saturation state of samples may not be at 100 percent.

The significant effects of the water saturation degree on the permeability of cementitious materials will be discussed in Section 1.3. In contrast to the water permeability test, measurement of gas permeability is easier and more reproductive, which is therefore preferred

by many researchers. However, the samples for air permeability measurements should be dried to a well-defined saturation degree, which may take more than a year (Zalzale, 2014). Considering all this, computer modelling seems an attractive alternative to perform the same task.

1.2.4 Modelling techniques

Computational models of fluid transport are generally determining the flow through a simulated pore structure of mature cement paste by solving the equation of Darcy. To obtain the virtual material for permeability calculation, fresh cement grains need to be first generated and distributed in a container. In general, two ways can be distinguished of generating and distributing the particles, *i.e.*, random sequential addition (RSA) and discrete element method (DEM). In contrast to RSA, the interactions between particles are well represented in DEM, which is considered more realistic for particle packing simulations and therefore chosen in this work. Similar to a real experimental setup, the so obtained densified structure then serves as input for hydration simulation. Hydration can be accomplished in two ways. In the first methodology, the full microstructure is discretized into a regular grid also referred to as voxels. Voxels located in pore space are assigned as pore while all other voxels are given chemical behavior. Hydration in this model means changing the characteristics of all voxels in time. In this way, a multiphase material with grains of any shape can be directly represented. These models are denoted as voxel-based systems, such as CEMHYD3D (Garboczi and Bentz, 2001). In the second methodology, each cement particle is described by its position and a set of radii representing an unhydrated spherical core that is covered by spherical shells of hydration products (Le *et al.*, 2013). Since the microstructure is not discretized but described by vectors and radii, it is known as a vector-based model (continuum approach). Hydration using a vector-based model means changing the radii of each particle and possibly the creation of new ones. Examples of this category are HYMOSTRUC (Breugel, 1995a, b), SPACE (Stroeven, 1999), µic (Bishnoi and Scrivener, 2009) and XIPKM (Le *et al.*, 2013). To calculate the permeability of simulated material, again two distinct methods can be applied to the structures that are generated by the abovementioned different systems. As for the voxel-based structure, a finite element method (FEM) or Lattice-Boltzmann approach can be employed to calculate the permeability of the voxel system that represent pore space. For the same purpose, the complex and tortuous pore structure of the vector-based system is approximated by a network of inter-connected cylindrical tubes. For each tube, the equations of laminar flow can be set up, whereas the flow through the entire system can be obtained by solving the system of equations. More information about the numerical methods used in this research work can be found in Chapter 2.

In contrast to the voxel-based systems, the vector-based approach to tube network modelling is resolution-free. The studies by Garboczi and Bentz (2001), Zalzale *et al.* (2013), Zhang *et al.* (2013) and Qin *et al.* (2016) reveal that the permeabilities obtained from the voxel-based models are very sensitive to the resolution of the microstructure. A higher resolution naturally

results in more accurate data, but also leads to a dramatic increase in the computational efforts. This can be considered as a main limitation of the voxel-based systems. Since permeability concerned in this work is a structure-sensitive property and heavily depends on the proper description of the pore structure, the network model approach seems to be more suitable for that purpose and is thus selected in this work. Pignat *et al.* (2005), Ye *et al.* (2006) and Le (2015) have conducted earlier studies following this approach. The reported outcomes differ significantly among the different researchers, although they all approximate the flow using network models of microstructures essentially composed of overlapping spheres of hydrated cement grains.

These differences can mainly be attributed to the different properties of specimens (*i.e.*, water/cement ratio, particle size range, hydration degree). The influence of these technological parameters on the permeability will be studied and presented in Chapter 3. Unfortunately, all these previous studies only deal with fully saturated samples which is a condition rarely realized in practice. Water evaporation inevitably occurs inside the specimens, resulting in partially saturated structures. The studies on permeability estimation of partly saturated cement paste using the network model are conducted and presented in Chapter 2. Basically, modelling techniques can be applied to various agents (*i.e.*, water or gas). However, most studies to date only concentrate on water transport. Only recently, gas permeability of cement paste has been numerically determined by Zalzale *et al.* (2013) using a voxel-based model. Hence, the estimation of gas permeability of cement paste by a tube network model is still an interesting topic and will be discussed in detail in Chapter 2 as well.

1.2.5 A mismatch between experiments and simulations?

In general, the permeabilities obtained from computer models seem to exceed experimental data by several orders of magnitude for samples with similar chemical composition, water/cement ratio, hydration age and particle size range. As stated earlier, a possible reason for this discrepancy may be that experimental samples in practice are almost never fully saturated as generally assumed and in fact a required condition for the use of Darcy's law. For numerical simulations, this state is easily obtained and commonly used. However, the specimens in experiments are probably never fully saturated, even though they are cured under water for a long period of time. In such underwater curing systems, it is not likely that additional water can be fully drawn into the chemical shrinkage voids of hydrated cement paste. Some pores remain devoid of water and cannot easily be refilled, as demonstrated by Muller *et al.* (2013) in quantitative nuclear magnetic resonance experiments. The influence of the water saturation degree on permeability of cementitious materials has been shown by Zalzale *et al.* (2013), Zhang (2013), Kameche *et al.* (2014) and Li *et al.* (2016a) to be severe, meaning several orders of magnitude can be bridged by a change of 65 percent water saturation degree. Hence, the measured permeabilities cannot be compared to the values from numerical simulations without matching the conditioning of the samples in the experiments with the degree of water saturation in the models (Zalzale, 2014). Since the water saturation

degree cannot be controlled in experiments, the water saturation degree needs to be taken into account in the numerical models to explain the mismatch. By doing so, the real state of specimens in practice can be well represented.

1.3 Pore characteristics and saturation degree in relationship to permeability

To produce cement paste, anhydrous cement powder has to be mixed with water. The chemical reactions between the anhydrous cement and water result in the formation of hydrates, which partly fill the original pore space to produce a porous solid (Zalzale, 2014). The remaining pore space (not occupied by solid phase) is referred to as capillary pores. These capillary pores (10 nm-10 μm) make the prime contribution to fluid flow though the material. The gel pores (3-5 nm) inside calcium silicate hydrate (the main hydrate phase) also affect fluid transport, however, its contribution to the permeability only becomes important when the capillary pores are fully de-percolated (Zalzale *et al.*, 2013). Moreover, the formation mechanism and structure of calcium silicate hydrate is still uncertain and controversial (Gartner *et al.*, 2000; Jennings, 2000, 2008), so in this study its contribution to permeability is ignored. As hydration progresses, water is gradually consumed and part of the pores will be drained from water. Unreacted water occupies the rest of the capillary pores with sizes ranging up to a few micrometers (Muller *et al.*, 2013). The empty pores, which cannot easily be refilled during underwater curing, act as barriers for water transport in a similar way as a solid phase would do. Hence, the effective porosity (*i.e.*, water-filled porosity for water transport) should be used to represent the permeability instead of the total porosity.

Consequently, the degree of water saturation is employed for characterizing the effective porosity; it is defined as the fraction of the porosity that is filled with water (Abbas *et al.*, 1999; Wong *et al.*, 2007; Baroghel-Bouny *et al.*, 2011). Note that the water-filled pores are the effective ones for water transport but they are actually impermeable to gas flow. In the case of gas permeability, air-filled porosity should be taken as the effective parameter. Although the specimens used in permeability measurements are required to be at fully saturated state by Darcy's law, this ideal situation is difficult (if not impossible) to reach and maintain, as stated earlier. Humidity changes in the environment inevitably result in water evaporation of the samples. According to the Kelvin-Laplace equation, large pores will drain easier in contrast to the smaller ones. Hence, large pores of the unsaturated samples are most probably emptied in practice. These empty pores block the original paths for water transport, resulting in a lower water permeability. The effects of the water saturation degree on permeability of cement-based materials have been experimentally and numerically studied, of which the results can be found in the international literature (Ye, 2003; Zalzale *et al.*, 2013; Kameche *et al.*, 2014; Li *et al.*, 2016a). To generate the specimens at various water saturation degrees, a blocking algorithm in which empty pores are replaced by solid material is proposed

and implemented in this work. Afterwards, the permeability of partially saturated cement paste can be numerically determined, as presented in detail in Chapter 2.

Although interesting on its own, it is not very common to use cement paste in experimental testing, because its behavior apparently deviates from the normal building material concrete. Therefore, the ultimate goal of this work is to model the behavior of partially saturated concrete. To eventually predict the permeability of concrete, the study starts by studying the flow transport through cement paste due to its simpler structure than concrete. Additionally, it is the cement paste that actually determines the permeability of concrete since aggregates are generally considered as impermeable. Hence, cement paste is chosen as the material to be first investigated in this thesis (Chapters 2 to 4). Then, the information obtained for cement paste can be used to calculate the permeability of concrete, as described in detail in Chapter 5.

1.4 Objectives of this research work

The objectives of this research work are to develop a computational methodology for numerically determining the permeability of cementitious materials and to systematically apply it for this purpose. The focus in this work is on cement and concrete. The water saturation degree that reveals the real state of specimens in service is taken into account in the developed models to bridge the gap between the permeability measured by experimental techniques and obtained from numerical simulations. The proposed computational methodology is intended to be an alternative to the laborious and expensive experimental techniques for durability assessment of concrete.

1.5 An overview of this thesis

The content of this thesis is presented in six chapters, in accordance with the flow chart in Figure 1.2.

To numerically determine the permeability of cement-based materials, a computational methodology is developed in this thesis. In general it consists of two stages, in similarity with the real experimental setup, *i.e.*, sample preparation and permeability measurement. In the stage of sample preparation, fresh cement grains are generated first and mixed by DEM in a large container that gradually shrinks in size. This process stops once the required packing density and sample size is reached. The densified structure then serves as an input for hydration simulation to obtain hardened cement paste. In the hydration simulation, each cement grain is represented by an unhydrated spherical core that is covered by spherical shells of hydration products. As hydration proceeds, cement grains gradually expand, and calcium hydroxide particles nucleate and grow in the empty region, resulting in a reduced pore space. The specimens at different hydration ages are selected for permeability estimation later. The sample preparation process allows to vary a number of parameters (*i.e.*, water/cement ratio,

particle size range) to generate different samples. The influence of these technological factors on the permeability of cement paste will be discussed in Chapter 3. In the following stage of permeability measurement, the pore structure of the obtained matured paste is investigated by a robotics-inspired technique that renders possible the assessment of topological and geometric properties of pore space. In short, points are randomly distributed in the structure and only those located in the pore space are used for determining global and local pore characteristic (Stroeven *et al.*, 2015). Connecting those points, pore channels are created that form paths between two opposite surfaces of the specimen. The information (*i.e.*, position, size) of all pores along the continuous channels is stored for further analysis. Due to the evaporation of water inside specimens, some pores (from the largest pores to the smallest ones) are drained and become impermeable for water transport. These pores are removed from the structure by filling them up by an impermeable material. For the so obtained structure, a tube network system as described earlier is built to calculate the permeability of the simulated cement paste. Chapter 2 presents the relevant details of how the permeability of partially saturated cement paste can be numerically determined, which is based on Li *et al.* (2016a), a paper published in *Cement and Concrete Research*.

Next, the developed methodology is applied to different samples to study the effects of hydration period, water/cement ratio, particle size range on the permeability of unsaturated cement paste. The outcomes observed in this work are in line with experimental findings, which can be seen as a qualitative validation of the presented methodology. Additionally, the controversial role of the interfacial transition zone between aggregates and bulk paste in determining the permeability of concrete is numerically studied, revealing that water or gas permeability behave differently with respect to the water saturation degree. All information can be found in Chapter 3, which is based on Li *et al.* (2016b), a paper submitted for publication in *Cement and Concrete Composites*.

Apart from the abovementioned methodology, an engineering approach is also developed for quick permeability estimation of cement paste on the basis of the pore characteristics obtained from the proposed numerical models. Using this method, permeability can be directly linked to the effective porosity, which is independent of the samples' conditions (*i.e.*, hydration time, water/cement ratio, particle size range). In contrast to the earlier mentioned complete methodology, the presented shortcut method for permeability estimation is able to reduce the computational efforts significantly. Chapter 4 contains all the relevant information on this engineering approach and is based on Li *et al.* (2016c), a paper published in *Construction and Building Materials*.

At the end of this thesis, the developed computational methodology is applied to the more commonly used construction material concrete. Concrete is on meso-level generally considered a three-phase material composed of aggregate particles and a cement matrix in which an interface transition zone (ITZ) is formed near the surface of aggregate particles. The ITZ contains larger pores and it has a higher porosity (resulting potentially in a higher

permeability) than the bulk paste. Consequently, permeability is expected to raise with an increasing aggregate fraction. This is verified by experiments, however, an opposite trend (that is, permeability decreases with an increasing aggregate content) is also observed. The permeability ratio between the ITZ and bulk matrix is found to be an important factor in explaining these controversial experimental observations. To quantitatively study this parameter at various conditions (*i.e.*, hydration degree, water/cement ratio, particle size range and water saturation degree), a ribbon structure including the ITZ and bulk matrix is constructed in particle packing simulations where aggregate surfaces and cement grains are modelled as rigid walls and spheres, respectively. The ITZ region is then extracted from the whole specimen, so that the ITZ and bulk paste can be treated as a separate sample for which the permeability is determined. This is how the respective contributions from the ITZ and bulk paste to the permeability of concrete can be determined. It is found that the ITZ is not likely to promote the transport properties of normal concrete. Chapter 5 presents all the information, which is based on Li *et al.* (2017), a paper submitted for publication in *Cement and Concrete Research*.

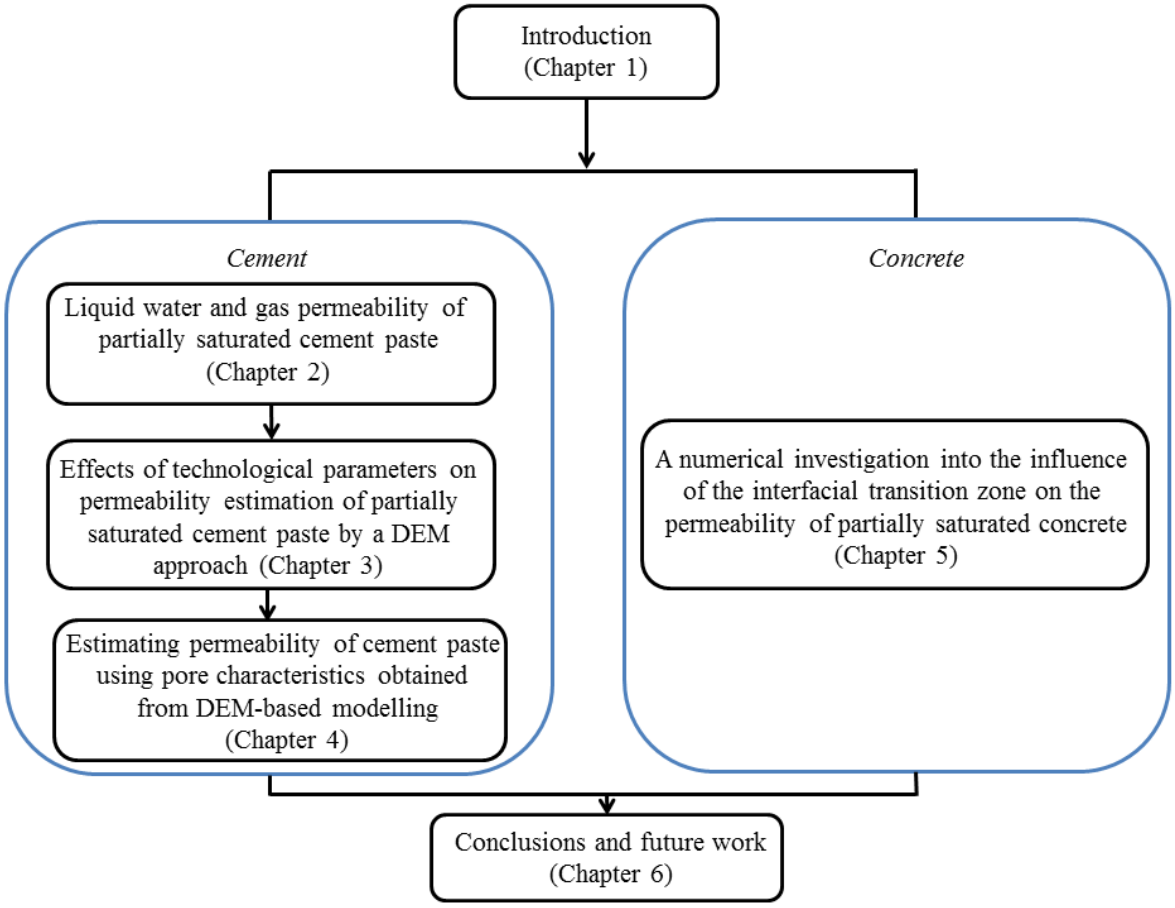

Figure 1.2 Flow chart of this thesis.

Chapter 2 Liquid water and gas permeability of partially saturated cement paste by DEM approach

This chapter is based on Kai Li et al. (2016a), a paper published in Cement and Concrete Research 83: 104-113.

Permeability of virtual cement seems to exceed experimental data by several orders of magnitude. The difference may not be that dramatic, since samples are in practice not always fully saturated as generally assumed. This has enormous effects on permeability. Therefore, a numerical study is conducted on water and gas permeability of partly saturated cement paste based on simulated microstructures. The results show that water permeability declines with the decreasing saturation degree. A similar but inverse relationship exists between gas permeability and saturation degree. The changes of pore size distribution and pore connectivity will be discussed in this chapter. The results in terms of relative water and gas permeability have been validated against lattice Boltzmann simulations and experimental data, respectively. A satisfactory agreement is found.

2.1 Introduction

Permeability is an important indicator for durability estimation of cement-based materials. It is defined as the movement of an agent (liquid or gas) through the porous medium under an applied pressure (Banthia *et al.*, 2005). Measurements of permeability in concrete structures are widely conducted in laboratories. Unfortunately, they are usually laborious, time-consuming and inevitably expensive. Wong *et al.* (2012) developed a convenient method for estimating the permeability of cement pastes and mortars based on backscattered electron micrographs (BEM). It seems that obtaining BEM images still requires significant efforts and may not be possible in some laboratories. As an alternative, digital modelling techniques constitute an attractive and economic solution. Pignat *et al.* (2005), Koster *et al.* (2006) and Ye *et al.* (2006) are the pioneers in the field of water transport simulation in cement pastes. Their so-called network models are subdivided into a series of nodes connected by cylindrical tubes. Each tube represents a local pore. Next, the equations of laminar flow inside this tube network are solved to obtain the intrinsic permeability. The reported outcomes in these earlier

studies range from 10^{-13} to 10^{-20} m^2 depending on the design of the hydrated pastes (*i.e.* porosity, water/cement ratio, particle size distribution and degree of hydration). The lattice Boltzmann method is another popular method because of its low requirement for computing resources. Garboczi and Bentz (2001), Zhang *et al.* (2013) and Zalzale (2014) have conducted studies of simulated fluid flow through the cement paste using this approach. It is also known as a discrete modelling method since the microstructure of the hydrated paste has to be discretized into numerous voxels (each one representing a certain phase such as pore, unhydrated cement or hydration product) before the equations of flow can be solved by the lattice Boltzmann approach. A general comparison between the network model and the discrete model has been presented in (Zalzale, 2014). The network model yields larger scatter in water permeability data as the discrete model. The network model seems to strongly depend on the structural representation of the specimens.

Nevertheless, in the aforementioned modelling techniques, the permeability of the virtual cement seems to exceed experimental data by several orders of magnitude. However, the differences may actually not be that dramatic since the saturation conditions of specimens in simulations and experiments are generally not the same. In fact, Darcy's law (Darcy, 1856) used in the conventional laboratory testing for obtaining permeability requires samples to be fully saturated. This is implicitly assumed in simulations, however the full saturation state is difficult if not impossible to realize in practice (Zalzale, 2014). Muller *et al.* (2013) experimentally showed that for a white cement paste (*w/c* = 0.4, hydration for 28 days) 85% of the total pore volume can be considered 'empty' due to chemical shrinkage. These pores cannot easily be filled. This means that those pores are not active in the water transport that defines the permeability.

Earlier experimental studies (Coussy *et al.*, 1998; Abbas *et al.*, 1999; Villain *et al.*, 2001; Monlouis-Bonnaire *et al.*, 2004; Sercombe *et al.*, 2007; Baroghel-Bouny *et al.*, 2011) show that the permeability of cementitious materials strongly depends on the degree of water saturation (defined as the volume fraction of the pores that is filled with water). However, these studies mainly deal with the case of gas as the penetrating agent. Only recently, Kameche *et al.* (2014) and Zamani *et al.* (2014) reported that the liquid water permeability of cementitious materials measured by experiments is governed by the degree of water saturation. The reason why only limited experimental data regarding water permeability are available has been discussed in (Kameche *et al.*, 2014). It is because gas permeability measurements require less time and produce better reproducible results since the fully saturated state as required in laboratory testing on water permeability is difficult to establish and maintain. Therefore, the concept of the water saturation degree is interesting and meaningful for the author, since this parameter was so far not taken into account in our network model. The specimens in our simulations were so far assumed to be in a full saturation state, so that the obtained results were inevitably not in a good agreement with the experimental data of incompletely saturated specimens (Le, 2015).

Zalzale *et al.* (2013) have conducted a study on the influence of water saturation on the permeability of cement paste by a 3D lattice Boltzmann approach. The water evaporation process inside the hydrated paste is modelled by means of the Kelvin-Laplace equation to obtain partially saturated samples. This equation states that large pores are easier loosing water because of low capillary pressure. In the study presented herein this assumption is also used but implemented in a different way. Instead of transferring pore-voxels into solid-voxels as described in (Zalzale *et al.*, 2013), an "empty" algorithm was developed for mimicking the reduced saturation, which is described in detail in Section 2.3. Moreover, the basic difference between the model presented here and that of Zalzale (2014) is the method chosen for fluid flow simulation. The lattice Boltzmann method in the latter is based on a voxel system, while in this work the flow transport in cement paste is simulated by a network model. Although Pignat *et al.* (2005), Ye *et al.* (2006) and Le (2015) have earlier conducted studies by using such tube network models, they only addressed the case of fully saturated porosity conditions. Hence, their simulation results cannot be compared to water-based experiments with a saturation degree lower than 100%. Besides, it should also be noted that only water permeability is concerned in those studies; the assessment of gas permeability by network models applied to simulated microstructures of mature cement paste was not considered.

The objective of this chapter is to quantitatively evaluate the effects of partial water saturation on the water/gas permeability of a virtual cement paste and to validate the developed methodology on the basis of available relevant literature information. Moreover, the changes in available channels for fluid permeation (as to pore size distribution and pore connectivity) will also be discussed. Note that cement paste is selected in this study for permeability studies instead of concrete since the aggregates are usually impermeable compared to cement paste. The methodology followed in this work has been thoroughly outlined in (Stroeven *et al.*, 2015), so the interested reader is referred to this publication for more information. We will only give a brief introduction about the full methodology in Section 2.2, including the hydration simulation set up, the porosimetry approach and the model for permeability calculation. The discrete element method (DEM) is used instead of random sequential addition (RSA) to more realistically distribute the individual cement grains in the container (Williams and Philipse, 2003; Chen *et al.*, 2006; Stroeven *et al.*, 2009). The dense structure obtained after DEM packing simulation is the input for hydration simulation. The effects of the degree of water saturation on the water and gas permeability of cement paste will be demonstrated in Section 2.3. When the saturation degree is reduced, the calculated water permeability decreases significantly. A similar relationship between gas permeability and the saturation degree does exist, but in an inverse way, implying that an increase in the saturation degree leads to a decrease in gas permeability. All findings are shown to agree well with experimental observations (Ai *et al.*, 2001; Vichit-Vadakan and Scherer, 2002; Ye, 2005; Grasley *et al.*, 2007).

The simulation results, in terms of relative permeability, are compared with outcomes of analytical models, with estimates obtained by a lattice Boltzmann approach, and with

experimental data, respectively. A satisfactory agreement is observed, validating the presented methodology.

2.2 Methodology

2.2.1 Three-dimensional microstructure

The vector-based XIPKM (Extended Integrated Particle Kinetics Model) was used to create the microstructures of hydrated cement pastes in this study (Le *et al.*, 2013). The major cement compounds, *i.e.*, tricalcium silicate (C_3S), dicalcium silicate (C_2S), tricalcium aluminate (C_3A) and tetracalcium aluminoferrite (C_4AF), together with the effect of rice husk ash blending, can be taken into account. The structures were generated in a cube container (100 µm in size) with a water/cement (*w/c*) ratio of 0.4. The phase composition of the cement clinker was 61% C_3S, 20% C_2S, 8% C_3A, 11% C_4AF by volume. The Rosin Rammler function was chosen to represent the particle size distribution, ranging from 1 to 30 µm. For more details on XIPKM, the reader is referred to (Le *et al.*, 2013). Although calcium silicate hydrate (C-S-H) has been proven to be porous and weakly-permeable, its contribution is only of importance for the total permeability at very low capillary saturation (Zalzale *et al.*, 2013). Its structure and formation mechanism is still uncertain and controversial (Feldman and Sereda, 1970; Gartner *et al.*, 2000; Jennings, 2000, 2008). Within the scope of this work, the C-S-H is considered impermeable. The volumetric density (64%) proposed by Jennings (2000) was used to determine the thickness of the outer layer hydration product surrounding the hydrating cement grains in XIPKM.

Microstructures were generated for different degrees of hydration and those with 9.5% total capillary porosity were selected for permeability tests. The reason for choosing this porosity is to ensure the cement paste to be matured and to compare it with other simulation results (Zalzale *et al.*, 2013). Compared to other vector models (Breugel, 1995a, b; Bishnoi and Scrivener, 2009), XIPKM was selected because of the dynamic generation of particles realized by a DEM simulation. In DEM, the particles are dynamically mixed rather than sequentially positioned, leading to realistically packed structures.

2.2.2 Porosimetry in matured cement paste

The Double Random Multiple-Tree Structuring (DRaMuTS) method, was chosen to perform the porosimetry operation of the aforementioned virtual matured material. After distributing random points into the virtual structure, the nodes situated in the solid phase are eliminated from further consideration. So what results are nodes dispersed inside pores as a detection system of the 3D capillary pore network of the specimen. Then, a structuring process starts in which the relationships between nodes are built up by unobstructed straight line segments connecting the nodes. Such randomized data structures are built incrementally like growing

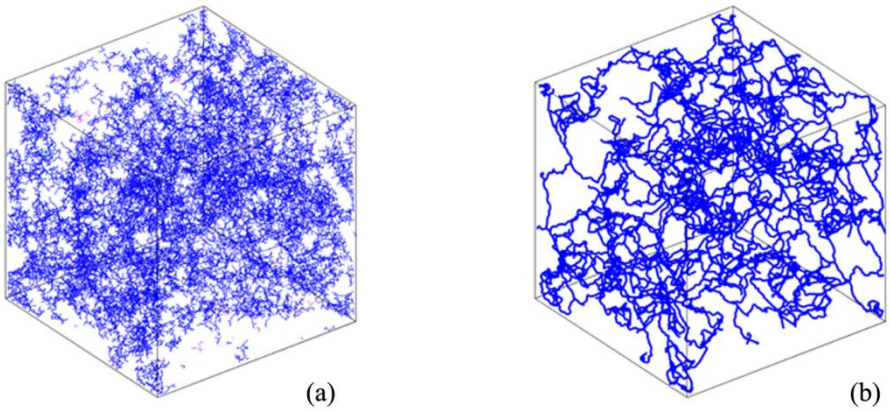

Figure 2.1 Pore delineation by DRaMuTS in 100 μm cubes for PC. All capillary pores are shown (a) as well as the continuous channels only (b). Hydration is simulated by XIPKM.

trees to characterize the pore network. Relevant details can be found in (Le and Stroeven, 2012; Stroeven *et al.*, 2012). An illustrative image about pore delineation by DRaMuTS is given in Figure 2.1. Compared to the serial sectioning and 3D reconstruction technique developed by Ye for porosimetry of virtual concrete (Ye, 2003) - a technique popular for applications on soft tissues in life sciences - DRaMuTS is more economical in assessing the full pore topology of virtual cement-based materials. For assessment of local pore volume, a method called star volume measuring (SVM) is applied (Stroeven *et al.*, 2012). Using information from DRaMuTS and applying SVM, the pore characteristics were assessed of matured cement paste, including the pore connectivity and the pore size distribution.

2.2.3 Microstructures at various degrees of water saturation

The modelling platform XIPKM generates the microstructure of the solid phases. As for the remaining space, it is usually assumed to be completely water-filled. This hypothesis indicates that the sample under this condition should be fully saturated; the water saturation degree will equal to 100%. However, this ideal situation is difficult to achieve in practice. Since an empty pore that always exists in the cement paste acts as a local barrier for water transport, such empty pores will permanently block the local transport of water. According to the Kelvin-Laplace equation, larger pores drain earlier than smaller ones because of the capillary force and are therefore the first to get empty. Zalzale *et al.* (2013) modelled the partially saturated samples by gradually transferring pore-voxels into solid-voxels. Thus, the voxel transfer starts from the largest pores. The same principle is also applied in our network model. However, we mimic the reduced saturation phenomenon by positioning solid objects in the presumed empty pores rather than using the voxel transfer technique.

To model permeability at various degrees of water saturation, an "empty" algorithm was implemented in our models. In this algorithm, water can be removed progressively from fully saturated microstructures. A pre-defined amount of water can be removed from a fully filled pore-structure by removing spherical amounts of water or equivalently placing spherical solid

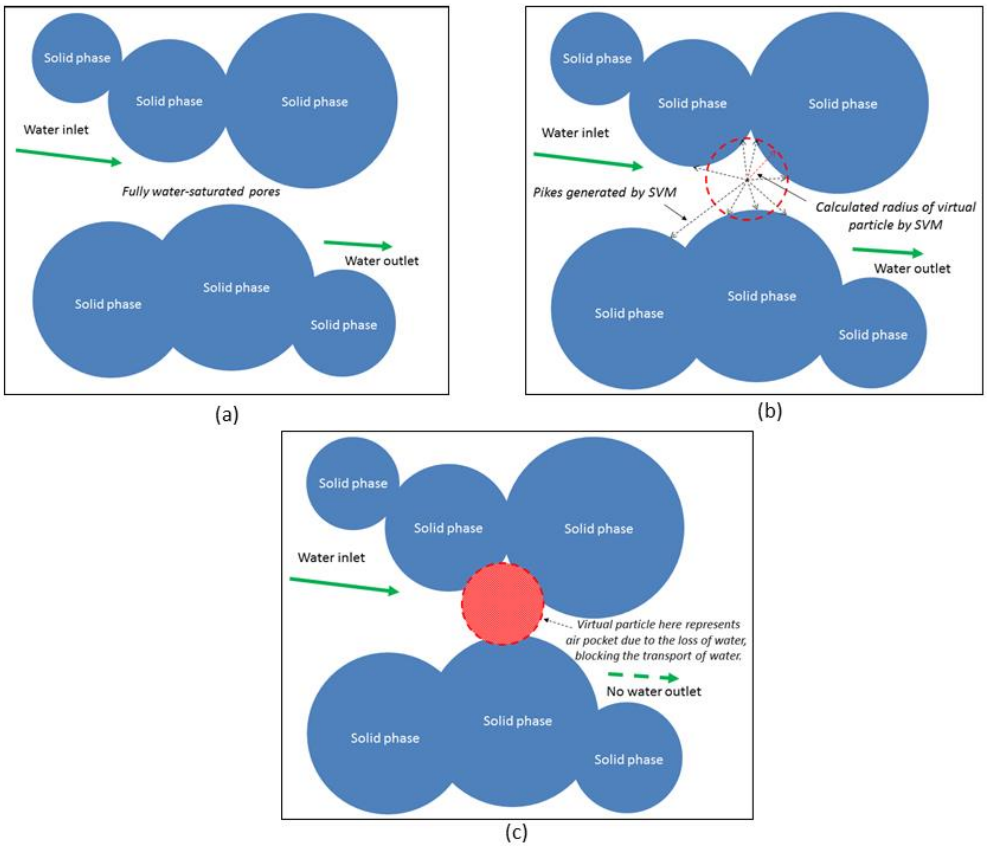

Figure 2.2 Illustration of the "empty" algorithm in 2D. (a) fully saturated state; (b) positioning of a solid sphere in water-filled pore; (c) partially saturated sate. The position and size of the solid sphere (virtual red circle) is obtained by DRaMuTS.

objects at those locations. This can easily be accomplished by DRaMuTS. All pores were characterized and sorted by their sizes and stored for further analysis. In accordance with Zalzale's work (Zalzale *et al.*, 2013), the "empty" algorithm starts from the largest pores in our simulation. Once positions of pores were determined, water can be removed by positioning solid spheres at the calculated center of the pore with a radius equal to the calculated pore-radius to block the original transport path of water. The procedure is illustrated in Figure 2.2. Since the empty pores are modelled by replacing them with a solid phase, the remaining open space is assumed 100% filled by water. Darcy's law still holds for permeability calculation. This allows for the investigation of the influence of the water saturation degree on the permeability.

In the case of air penetration, pores filled by water become impermeable to gas, as gas transport can only occur in percolated air-filled pores. The penetrative phenomenon of air in a water environment is usually too insignificant to be taken into account. The capillary pressure in small pores causes the smallest pores filling up with water before the larger pores do. Hence, these small pores are the first ones to become impermeable to air while the large ones remain open for the transport of gas. The "empty" algorithm in this case starts from the same pore structure as with the water permeability simulation. However, this time it starts blocking

the smallest pores first. To increase the reliability of the results, multiple repeats of the algorithm were run with different parent structures (8 samples) all with the same overall capillary porosity (9.5%).

2.2.4 Permeability calculation

A network structure, consisting of cylindrical tubes, was constructed to represent the pore channels. The main trunks represent the direct paths through the pore space from the bottom to the top of the sample. In contrast to isolated paths and dead-end branches, the main trunks are assumed to play a key role in the transport process. They can be extracted from the system and then used for permeability calculations, while the other pores are neglected. The diameters of the tubes along the main trunks were estimated by using SVM on the underlying point structure. The flow inside a tube is assumed to be slow, saturated, incompressible and laminar, so that the Hagen-Poiseuille law applies. A pressure gradient is applied between inlet and outlet nodes located at the bottom and top boundary of the specimen. In a tube segment with a pressure difference Δp_{ij} (Pa) between the two ends (i and j), the volumetric flow, Q_{ij} can be expressed by:

$$Q_{ij} = G_{ij}\,\Delta p_{ij} \tag{2.1}$$

where G_{ij} denotes the hydraulic conductance of the tube segment. At each node i that connects a number of the tube segments, the mass conservation law of flow gives:

$$\sum_{j=1}^{n_i} Q_{ij} = 0 \tag{2.2}$$

where n_i is the total number of tubes having node i as the common end, and j denotes the other end of the tube. Substituting Eq. (2.1) into Eq. (2.2), a set of algebraic linear equations with nodal pressures as unknowns are obtained. Applying the prescribed pressures at the nodes (tube ends) located at the bottom and top surfaces of the specimen, the nodal pressures are determined by solving this set of equations. The flow rate in each tube and thus the total outlet (inlet) flow rate can be calculated, whereby the average velocity of flow and therefore the permeability can be estimated by using an adapted version of Darcy's equation (the normal form of Darcy's equation is Eq. (2.3) while the adapted one is Eq. (2.4)):

$$\kappa = \frac{L}{A}\frac{Q\,\mu}{\Delta P} \tag{2.3}$$

$$\kappa = \frac{\mu \langle u \rangle L}{\Delta P} \tag{2.4}$$

where κ = intrinsic permeability [m^2] and $\langle u \rangle$ represents the average velocity which can be obtained by either volume averaging or area averaging on the inlet (or outlet) surface [m/s]. L

(m) and A (m^2) are the length and cross sectional area of a test sample subjected to a fluid flow Q (m^3/s). μ denotes the dynamic viscosity of the intruding fluid [Pa·s]. To distinguish water permeability and gas permeability discussed in the scope of this study, the former is denoted as κ_w while the latter is κ_g.

The hydraulic conductance G_{ij} given in Eq. (2.1) should be available to solve the algebraic linear equations derived from Eq. (2.1) and Eq. (2.2). The conductance G_{ij} of a tube segment of length L_t, with the cross-section varying along its length, is given by (Le, 2015):

$$G_{ij} = \frac{1}{L_t} <C(x)^{-1}>^{-1} \tag{2.5}$$

in which <•> denotes the average value along the length of the tube. The conductance of a cross-section, C, is therefore the remaining unknown parameter. For an ideal circular cross-section, the conductance C_c is equal to $\pi D^4/128\mu$ under no slip conditions at the wall and a parabolic distribution of flow, where D is the diameter of the circular section. However, the cross-sections of capillary pores in cement paste, even originating from spherical particles, are generally very irregularly shaped. To account for the inefficiency with respect to the transport capacity of an actual throat section as compared to that of the tube's adopted representative circle section, a conductance ratio $\xi = C_t/C_c$ was defined, whereby C_t and C_c stand for the conductance of the real throat and of the cylinder sections, respectively. At each local pore, FEM (finite element method) is used to calculate ξ and thus C_t. Reference (Le, 2015) presents all details. Figure 2.3 is an example of the velocity field in the cross-section of an irregular-shaped pore in the simulated cement paste. This operation rendered possible providing the network model for all random points on the basis of the actual pore section's shape with relevant information on its conductance, C_t.

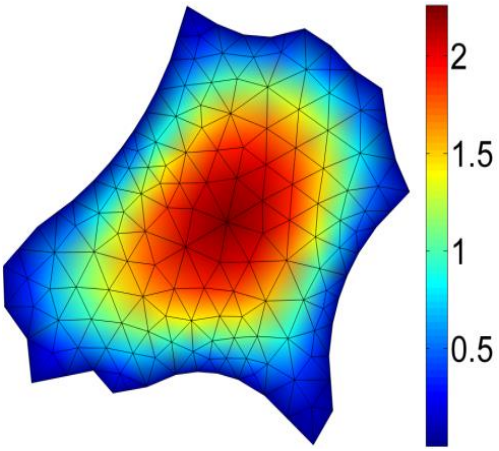

Figure 2.3 Velocity field solved by FEM of flow through an irregular cross-section of an arbitrary pore in the vector-based system.

2.3 Results and discussion

2.3.1 Water permeability

In the first part of this section, the results of a water permeability study of mature cement paste at various degrees of water saturation are discussed.

2.3.1.1 Evolution of water permeability with the degree of saturation

The whole methodology consisting of XIPKM-DRaMuTS-SVM-Pore blocking-Tube network modelling as described in Section 2.2 was applied to obtain specimens at different saturation degrees of which permeability has been assessed. The results are presented in Figure 2.4.

This figure shows the evolution of the measured intrinsic water permeability (K_w) with the degree of saturation (S) obtained by our numerical simulation approach. A significant influence of the degree of capillary water saturation can be observed, as reported in the literature (Baroghel-Bouny, 2007; Wong *et al.*, 2007; Baroghel-Bouny, 2008; Zalzale *et al.*, 2013; Kameche *et al.*, 2014). As a first result in our simulation, the intrinsic water permeability of cement paste at a fully saturated state ($S = 1$) was found equal to 3.27×10^{-16} m^2, which is almost one order of magnitude higher than the experimentally value of 5.7×10^{-17} m^2 obtained under presumably the same conditions (Kameche *et al.*, 2014). The difference can be explained by the fact that although experimentalists try to ensure water saturation before measuring water permeability, it is quite impossible to establish and maintain full saturation. In Figure 2.4, the measured water permeability of 5.7×10^{-17} m^2 would be obtained at a saturation degree that is equal to 0.71.

In general, as the water saturation degree decreases, the number of connected pores filled by water will decline, resulting in a reduction of the available paths for water transport in the system. In other words, the system is de-percolating. Moreover, the large pores will dry-up first, additionally contributing to a lower permeability. For $S \leq 0.42$, the estimated water permeability will drop faster until S reaches 0.22 or so. At that point, the remaining fully water-filled pores will be completely disconnected, thus, leading to a permeability equal to zero.

The validation of our simulation results is difficult because only a limited number of experimental data on liquid water permeability of partially saturated cement-based materials is available. However, analytical expressions popular in the field of inert porous media and/or soils can serve as an alternative. Kameche *et al.* (2014) used three different types of analytical expressions to verify experimental results. These expressions are the Corey model (Marechal and Beaudoux, 1992) (see Eq.(2.6)), the Fatt & Klikoff model (Udell, 1985) (see Eq.(2.7)) and the Van-Genuchten-Mualem (V.G.M) model (Mualem, 1976; Genuchten, 1980) (see

Eq.(2.8)). We use the same analytical expressions to preliminarily validate our simulation results.

$$\kappa_{rw} = [(S-0.05)/(1-0.05)]^4 \tag{2.6}$$

$$\kappa_{rw} = S^3 \tag{2.7}$$

$$\kappa_{rw} = S^q (1-(1-S^{1/m})^m)^2 \tag{2.8}$$

In Eqs. (2.6) - (2.8), S represents the liquid water saturation degree, and κ_{rw} is the relative water permeability. The parameter κ_{rw} is defined as the ratio of the intrinsic water permeability at a certain degree of saturation (S) to the intrinsic water permeability measured in the fully saturated state (S = 1). In Eq. (2.8), there are two additional parameters (q and m), which are related to the material. Parameter q is a factor that accounts for the pore connectivity and tortuosity. Monlouis-Bonnaire *et al.* (2004) proposed for concrete an adjustment with a value of q equal to 5.5, instead of the value of 0.5 used for other porous materials. Both values of 0.5 and 5.5 are adapted in our case to see the effect of such a variation. Parameter m is to be determined from the capillary pressure curve of the material. In this work, it is taken as 0.5, which is the mean value given for concrete in the literature (Kameche *et al.*, 2014).

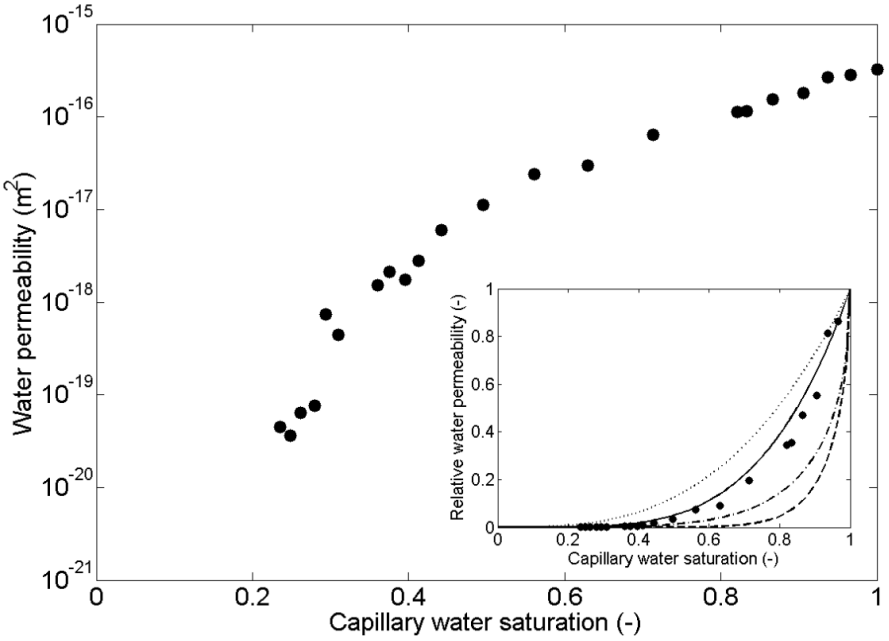

Figure 2.4 Intrinsic water permeability as a function of capillary water saturation. Insert: validation of our data (solid points) in terms of relative water permeability with analytical results. Solid line, double dot dash line, dot dash line and dash line represents the results obtained by the Corey model, the Fatt & Klikoff model and the V.G.M model (q=0.5 and 5.5), respectively.

To compare our model with the analytical expressions given in Eqs. (2.6) - (2.8), the intrinsic water permeability of Eq. (2.4) was transformed into relative water permeability ($\kappa_{rw} = \kappa_{w(s)}/\kappa_{w(s=1)}$). Outcomes of our simulations and the results from three different analytical expressions are plotted in Figure 2.4 as an insert. It can be observed that our simulation results are in the range covered by the analytical formulas. The Corey model seems to fit the best with our simulations.

2.3.1.2 Porosimetry analysis

Pore size distribution (PoSD) and connected pore fraction are the two key factors affecting the transport process in cementitious materials. In this work, these two parameters were investigated by SVM and DRaMuTS for cement paste at five different capillary water saturations (100%, 73.7%, 53.2%, 44.0%, 26.2%). In Figure 2.5, we can see that the volume-based PoSD curve of cement paste shifts to the left side as capillary water saturation decreases. Remember that water was progressively removed from the largest pores according to Kelvin-Laplace equation to reach a lower saturation degree. Since these larger pores are gradually replaced by solid particles as a result of the "empty" algorithm, they are no longer considered as pores contributing to the water transport. Moreover, the curve areas in Figure 2.5 are normalized to the corresponding saturation degrees (*i.e.* 100%, 73.7%, 53.2%, 44.0% and 26.2%), this is why the total area below each curve declines with the decreasing saturation degrees. This causes the shift to the left of the PoSD curve for lower degrees of saturation.

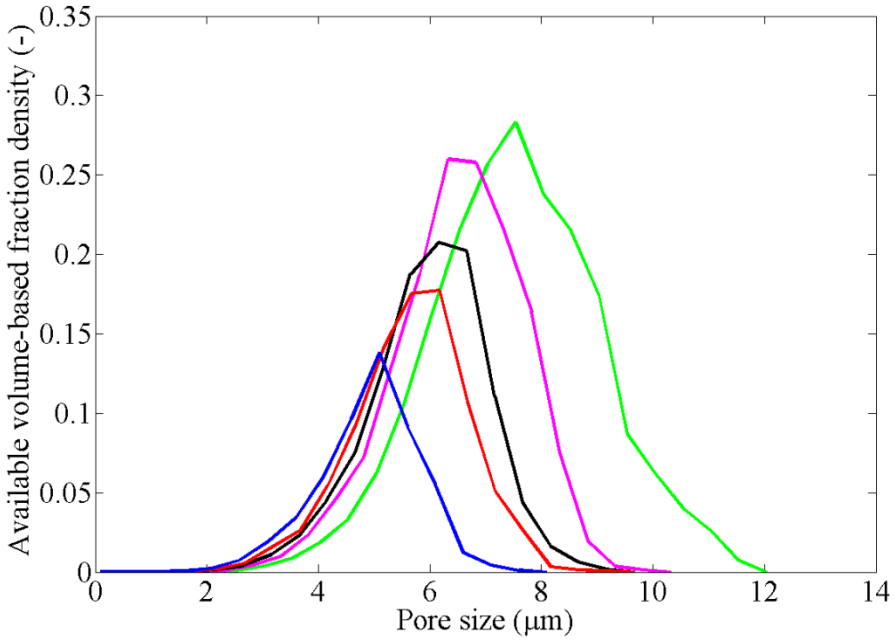

Figure 2.5 Pore size distribution of samples at various degrees of water saturation normalized for the corresponding saturation degrees. The curves in green, pink, black, red and blue show the results of the specimens at various saturation degrees (100%, 73.7%, 53.2%, 44.0% and 26.2%), respectively.

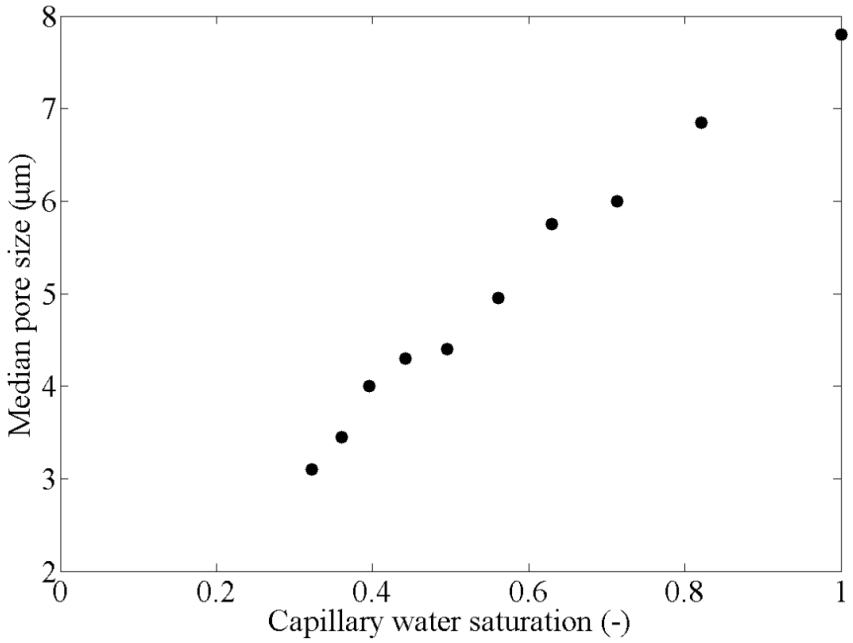

Figure 2.6 Almost linear reduction in volume-based median pore size with declining degree of water saturation in the capillary pore network structure.

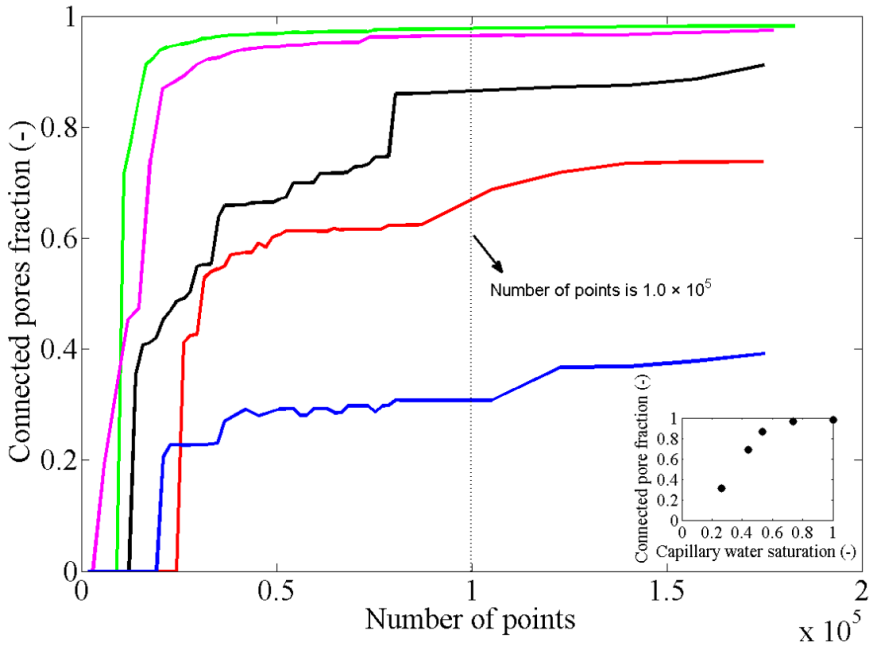

Figure 2.7 Sensitivity analysis of connected pore fraction at various degrees of water saturation. The curves in green, pink, black, red and blue show the results of the specimens at various saturation degrees (100%, 73.7%, 53.2%, 44.0% and 26.2%), respectively. Insert: connected pore fraction of the five specimens in the main figure when number of points for connectivity analysis is set as 1.0×10^5.

Figure 2.6 reveals an almost linear decline in median pore size with diminishing degree of water saturation in the pores. Note that the calculated median pore size here is also volume-

based instead of number-based, as already shown in Figure 2.5. So, PoSD of water filled pores is very sensitive to the degree of water saturation.

The other important parameter, pore connectivity in mature cement paste, was studied as well. DRaMuTS is based on a system of randomly distributed points, so the confidence of results depends strongly on their numbers. A large number of points usually leads to more accurate results, but makes the computations more expensive. Although the PoSD also depends on these numbers, the sensitivity is larger within the case of connectivity. Therefore, a sensitivity analysis of the connected pore fraction (= number of connected pores divided by the total number of pores) at various degrees of water saturation was carried out first. The results are plotted in Figure 2.7. At first, the connected pore fraction increases sharply as the number of points distributed in the remaining water-filled pores goes up. The curves seem to gradually converge to a steady number. In this work, the number of points was set to 10^5 to limit the computation time without a significant loss of accuracy in the results. For the five samples in Figure 2.7, their connected pore fractions are plotted in Figure 2.7 as an insert. With a decreasing capillary water saturation, the initially fully water-filled pores will gradually become empty, leading to a reduced fraction of connected pores. A smaller number of connected pores involve a lower water permeability.

2.3.2 Gas permeability

The results of gas permeability investigation of hydrated cement paste at different degrees of water saturation are given in the second part of this section.

2.3.2.1 Evolution of gas permeability with the degree of saturation

When, instead of a liquid, a gas is taken as the penetrating agent, a similar simulation can be performed. However, gas flows only through the air-filled pores instead of the water-filled pores. Basically, air is able to penetrate water but its permeability is too low to be taken into account (4 to 5 orders of magnitude smaller than the value in empty space). So, it is reasonable to ignore the permeation of gas in water-filled pores. To demonstrate the influence of the water saturation degree (S) on the intrinsic gas permeability (K_g), capillary water saturation was varied from totally dry (S = 0) to partially saturated conditions (S = 0.65). In this case, the pores are gradually filled with water. Since the smallest pores fill up the easiest, they will be blocked first. The de-percolation process is similar to the water permeability approach. The evolution of intrinsic gas permeability with the degree of saturation is shown in Figure 2.8. As a first result, the intrinsic gas permeability of cement paste at the fully-dry state is equal to 3.27×10^{-16} m^2, the same value as the water permeability at the fully-saturated situation. This is logical because the transport paths at fully-saturated states are the same, independent of the penetrating agent. This value agrees well with the experimentally obtained values in (Zalzale *et al.*, 2013; Kameche *et al.*, 2014; Zamani *et al.*, 2014).

The simulation results show that the intrinsic gas permeability is also strongly influenced by the degree of water saturation of cement paste. This observation confirms the results obtained by several researchers(Zalzale *et al.*, 2013; Kameche *et al.*, 2014; Zamani *et al.*, 2014). The permeability due to gas decreases when the water saturation increases as a result of the progressing "blocking" effect due to the capillary water.

The relative gas permeability κ_{rg} is defined as the ratio of intrinsic gas permeability at a certain degree of saturation to the intrinsic gas permeability measured in the fully gas saturated state (no water exists in the sample, *i.e.* $S = 0$). Similar to the preliminary validation in the water permeability study, the Jason model (Jason, 2004) used in Kameche's work (Kameche *et al.*, 2014) for ordinary concrete is used in this study for describing the evolution of the relative gas permeability as a function of the degree of saturation. So,

$$\kappa_{rg} = \left(1-S\right)^{p} \left(1-S^{2}\right) \tag{2.9}$$

in which S represents the capillary water saturation, and p is a so-called tortuosity parameter that depends on the material. As Jason's equation is just an adjustment of the V.G.M model (see Eq.(2.8)), Eq. (2.9) is still referred to as the V.G.M model. Although many researches have been conducted to determine the parameter p in Eq. (2.9) for various porous media (Baroghel-Bouny, 1994; Savage and Janssen, 1997; Monlouis-Bonnaire *et al.*, 2004), the

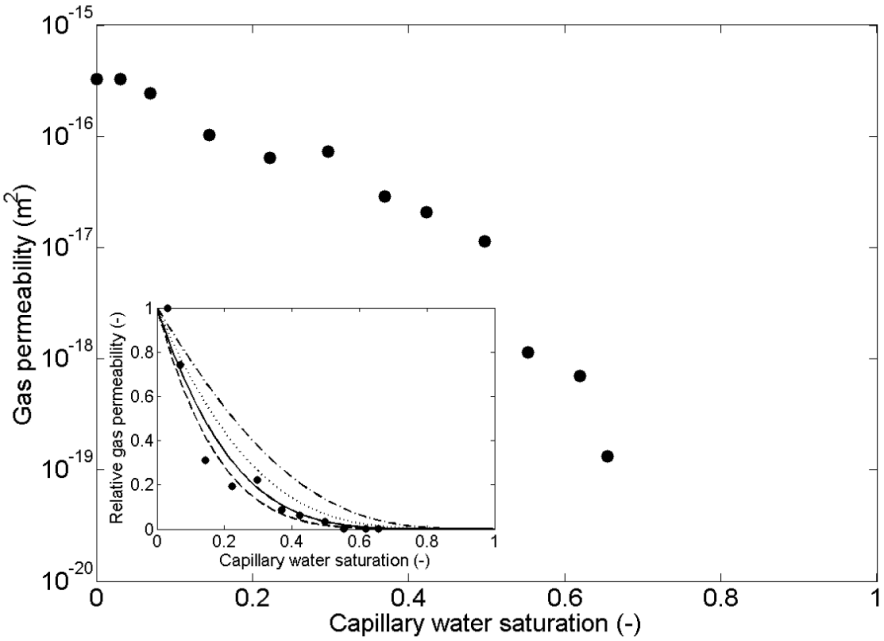

Figure 2.8 Intrinsic gas permeability as a function of capillary water saturation. Insert: validation of our data (solid points) in term of relative gas permeability with the results calculated by the V.G.M model. Dot dash line, double dot dash line, solid line and dash line represent the results obtained by the V.G.M model when p is equal to 2.5, 3.5, 4.5 and 5.5, respectively.

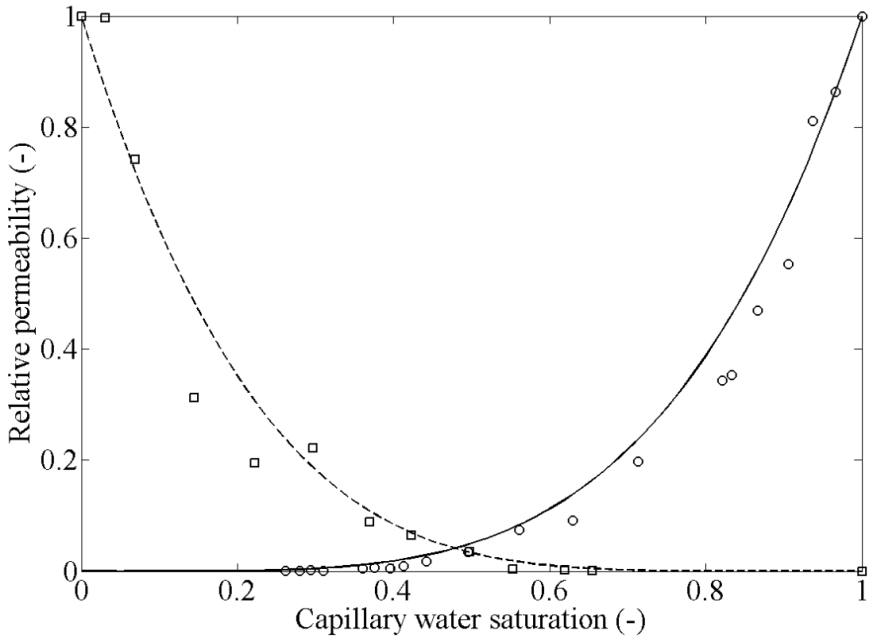

Figure 2.9 Relative gas and water permeability as a function of the degree of water saturation. Circles and squares represent the relative water permeability and relative gas permeability obtained by our model, while solid line and dash line the results calculated by the Corey model and the V.G.M model with p = 4.5, respectively.

value of parameter p is still uncertain for cement paste. Usually, p ranges from 2.5 to 5.5 for cementitious materials, as presented in (Kameche *et al.*, 2014). The parameter p with the same range is used in this research for preliminary validation of the relative gas permeability. The analytical curves obtained with the V.G.M. model for values of p between 2.5 and 5.5, are shown in Figure 2.8 as an insert, together with the results of the relative gas permeability of cement paste obtained from our simulation.

κ_{rg} calculated by our methodology reveals a strong decline down from 1.0 to 0.1 over the range of $0 \leq S \leq 0.4$. As $S \geq 0.55$, κ_{rg} tends to approach zero. This highlights the influence of S on transport properties, as already earlier depicted through quantitative and qualitative studies by Picandet *et al.* (2001) and Zamani *et al.* (2014), respectively. Moreover, κ_{rg} calculated by the V.G.M. model with p = 4.5 seems to fit best with our simulation results. This value is in the range between 3.5 and 5.5 as proposed by Savage and Jensen (1997) for concrete, validating our model.

The relative gas and water permeability versus capillary water saturation degree obtained by our simulation methodology are combined in Figure 2.9 with the best-fitting analytical results. Obvious inverse tendencies can be observed for water and gas permeability at various water saturation degrees.

2.3.2.2 Porosimetry analysis

Similar to the porosimetry approach in the water permeability study of mature cement paste, as described in Section 2.3.1.2, the PoSD and connected pore fraction in the gas permeability modelling approach were investigated at five different degrees of capillary water saturations (0, 14.4%, 29.6%, 42.3%, 55.3%). Pore size distribution curves of samples at various degrees of water saturation are plotted in Figure 2.10. As the process of capillary water saturation proceeds, small pores are filled by water first because of the capillary pressure. These pores are no longer considered for gas transport. This yields a shift to the right ("absence" of small pores) in Figure 2.10. Investigating the specimens with these five water saturation degrees yields the volume-based median pore size to range from 6.8 µm to 7.8 µm. Compared to the curve shown in Figure 2.5, the changes are less significant. The curve areas in Figure 2.10 are also normalized to the corresponding saturation degrees (*i.e.* 0, 14.4%, 29.6%, 42.3% and 25.3%). However, water-filled pores become impermeable to gas so the available pore fraction for gas transport should be calculated by 100% subtracting the water saturation degree. This is why an inverse tendency can be observed in comparison to Figure 2.5. Also in this case, a sensitivity analysis was performed to investigate the number of points (distributed in the remaining gas-filled pores) required for a reliable assessment of the connected pore fraction; 10^5 points were selected as well. The resulting connected pore fraction versus the degree of water saturation is plotted in Figure 2.11. Pore connectivity goes down as the water saturation degree increases. This is in good agreement with the relationship already found in

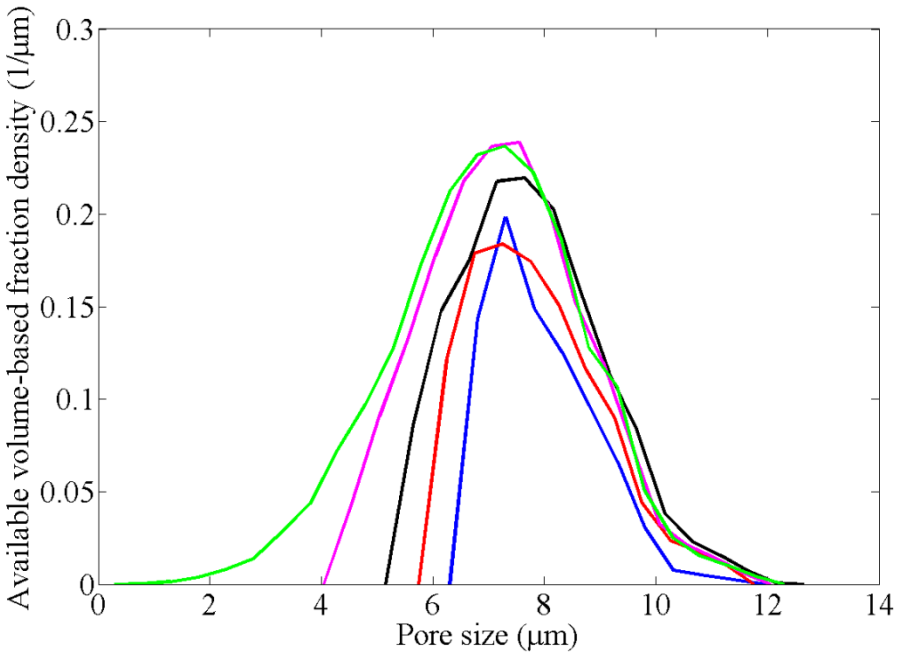

Figure 2.10 Pore size distribution of samples at various degrees of water saturation normalized for the corresponding saturation degrees. The curves in green, pink, black, red and blue show the results of the specimens at various saturation degrees (0, 14.4%, 29.6%, 42.3%, 55.3%), respectively.

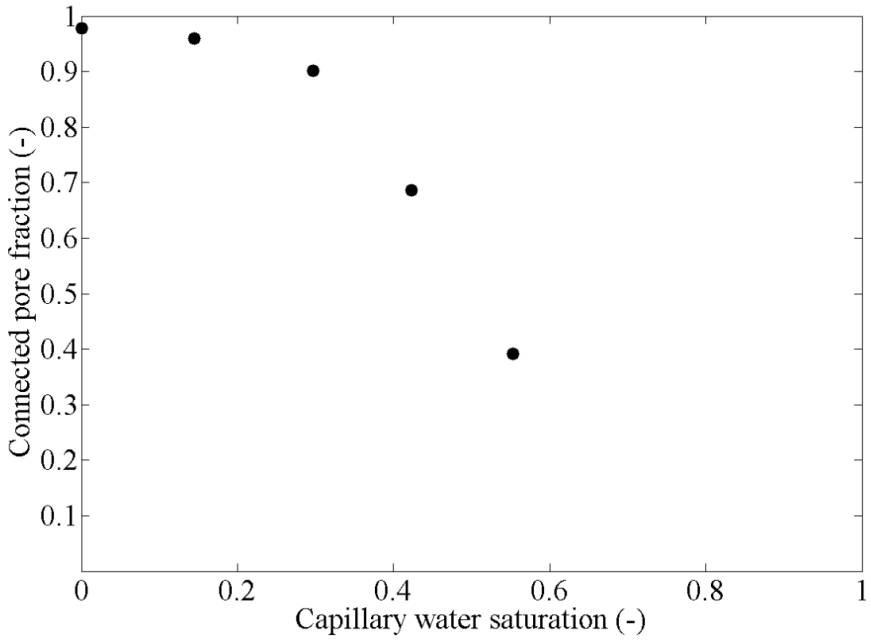

Figure 2.11 Connected pore fraction of the five specimens in Figure 2.10 when the number of points for connectivity analysis is set as 1.0×10^5.

Figure 2.7. A similar but inverse tendency was found in pore connectivity versus water permeability.

2.3.3 Validation

A limited number of experimental studies on liquid water permeability and gas permeability of partially saturated cement paste are available. Only very recently, Kameche *et al.* (2014) and Zamani *et al.* (2014) published two papers in this field. The experimental data in (Kameche *et al.*, 2014) are used here to validate our simulation results. Even though the specimens in the experiments are not exactly the same as the ones used in our simulations, the tendency should be similar between the cementitious materials. It makes the comparison in this study acceptable. This is the reason why we choose relative permeability instead of absolute value as a criterion. In addition to the experimental data, the permeability results of the cement paste from the 3D Lattice-Boltzmann modelling by Zalzale *et al.* (2013) are also used for comparison reasons. The outcomes of the comparison are shown in Figure 2.12. In the case of both water permeability and gas permeability (Figure 2.12), a satisfactory agreement is observed between our simulation data and both other results. Moreover, the tendency shown in Figure 2.12 also agrees well with the observation reported in (Zamani *et al.*, 2014).

However, a slight difference can be found between the numerical simulations and real experiments. In general, the results from our simulation as well as well as those due to the Lattice-Boltzmann (LB) simulation slightly underestimate the experimental values. Three

factors can be mentioned that may contribute to this difference when the experimental material is concrete rather than cement paste. Concrete contains relatively porous ITZs between aggregate grains and the cement paste that would facilitate the ingress of water. Moreover, micro-cracking along the particle-matrix interfaces may also contribute to the water transport. Finally, the experimental assessment of water saturation degrees of 0 and 100% in the concrete experiments may be considered with care. All these factors contribute to obtaining relatively high experimental permeability values.

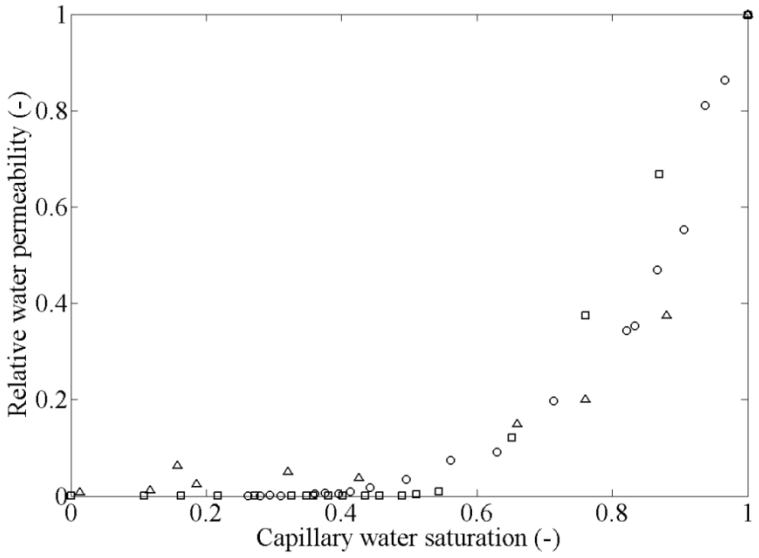

(a)

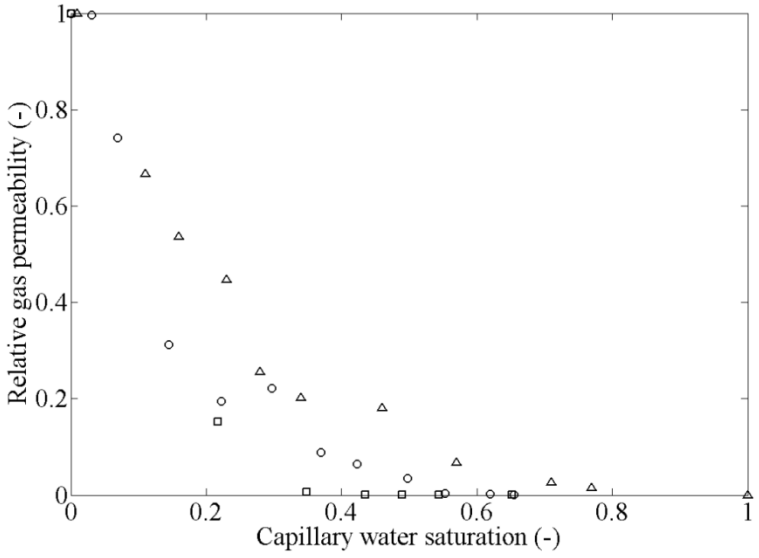

(b)

Figure 2.12 Validation of our simulation results by comparing with experimental data (Kameche *et al.*, 2014) and the values obtained by the LB method (Zalzale *et al.*, 2013). (a) Water permeability; (b) Gas permeability. Circles, triangles and squares represent the data from the present work, and from (Kameche *et al.*, 2014) and (Zalzale *et al.*, 2013), respectively.

In contrast to the lattice Boltzmann approach, the *w/c* (0.4) and the porosity of the fully saturated specimen (9.5%) are kept the same in our study. The minor difference between the values of relative permeability by our simulation and lattice Boltzmann method can be attributed to the fact that the inherent mechanism of generating cement particles for hydration simulation is different. In the latter case, a RSA algorithm is implemented for modelling cement grains distribution prior to the hydration simulation. Contrary, in our case, a dynamic concurrent algorithm-based DEM system is used to obtain a more realistic distribution of cement grains, as demonstrated in (O'Connor, 1996; Stroeven, 1999). However, the differences are not dramatic implying the results to be relatively independent of the model used in the simulation.

2.4 Conclusions

The intrinsic permeability can be a better parameter for estimating transport-based durability properties of concrete, as compared to the traditional Darcy's coefficient of permeability, as suggested by Kameche *et al.* (2014). Conceptually, the intrinsic permeability is independent of the applied pressure gradient and the transport agent's properties; it is a characteristic of the porous medium alone. Hence, the intrinsic permeability of cement paste fully saturated with water should be the same as the intrinsic permeability of the material when completely dried and saturated with air in an ideal gas permeability experiment. However, this is not always true in practice as observed experimentally (Loosveldt *et al.*, 2002). The reported experimental values of the gas permeability are generally 3-5 orders of magnitude higher than that of the water permeability. This is most probably due to the degree of water saturation not being zero percent, respectively 100 percent as assumed in the experiments.

A new methodology (XIPKM-DRaMuTS-SVM-Pore blocking-Tube network modelling) has been applied in this work to determine the permeability of partially saturated pastes. The outcomes in terms of relative water and gas permeability are found in good agreement with the experimental data (Kameche *et al.*, 2014) and lattice Boltzmann simulations (Zalzale *et al.*, 2013), validating the presented methodology. Moreover, the relationship between water/gas permeability and water saturation degree shown in this study also agrees well with the observation reported in (Zamani *et al.*, 2014).

This work confirms that there is an important influence of the water saturation degree on the values of both the liquid water permeability and gas permeability of cement paste, in good agreement with outcomes of experimental tests and of lattice Boltzmann simulations (Zalzale *et al.*, 2013; Kameche *et al.*, 2014; Zamani *et al.*, 2014). In case of water permeability, the water permeability decreases slowly at first when the water saturation is decreased from 100 percent. When the water saturation reaches values of 50 percent and lower, the water permeability decreases more rapidly and a sharp drop in the water permeability can be observed for values below 40 percent, as illustrated in Figure 2.4. This can be explained by the fact that the water-filled capillary porosity gradually becomes de-percolated, as a sharp

drop at a similar range of water saturation can also be found in the connected pore fraction. The degree of water saturation ends at 25 percent, where the fraction of connected pores is 30 percent. Upon further decreasing the water saturation degree, the remaining connected pores will be blocked; the system is fully de-percolated. Therefore, no transport is possible. In reality, this may not be true as C-S-H containing nano-porosity is conceived as a weakly-permeable substance to water, as shown by (Zalzale *et al.*, 2013; Zalzale, 2014; Ma and Li, 2013). Even when the main trunk for water transport is completely blocked, C-S-H as the major compound of mature cement paste, can still make contributions to the water transport. But, the role of C-S-H is only critical for determining the permeability at low capillary water saturation.

Compared to water permeability, an inverse tendency can be observed for gas permeability at various degrees of water saturation. At the start, we assume no water in the sample, so the degree of water saturation is 0, whereas for water permeability the start is at the 100 percent degree of water saturation. In the two (extreme) cases, the intrinsic permeability for air or water is at its maximum. The gas permeability of cement paste at the fully-dried state is equal to 3.27×10^{-16} m^2, close to the experimental data (Kameche *et al.*, 2014). From their respective abovementioned start situations on, the air permeability decreases when the degree of water saturation increases, whereas the water permeability decreases with decreasing water saturation degree. The extreme degree of water saturation above which no transport is possible in the gas permeability case is approximately 65%, whereas for water permeability this amounts to approximately 25%. It is quite interesting to point out that similar thresholds also exists in lattice Boltzmann modelling (Zalzale *et al.*, 2013). According to the porosimetry study of the hydrated microstructure, both pore size and pore connectivity seem to affect the water/gas permeability, in agreement with the previous study (Zhang, 2013). They seem able explaining the observed structural changes of the specimen.

Analytical expressions as used in (Kameche *et al.*, 2014), largely validated for porous materials, including the model by Correy, Fatt & Klikoff and Van-Genuchten-Mualem, are therefore used for preliminary validation. In the case of water permeability, our simulation results fall inside the range of predictions obtained by the analytical formulas and specifically agree well with those by the Correy model. When the penetrating agent is air, our simulation data better fit the VGM predictions with p=4.5. This value is in between the ones reported by Kameche (p=3.5) (Kameche *et al.*, 2014) and by Monlouis-Bonnaire (p=5.5) (Monlouis-Bonnaire *et al.*, 2004). This difference may be attributed to the fact that cement paste is used in our case instead of concrete in the other cases.

Furthermore, our simulation results are validated also by the limited number of experimental data and by the outcomes of the Lattice-Boltzmann simulation. A good agreement is observed, validating the presented methodological approach.

Chapter 3 Effects of technological parameters on permeability estimation of partially saturated cement paste by a DEM approach

This chapter is based on Kai Li et al. (2016b), a paper submitted for publication in Cement and Concrete Composites.

In this chapter, a numerical approach developed in our group is used to assess the permeability of partially saturated cement paste based on a discrete element modelling (DEM) technique. The relationship between saturation degree and permeability is found to be in good agreement with experimental observations. Also, outcomes of a systematic study of the effects of technological parameters (*i.e.*, hydration period, water/cement ratio and cement particle size range) on the permeability of partially saturated specimens follow expected trends. Moreover, permeability is found to be correlated to effective porosity. This is a sound basis for investigating the impact of the interfacial transition zone on water and gas permeability. Effects of partial saturation are demonstrated different for water and gas transport. Possible mechanisms underlying these permeability characteristics are discussed herein.

3.1 Introduction

The ingress of aggressive agents (*i.e.*, water, chloride and carbon dioxide) into cementitious materials often leads to premature degradation and even failure of many reinforced concrete structures (Zhang and Zhang, 2014). Therefore, transport-related properties (*i.e.*, permeability, chloride diffusivity and electrical conductivity) are generally considered as important indicators for durability assessment of concrete. In this study, we only consider permeability while the other two factors are outside the scope. Permeability is defined as the movement of an agent through a porous medium under an applied pressure load (Banthia *et al.*, 2005). For cement and concrete, permeability is usually determined by laboratory testing. Applying a pressure gradient and measuring the steady fluid flow through the fully saturated sample are generally involved in the conventional testing, as described in (Wong *et al.*, 2012). Afterwards, Darcy's law can be applied to calculate the permeability.

Unfortunately, direct permeability measurements require specialized equipment and a long period of time to finish. Simulation techniques are therefore considered as an attractive alternative for their efficient and economic benefits. In general, network models (Pignat *et al.*, 2005; Koster *et al.*, 2006; Ye *et al.*, 2006) and discrete models (Garboczi and Bentz, 2001; Zalzale and McDonald, 2012; Zhang *et al.*, 2013) are popular for modelling the transport of fluid flow through cementitious materials. The latter, voxel-based models pursue solving the equations of flow by numerical methods such as lattice Boltzmann or finite element method. Garboczi and Bentz (2001), Zhang *et al.* (2013) and Zalzale (2014) have conducted studies of fluid flow simulation through the cement paste by this approach. In contrast to the discrete model, a different principle is implemented in network models for obtaining the permeability. Instead of discretizing the structure into numerous voxels, a series of inter-connected cylindrical tubes are constructed to represent the pore network for fluid transport. Afterwards, the intrinsic permeability can be obtained by solving the equations of laminar flow inside this tube network. The tube model is selected in our case since we believe this approach is closer to the realistic situation and it fits well with the discrete element modelling of our hydrated cement. A comparison between the network model and the discrete model has been made in (Zalzale, 2014). Earlier studies by the tube network model are conducted by Pignat *et al.* (2005), Ye *et al.* (2006) and Le (2015).

Comparing the simulated permeability measurements with of experimental investigations is very difficult due to the difference in the conditions of the specimens in experiments and in simulations. In fact, the samples in experiments are required by Darcy's law to be fully saturated. Although this can be easily achieved in simulations, a fully saturated state of the material is difficult to establish and maintain in practice. Concrete has been proven to remain unsaturated during construction and throughout its lifetime (Glasser and Zhang, 2001; Chatterji, 2004). In the past decade, the effects of water saturation degree on the permeability of cementitious materials have been studied by many researchers (Coussy *et al.*, 1998; Abbas *et al.*, 1999; Villain *et al.*, 2001; Monlouis-Bonnaire *et al.*, 2004; Sercombe *et al.*, 2007; Baroghel-Bouny *et al.*, 2011; Kameche *et al.*, 2014). These studies show that the degree of water saturation has a major influence on the permeability and could easily explain the orders of difference in magnitude between experiments and simulations (Zalzale, 2014). Water saturation degree is therefore taken into account in this numerical work. A review of the studies on transport properties in unsaturated cement-based materials is given by Zhang and Zhang (2014). Note that drying-induced microcracks in experiments have a significant effect on transport properties of cementitious materials, as shown by recent experimental and modelling work (Lee *et al.*, 2016; Liu *et al.*, 2016; Fahy *et al.*, 2017; Plague *et al.*, 2017). These cracks tend to initiate at the interfacial transition zone (ITZ) and may coalesce. In this case, the transport properties (*i.e.*, permeability) are enhanced. However, the influence of microcracks on permeability of cement-based materials is not within the scope of this work.

A simulation methodology for numerical determination of permeability of cement paste developed in our group (Li *et al.*, 2015; Stroeven *et al.*, 2015) has been recently extended with

a parameter that indicates the saturation degree. This is considered an important improvement since samples in service can now properly be represented. Although methodological details have been given in (Li *et al.*, 2016a), enough information will still be provided in this paper to enable the reader to understand how the simulations are conducted. The various stages of the methodology, to be shortly introduced later, have also been validated and published separately (Stroeven *et al.*, 2010; Stroeven *et al.*, 2012; Le *et al.*, 2013). The developed methodology is applied to a series of samples representing different conditions met in practice. In this paper, only the final outcomes from our numerical studies (in terms of permeability) are shown and compared with results from other studies (Zalzale *et al.*, 2013; Zamani *et al.*, 2014). The effects of parameters such as hydration age, water-cement ratio (*w/c*) and cement particle size range (PSR), on permeability of partially saturated cement paste have been systematically studied on the basis of a DEM-based particle structure. The influence of the interfacial transition zone (ITZ) on permeability estimation is also included. Although concrete is more often investigated in practical studies, cement paste is selected in this study since the aggregates are usually treated as impermeable phases in concrete. DEM is used to more realistically distribute the individual cement grains in the container. For more details on DEM, see (Williams and Philipse, 2003; Chen *et al.*, 2006; Stroeven *et al.*, 2009). The background of our computational methodology will be briefly overviewed in Section 3.2. Next, the influence of hydration age, *w/c* and PSR on the water permeability of cement paste at different degrees of water saturation will be discussed in Section 3.3. Finally, the effects of the ITZ on both water and gas permeability of partially saturated paste are studied and underlying mechanisms behind this phenomenon are discussed in the same section.

3.2 Computational methodology

Roughly, two stages can be distinguished in laboratory testing of the permeability of cementitious materials, *i.e.*, sample preparation and permeability assessment. In the first stage, the fresh cement grains of the targeted particular material are mixed with water, hydrated and cured for a period of time in experiments. In the case of water permeability measurements, the specimens need to be cured underwater for a long period of time to ensure their fully saturated states as required by Darcy's equation. In the second stage, water is penetrating through the samples under an applied pressure gradient. When the water flow reaches a steady state, the amount of flow through the materials is measured using precision instrument; Darcy's law is used to calculate the permeability. The complete process of our computational methodology (consisting of five steps) is in accordance with the experimental procedure, as illustrated in Figure 3.1. Step 1 and 2 represent the sample preparation whereas steps 3 to 5 correspond to the permeability assessment stage. A short description of each step is given as follows:

- Step 1: spherical cement grains are dynamically mixed by a force-based DEM system (HADES) to reach the required packing density (that is, *w/c*);

- Step 2: the dense structure after packing simulation is used as an input for hydration simulation by XIPKM (Extended Integrated Particle Kinetics Model). The cement particles are given chemical compositions and react with water to obtain matured cement paste;
- Step 3: DRaMuTS (Double Random Multiple-Tree Structuring) and SVM (Star Volume Method) are used to assess topological and geometric pore characteristics of the hydrated cement paste; this information is stored for permeability estimation;
- Step 4: an "empty" algorithm is developed to model the microstructure of the hydrated paste at various water saturation degrees for the partially saturated samples.
- Step 5: the tube network is constructed for permeability calculation on the basis of the pore information resulting from Step 3 while shape information is additionally obtained by FEM (Finite Element Method) and also used as input for permeability estimation.

More information about each stage will be given below in this section. Interested readers can also find all relevant details in (Li *et al.*, 2015; Stroeven *et al.*, 2015).

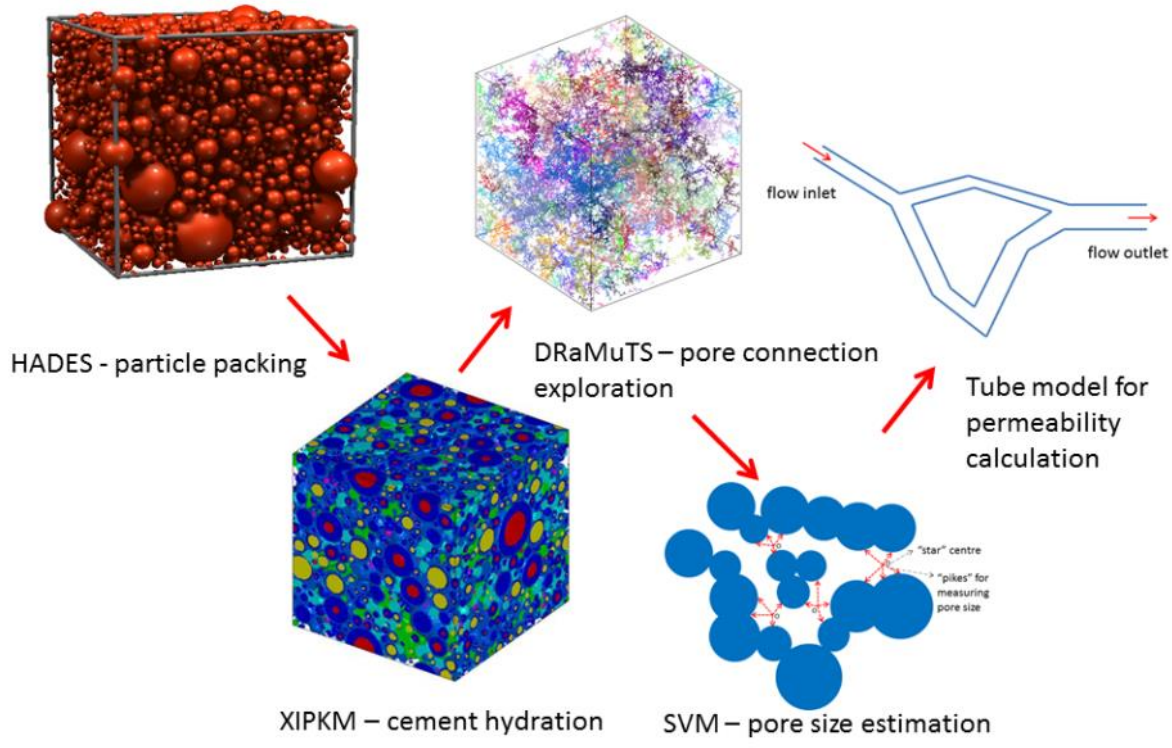

Figure 3.1 A schematic diagram of HADES-XIPKM-DRaMuTS-SVM-Tube model framework.

3.2.1 Packing of cement grains

In this step, cement grains are modelled as spheres that are dynamically mixed and compressed in a cuboidal container. The so obtained the densified structure can be used as input for the next step, namely the hydration simulation. During the mixing step, Newtonian laws govern the dynamics of the particles inside the container. The container can be gradually reduced in size so that an arbitary *w/c* can be obtained at the targeted cube size of 100 µm. The size of 100 µm is selected because this is a commonly chosen size for virtual cement paste. The Rosin Rammler function was chosen to represent the particle size distribution, ranging from 1 to 30 µm. Note that the parameters for the Rosin Rammler distribution are kept the same in this paper, while only the range of particle sizes will change in the presented parameter study. Six periodic boundaries were used to properly represent bulk paste. The DEM system HADES is used for the generation of the packed particles system, because parameters determining the fluid transport are basically structure-sensitive, which include pore size, connectivity and tortuosity. A DEM approach seems to be more appropriate than static random addition methods. Additional details on the particle packing stage of the fresh binder paste can be found in (Stroeven, 1999; He, 2010).

3.2.2 Cement hydration simulation

The densified structure obtained from the particle packing simulation serves as input for modelling the hydration process. The cement particles are given chemical compositions of Portland cement, *i.e.*, tricalcium silicate (C_3S), dicalcium silicate (C_2S), tricalcium aluminate (C_3A) and tetracalcium aluminoferrite (C_4AF). The ratios of each compound in the clinker were 60%, 20%, 7.8%, 12.2% by weight. The state of fresh (unhydrated) cement particles is set as the starting point of hydration simulation. As the reaction between cement grain and water starts and continues, calcium silicate hydrate (C-S-H) and calcium hydroxide (CH) are formed. C-S-H is treated as a substance that partly compensates for the consumed cement grains and the rest evenly covers the free surface of hydrating spherical particles (leading to an expansion of the original particle), while CH nucleates and grows in the open pore space, resulting in a diminishing pore space. XIPKM (Extended Integrated Particle Kinetics Model) was utilized in this study for hydration simulation, and the interested reader is referred to (Le *et al.*, 2013) for more information. In XIPKM, the hydration proceeds in hours and ultimately stops when there does not exist available water or cement for further hydration in the structure. The hydrated pastes at different curing age can therefore be selected for permeability estimation. The validation of XIPKM is also included in (Le *et al.*, 2013). Although C-S-H has been proven porous and weakly-permeable (Feldman and Sereda, 1970; Jennings, 2000; Jennings, 2008; Ma and Li, 2013; Muller *et al.*, 2013; Ma *et al.*, 2014b), its contribution is only of importance for the total permeability at very low capillary saturation (Zalzale *et al.*, 2013) when the much larger pores are “emptied”. Within the scope of this work, the C-S-H is considered impermeable and its contribution to fluid transport is ignored.

3.2.3 Porosimetry operation

It is the pore structure of hydrated paste that determines the fluid flow through the material since the solid phase is generally considered as an impermeable medium. Hence, it is necessary to delineate the pore network structure in the produced virtual matured. A robotics-inspired DRaMuTS method was used for that purpose. In this method, points are randomly distributed into pore space and connected by straight lines to find paths through the specimen. Only the connecting lines without intersections with the solid phase are considered as the effective connections, which look like growing trees. In this way, the complete pore network can be delineated by such trees thereby defining pore topology in the pore network system. De-percolated pores and continuous channels can be easily distinguished in this way. Relevant details can be found in (Stroeven *et al.*, 2010; Stroeven *et al.*, 2012). For the assessment of local pore volume, a SVM method popular in life sciences is applied (Stroeven *et al.*, 2010). Basically, a large number of random pikes from the previously distributed points are shot until they reach the surfaces of particles. The lengths of such rays are measured and averaged per point. The mean value is taken as the representative size of that pore, and then its local volume can be easily estimated. We used 10^5 points to produce reliable outputs with reasonable computational efforts since this amount of points is proven to be sufficient for porosimetry operation in (Li *et al.*, 2016a). Due to the well-known limitations in MIP (Mercury Intrusion Porosimetry) tests, the outcomes of our numerical porosimetry operation were verified with the results from image analysis, as discussed in (Le, 2015).

3.2.4 Structures at various water saturation degrees

As mentioned earlier, a 100 percent saturated specimen is seldom the case in practice since this fully saturated state is difficult to establish and maintain. The major influence of the water saturation degree on the permeability of cement paste has been reviewed in (Zhang and Zhang, 2014). The permeability is found to be a function of water saturation degree. To model the structure of cement pastes at various degrees of water saturation, Zalzale *et al.* (2013) used a 3D lattice Boltzmann method to gradually change the pore voxels into solid voxels as water saturation degree decreases. Larger pores will dry out earlier than smaller ones in accordance with the Kelvin-Laplace equation. A gas-filled pore acts as a barrier for the water transport in an identical way as the solid phase does. This phenomenon is mimicked in our simulation by positioning solid objects in the dried-out pores, as illustrated in Figure 3.2. This procedure, denoted as "empty" algorithm, can easily be implemented since DRaMuTS locates and characterizes individual pores. The "empty" algorithm starts simply from the largest pores. Once positions of pores are determined, water can be removed by positioning solid spheres at the calculated centres of the largest pores to block the transport path for water, representing the partially saturated state. In the case of air penetration, the reverse occurs since gas transport only occurs in percolated air-filled pores. Pores filled by water are considered impermeable to gas. The penetrative phenomenon of air in a water environment is usually too small to be taken into account. The capillary pressure causes the smallest pores first to absorb

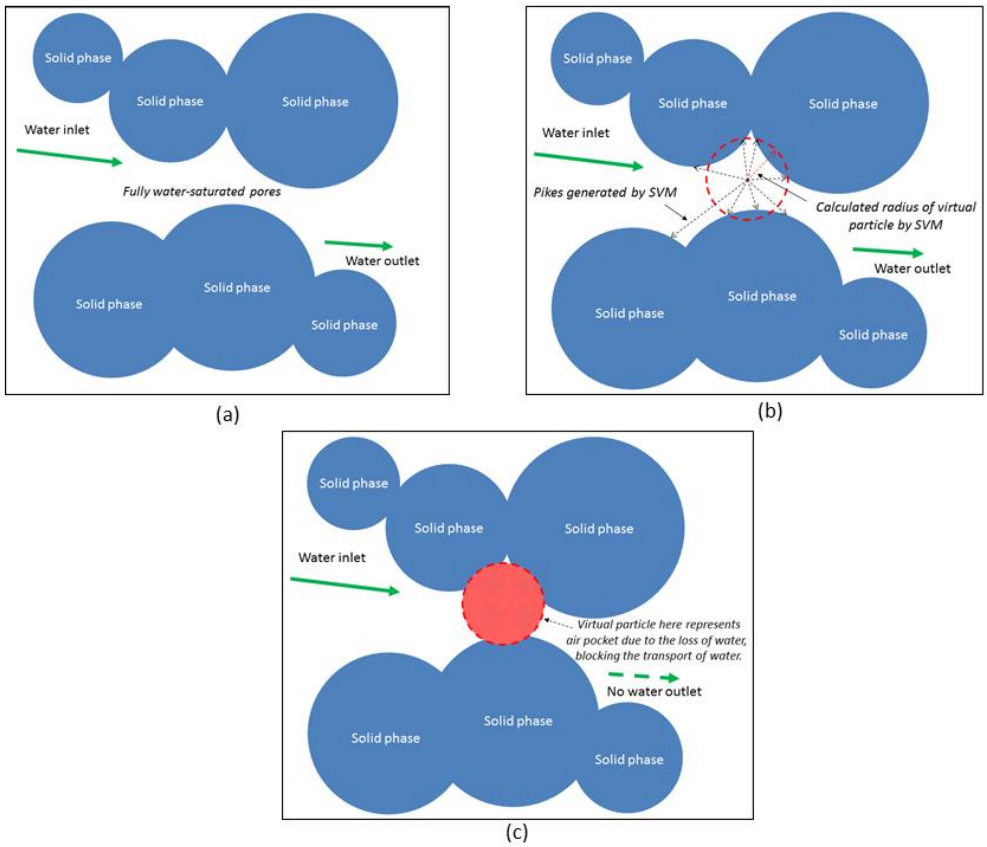

Figure 3.2 Illustration of the "empty" algorithm in 2D; (a) fully saturated state; (b) positioning of a solid circle in water-filled pore; (c) partially saturated sate. The position and size of the virtual red circle (in 3D: solid sphere) is obtained by DRaMuTS.

water thereby blocking the gas transport. Hence, these small pores become impermeable to air while the large ones remain open for the transport of gas. In case the air permeability was measured as a function of water saturation degree, we started with a completely empty pore-space and blocked the pores one by one starting from the smallest pores. To ensure the efficiency of the developed numerical models, pores are assumed to be either completely filled by water or to be completely filled by gas in this work. The influence on the permeability of cementitious materials of a water film existing in reality on the surface of solid phase is not considered herein.

3.2.5 Tube network model for permeability calculation

To model the fluid flow through the material, a network structure consisting of cylindrical tubes was designed to represent the transport channels. The tube network was constructed by using the pore connectivity information from DRaMuTS (tube length) and the pore size information from the SVM method (tube size). The main trunks represent the direct pore paths through the specimen from its bottom to the top surface. In contrast to isolated paths and dead-end branches, the main trunks are assumed to play a key role in the transport process.

They can be extracted from the system and used for permeability calculations, while the other pores are neglected. For detailed information, see (Le, 2015). The flow inside a tube is assumed to be slow, saturated, incompressible and laminar. By applying a pressure gradient between inlet and outlet nodes located at the bottom and top surfaces of the specimen and solving the flow equations in the entire system on interconnected tube elements, the intrinsic permeability κ , in m^2, can be calculated by Darcy's equation.

$$\kappa = \frac{L}{A}\frac{Q\,\mu}{\Delta P} \tag{3.1}$$

where L (m) and A (m^2) are the length and cross sectional area of a test sample. An external pressure gradient ΔP (Pa) is applied to ensure a fluid flow Q (m^3/s) go through the sample. μ (Pa·s) is the dynamic viscosity of the fluid. The influence of the actual shape of the pores on conductivity can be explicitly taken into account, as described in (Le, 2015). Note that using Darcy's law for permeability calculation may be problematic at nanoscale since liquid water viscosity in nanoscale pores increases notably and Knudsen diffusion dominates the permeation (Pivonka *et al.*, 2004). However, the influence of nanoscale pores on the permeability of cement paste is shown to be only significant at low water saturation degree (Zalzale *et al.*, 2013). As a result, this work only focuses on the structure of cement paste at microscale and the nanoscale pores mainly existing in C-S-H are not taken into account. Hence, Eq. (1) is still valid for permeability calculation in this work.

To avoid systematic computational biases, multiple repeats of the algorithm were run with 8 different randomly generated microstructures at a certain water saturation degree with the same *w/c* ratio, hydration time and cement particle size range. The simulated water

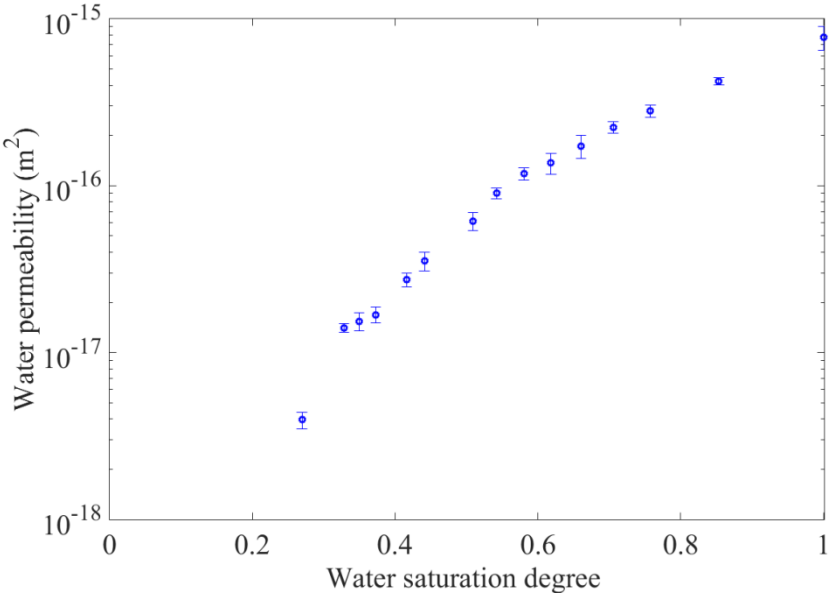

Figure 3.3 Water permeability data pertaining to virtual cement pastes with standard deviation error bars (*w/c*=0.4, hydration age: 28 days, PSR: 1-30 µm).

permeability data from our models with standard deviation error bars are displayed in Figure 3.3. The minimal spread in the results gives us confidence that the result of a single experiment is reasonably accurate.

3.3 Results

3.3.1 General

In the past decade, many experimental studies have been performed to investigate the influence of the degree of water saturation on the permeability of cement-based materials. The tested samples were usually underwater-cured and then dried to different saturation degrees. Subsequently, the specimens were subjected to flow of an agent (water or gas), whereupon permeability was calculated by Darcy's equation (Eq. (3.1)).

The simulation technique presented in Section 3.2 is an attractive alternative to study the relationship between water saturation degree and permeability. It follows basically the same steps as in the above-mentioned experimental approaches. In both cases, the relative water permeability is defined as the water permeability at given saturation degree relative to the permeability measured at the fully saturated state. This is a key indicator to evaluate the ingress of water into unsaturated cement-based materials. Although available experimentally measured permeability of cement paste is extremely limited and show a large scatter, the work done by Zamani *et al.* (2014) provides us a chance to make a direct comparison with the simulated permeability (Zalzale *et al.*, 2013; Li *et al.*, 2016a). The outcomes are shown in Fig. 3.4. Note that the relative permeability is used here since cement pastes in experiments and

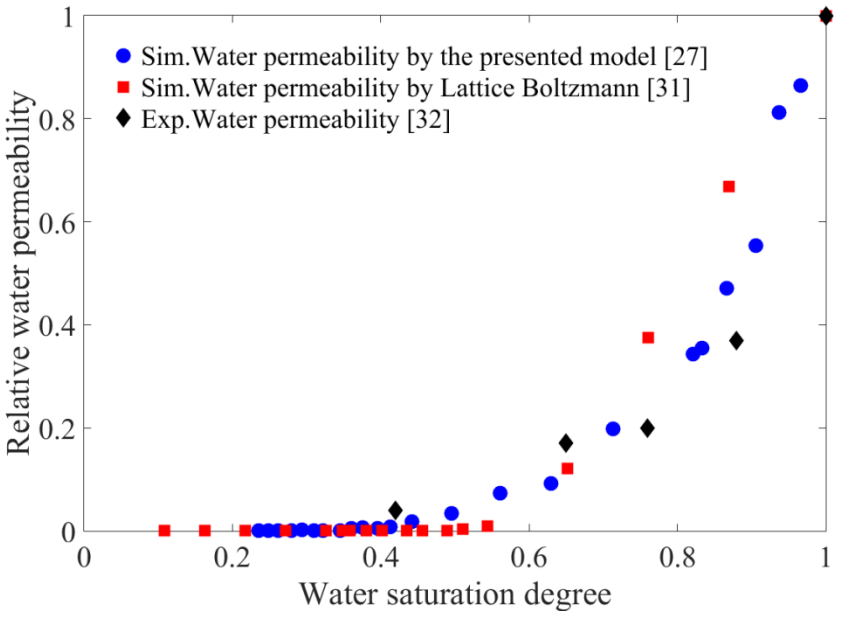

Figure 3.4 Influence of saturation degree on relative water permeability in cement pastes.

simulations are not exactly the same (*i.e.*, *w/c* and porosity). Comparison on the basis of the relative water permeability seems more reasonable. The relative water permeability versus saturation degree in these data sets reveal similar patterns, indicating that the relative permeability strongly depends on the saturation degree. In unsaturated porous cement-based materials under equilibrium conditions of moisture, water prefers to occupy smaller micro pores due to the capillary pressure, while the larger voids are filled by gas. With a decline in the water saturation level, water will gradually move out of these capillary pores, reducing the number of transport paths for water penetration. Hence, the decline in water permeability. Finally, at a water saturation degree of about 30%, the water-filled pores approach a fully de-percolated state, so that only a few transport paths are left for water transport. However, the simulation results do not coincide exactly with the experimental data in Fig. 4. This can be attributed to the fact that the assessment of water saturation degrees of 0 and 100% in experiments may be considered with care since a completely saturated state for cementitious materials is always problematic. This inevitably results in the biased experimentally measured relative permeability. Moreover, nanoscale pores and water film existing in the real cement paste that are not considered in modelling work could be possible reasons for that difference in relative water permeability.

Numerical experiments performed by Li *et al.* (2016c) have demonstrated that both the pore size and pore connectivity play an important role in governing water permeability. In this study, we extend the research by investigating the influence of hydration duration, *w/c* and PSR on the permeability of cement paste. Those three being the main technological parameters that define the concrete structure, significantly affect the microstructures of the mature paste and are likely to affect the water permeability. In fact, this is also to further validate the developed methodology (Li *et al.*, 2016a) in various samples since a general tendency can be anticipated for such parameter study. The existence of aggregates in concrete results in the generation of interfacial transition zones, which facilitate the ingress of water and gas and should be considered as an important factor as well. Hence, we also investigated the effects of ITZs on both water permeability and gas permeability by our methodology.

3.3.2 Effect of hydration age on permeability

As introduced in Section 3.2.2, the continuous hydration process was modelled by XIPKM in hours until the ultimate hydration degree was attained, or until attainment of the different curing ages (*i.e.*, 3 days, 7 days, 28 days and 4 months) for studying the influence of this parameter on water permeability of samples with various degrees of water saturation. Other parameters were kept the same for all samples (*w/c* = 0.4, PSR between 1 and 30 μm). The results are plotted in Figure 3.5. For the different hydration ages, the curves obtained for water saturation versus water permeability seem to be vertically shifted. As expected, the specimen hydrated for 4 months has the smallest permeability in contrast to the other samples. This can easily be explained by the increasing density in hydrate structure at a longer

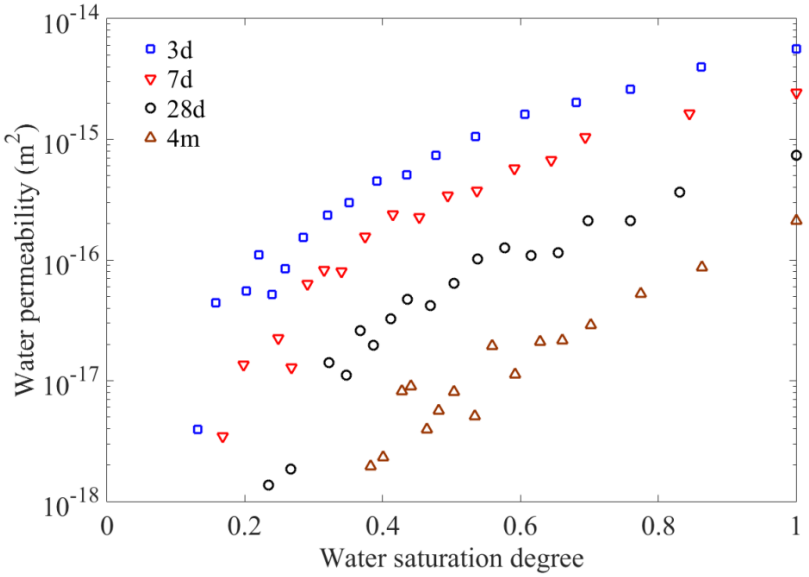

Figure 3.5 Influence of hydration age on water permeability of partially saturated bulk pastes (*w/c*=0.4, PSR: 1-30 μm). Each plot represents simulation data of a single specimen.

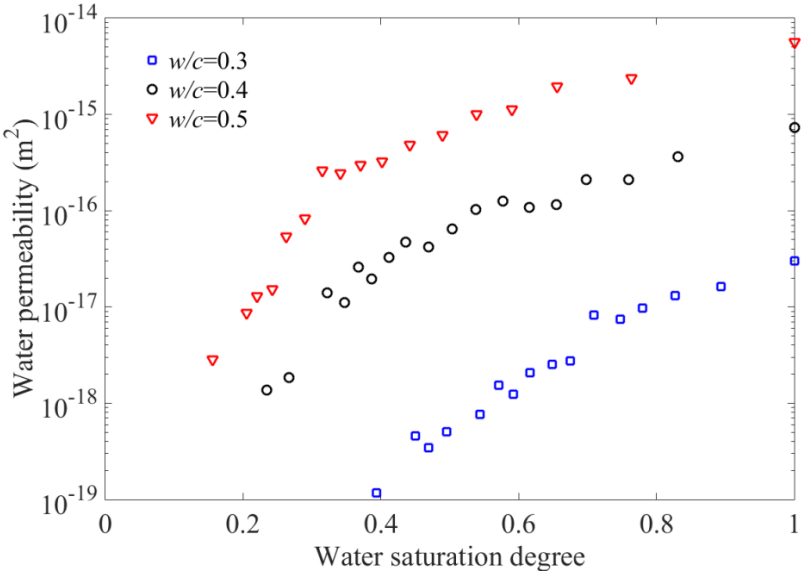

Figure 3.6 Influence of *w/c* on water permeability of partially saturated bulk pastes (hydration age: 28 days, PSR: 1-30 μm). Each plot represents simulation data of a single specimen.

hydration period and, as a result, in reduced pore space. The latter involves both smaller pores and more advanced pore de-percolation, both leading to reduced permeability.

3.3.3 Effect of w/c on permeability

It is generally considered that *w/c* is an important design parameter influencing the microstructure and thus the permeability of the material. Unfortunately, sufficient evidence is

lacking as to the relationship between *w/c* and water permeability of an incompletely saturated specimen. In this section, specimens with *w/c* = 0.3, 0.4 and 0.5, respectively, at 28 days of hydration, and with PSR between 1 and 30 µm were selected for the permeability analysis. The results are illustrated in Figure 3.6. For the different water to cement ratios, the curves obtained for water saturation versus water permeability seem to be vertically shifted. An increasing *w/c* actually means that the volume of the cement in the container space is declining. Hence, a lower packing density (that is, a higher porosity) is the inevitable result, resulting in a lower degree of pore de-percolation. Therefore, permeability is increased. This agrees well with the general acknowledged influence of *w/c* on the transport-based properties of cementitious materials.

3.3.4 Effect of PSR on permeability

PSR is also an important technological parameter in designing cement-based materials. In this paper, three different PSRs were chosen for samples with otherwise similar parameters (*w/c* = 0.4, hydration age = 28 days). The minimum particle size in these PSRs is maintained at 1 µm, only the maximum size is increased from 20 µm via 30 µm to 45 µm, denoted as PSR20, PSR30 and PSR45, respectively. Since *w/c* is a constant, the packed volume of cement grains in these three systems is the same. However, with a wider particle range, the number of particles is declining. This also involves the fraction of smaller particles of which the hydration rate is relatively high. Hence, the degree of hydration at the same hydration period of 28 days is the highest in PSR20 (70%), followed by PSR30 (64.2%) and PSR45 (60%). This leads to structures with different porosity of the three samples, PSR20 leads to the lowest porosity, causing the water permeability curve to fall beneath that of PSR30 and PSR45, as shown in Figure 3.7.

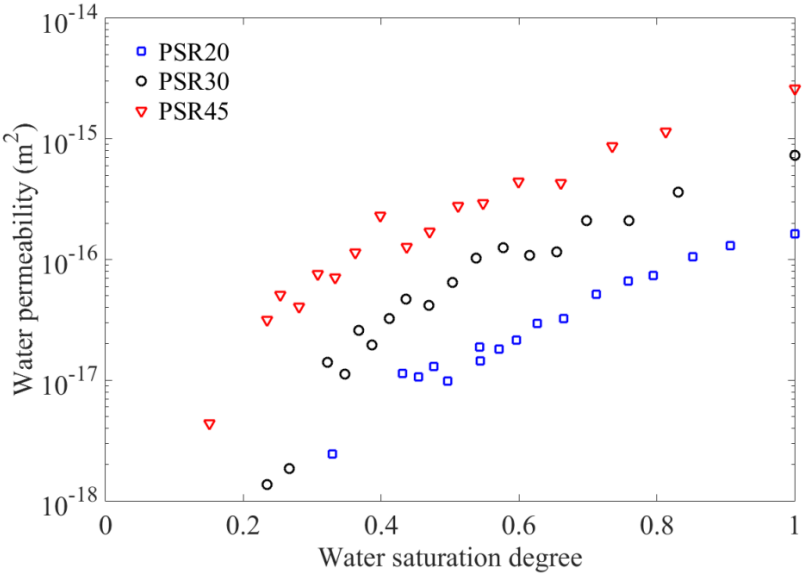

Figure 3.7 Influence of PSR on water permeability of partially saturated bulk pastes (*w/c*=0.4, hydration age: 28 days). Each plot represents simulation data of a single specimen.

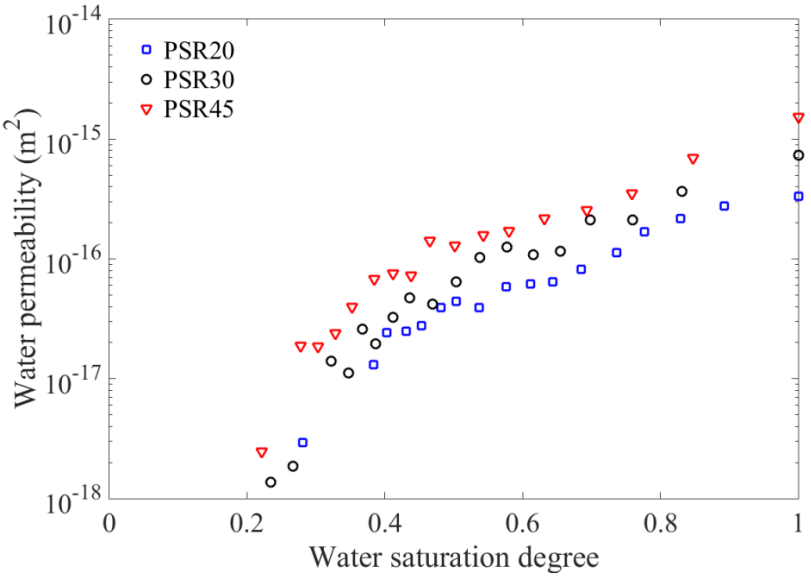

Figure 3.8 Water permeability of partially saturated bulk pastes with different PSR at the same degree of hydration (64.2%). Each plot represents simulation data of a single specimen.

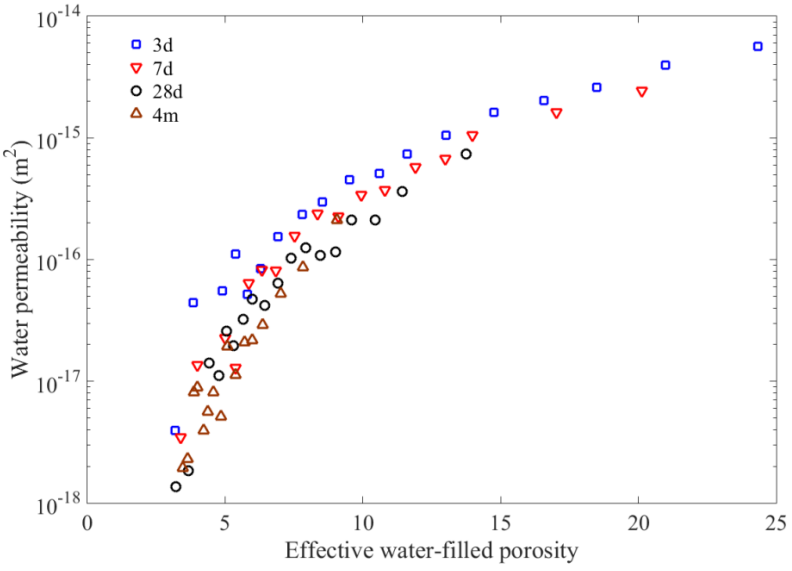

Figure 3.9 Water permeability versus water-filled porosity of cement pastes at different hydration age (the same data as presented in Figure 3.5).

To validate the hypothesis of hydration rate outlined above, the microstructures with different PSR but at the same degree of hydration (64.2%) were selected for permeability analysis. The results are plotted in Figure 3.8. Obviously, the differences between different curves in Figure 3.7 are less pronounced. A slight difference in the estimated water permeability of the different samples can be still observed in Figure 3.8. This is because the distribution of particles in these three cases is not the same which leads to different structures of matured cement paste.

The different but parallel curves shown in Figs. 3.5-3.7 are interesting since there seems to exist a relationship between permeability and pore characteristic of the specimens. This relation can be obtained by plotting the results shown in Figs. 3.5-3.7 in a different way, as illustrated as follows. According to the definition of water saturation degree, it can be obtained by dividing water-filled porosity at a specific saturation degree to that at fully saturated state. Since the porosity of a fully saturated specimen can be easily assessed by DRaMuTS, the water saturation degree can be directly transferred into water-filled porosity. Take the results shown in Fig. 3.5 for example, the same data can be plotted in another way (water permeability versus effective water-filled porosity), as illustrated in Fig. 3.9. It is found that water permeability can be directly correlated to water-filled porosity and is independent of the specimens' states (*i.e.*, hydration age), which is in accordance with recent findings (Zhang, 2017). A similar relationship can also be observed for the samples with different *w/c* and PSR, please refer to (Li *et al.*, 2016c) for more details.

Note that the presented permeability values of partially saturated cement pastes in this paper agree well with the data from other numerical work (Zalzale *et al.*, 2013; Zhang, 2017). However, the simulated permeability (in absolute value) in general exceeds the experimental data by 2-3 orders of magnitude. Reasons for this difference could be: (1) The "real' saturation degree of specimens in experiments could be lower than the expected value; (2) In contrast to virtual cement paste, supplementary water provided in water permeability measurements in reality may result in further hydration of the specimen and thereby lowers the porosity and permeability.

3.3.5 Effect of the ITZ on permeability

Since the ITZ constitutes probably the major difference between cement paste and concrete, it may be of interest to investigate the role of the ITZ in the global permeability. The effects of the ITZ on both water and gas permeability of unsaturated specimen are studied in the next sections. Note that drying-induced microcracks may initiate at the ITZ and coalesce, which has a significant effect on the experimentally measured permeability (Lee *et al.*, 2016; Liu *et al.*, 2016; Fahy *et al.*, 2017; Plague *et al.*, 2017). Moreover, the aggregate dilution and pore tortuosity effects in real concrete may also affect the transport. However, the influence of these factors on permeability are not taken into account in this numerical work. The origin of the ITZ lies in the so called "wall" effect of packing of cement grains against the relatively flat aggregate surface (Scrivener *et al.*, 2004). Since aggregate particles are generally much larger than cement grains, their surfaces can be actually considered as flat planes. The involved aggregate surfaces cause structural modifications due to imposed particle packing differences in the interface zone and in the bulk of the cementitious material. The ITZ region in general contains higher porosity and smaller cement grains. To simulate the rigid surfaces of the much larger aggregate grains in concrete, the periodic boundaries in X direction were replaced with rigid ones while remaining periodicity in other directions. This renders possible modelling the structural gradient between the rigid surfaces involving the ITZs and the bulk

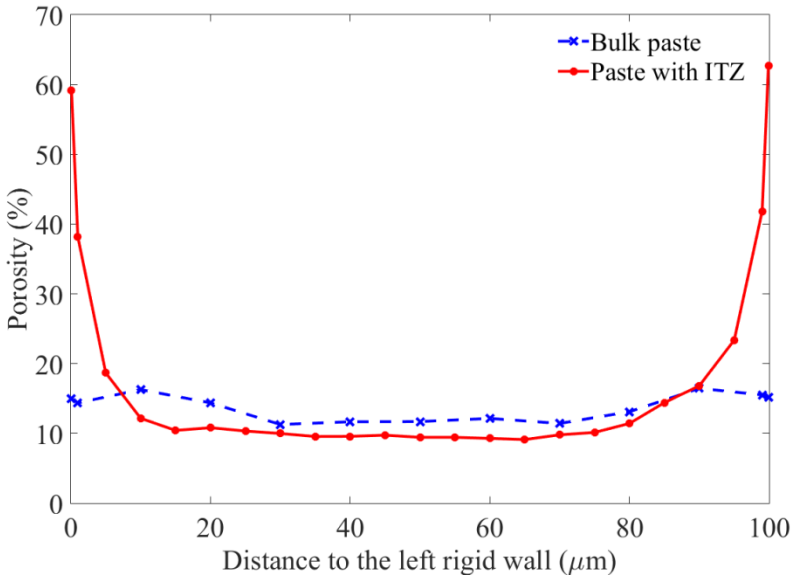

Figure 3.10 Porosity gradients over the full section of a specimen made in a container with six periodic boundaries (modelling bulk paste) and in a container having instead two rigid walls (modelling bulk paste and ITZ). In both cases, *w/c* = 0.4, hydration age: 28 days, PSR between 1 and 30 µm.

phase. It is assumed that the rigid boundaries are sufficiently far apart so that they do not mutually interfere with each other. Please see (Hu *et al.*, 2006; Chen *et al.*, 2011) for information on the aggregate surface spacing distribution. The technological parameters are set the same for pure paste and sample containing ITZ (*w/c* = 0.4, hydration age: 28 days, PSR between 1 and 30 µm). The porosity gradients of fully saturated specimens with or without ITZs are plotted in Figure 3.10. The structural gradient can be found in the sample with ITZ, while the porosity of pure paste evenly distributes through the whole range. Looser packing indeed happens in the ITZ and also the local particle size distribution differs from that in bulk phase (Stroeven, 1999). Both higher porosity and different particle size distribution of the ITZ affect the hydration process and ultimately the porosity and permeability of the specimens.

3.3.5.1 Effect of the ITZ on water permeability

Figure 3.11 shows the influence of the ITZ on water permeability of partially saturated cement paste (*w/c* = 0.4, PSR: 1-30 µm) after 28 days hydration. Obviously, the specimen with ITZs has a higher water permeability than pure (bulk) paste at different water saturation degrees. Of course, the existence of an ITZ with higher porosity and larger pores will promote the ingress of water and will lead to higher permeability. However, the difference in permeability of the samples is declining at lower saturation degrees. Especially, when the saturation degree is below 40 percent, the calculated water permeability of pure paste is close to that of the sample with ITZs. Hence, the ITZ effect on the permeability seems to diminish

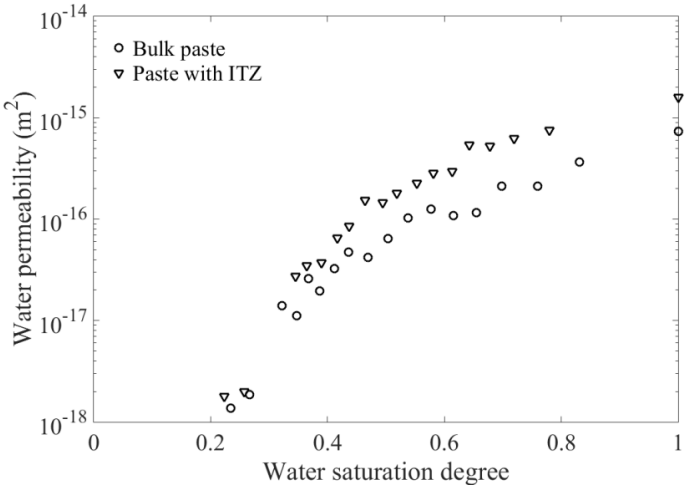

Figure 3.11 Influence of ITZ on water permeability of cement pastes (*w/c*=0.4, hydration age: 28 days, PSR:1-30 µm).

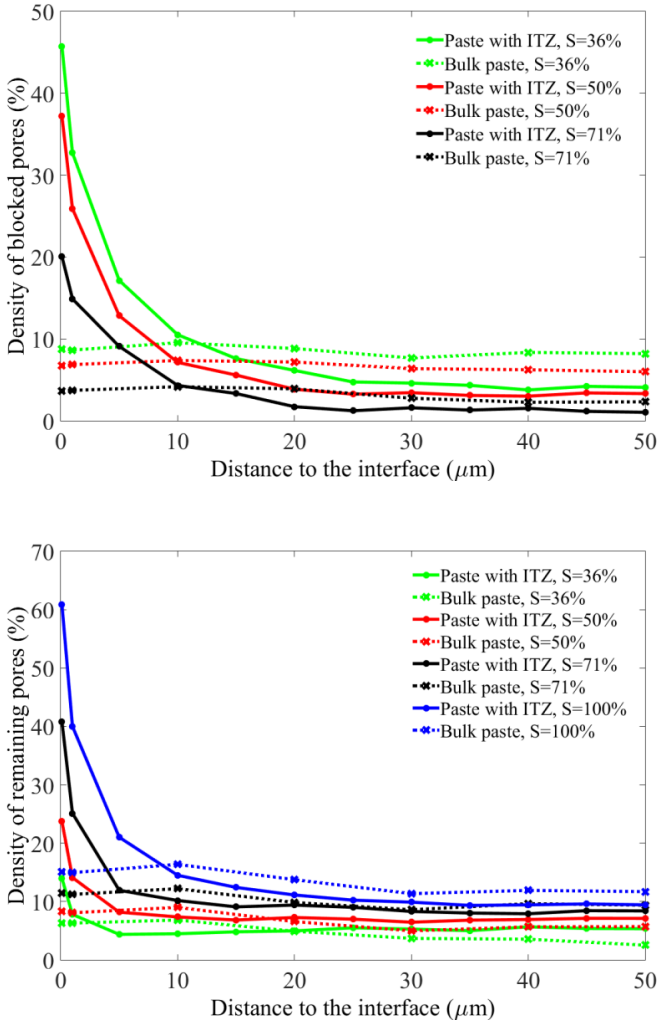

Figure 3.12 Porosity over the width of the specimens used in water permeability study (*w/c*=0.4, hydration age: 28 days, PSR:1-30 µm); (top) blocked pores; (bottom) remaining pores.

at lower saturation degrees. The underlying mechanism will be discussed in what follows. The specimens at different degrees of water saturation were then serially sliced perpendicular to the X axis to study the density distribution of the blocked and of the remaining pores. Results are presented in Figure 3.12. It is clear that pores existing in the ITZ zones are predominantly blocked. When the saturation degree is equal to 36 percent, the density of remaining pores in the sample containing ITZs is close to that in the bulk paste, leading to similar permeability data.

3.3.5.2 Effect of the ITZ on gas permeability

Similar to the water permeability study, pores are gradually blocked in the case of gas penetration, to model the microstructures at various saturation degrees. However, the simulation here starts from fully air-filled pores indicating the (water) saturation degree to be zero. As the saturation degree goes up, water will enter into the structure and occupy the small pores first due to the capillary pressure. These water-filled pores will be considered as impermeable to gas, since the permeability of air in water is too small to take into account. The large ones are air-filled and still contribute to the gas transport. This is the reason why an inverse tendency between gas permeability and saturation degree can be observed in Figure 3.13. With the increase of the saturation degree, more pores are filled by water and are thus considered not contributing anymore to gas transport. Thus, a decline in gas permeability with an increasing saturation degree can be found in Figure 3.13.

As already discussed in Section 3.3.5.1, the sample containing ITZs should have larger permeability than that without ITZs. This also holds for gas permeability. In addition, the two curves in Fig. 3.13 both significantly decrease at higher saturation degrees, indicating that the specimens become de-percolated (bulk paste first followed by the paste with ITZ). However, in contrast to water permeability where the values in the ITZ and bulk converge at low saturation degree, the values of the gas permeability in the ITZ and cement matrix do not seem to converge at high saturation degree. The reasons for this phenomenon will be discussed next.

Figure 3.14 shows that the porosity in the zone close to the interface is still larger than in the bulk zone when the saturation degree reaches 60 percent. So, high porosity ITZs play an important role in determining gas permeability. This gives a reasonable explanation why larger gas permeability at higher water saturation degree can still be found in the sample with ITZs.

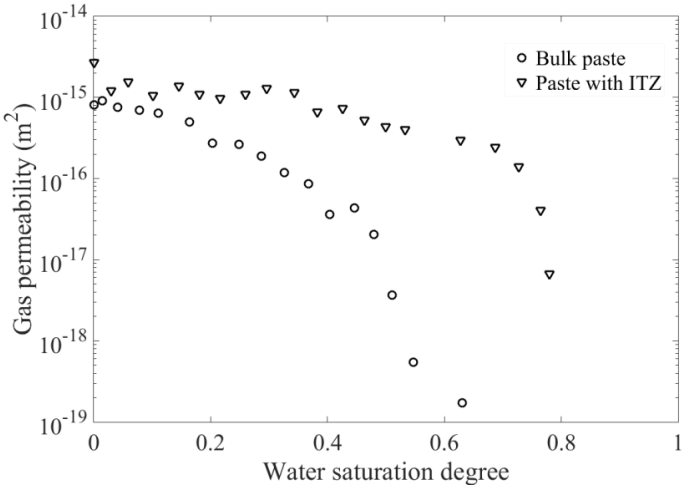

Figure 3.13 Influence of ITZs on gas permeability of cement pastes (*w/c*=0.4, hydration age: 28 days, PSR:1-30 μm).

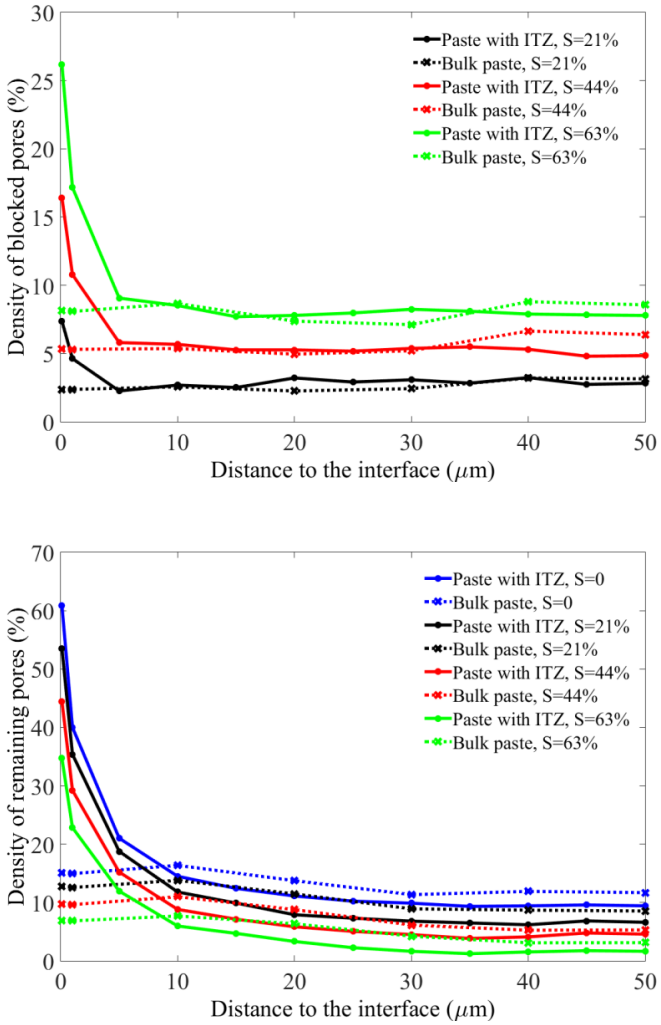

Figure 3.14 Porosity over the width of the specimens used in gas permeability study (*w/c*=0.4, hydration age: 28 days, PSR:1-30 μm); (top) blocked pores; (bottom) remaining pores.

3.4 Discussion and Conclusions

An effective numerical tool for permeability estimation of partially saturated cementitious materials has been developed and presented in an earlier publication of the present authors (Li *et al.*, 2016a). Here, a systematic study by our methodology is presented on the influence of technological parameters on permeability of partially saturated paste. This parameter study is of interests for practical implementation and to better understand the possible underlying structural phenomena. Further, it offers a far more economic approach as compared to experiments. Moreover, the ITZ study performed herein cannot easily be accomplished experimentally. Note that the following phenomena (except for the ITZ) may also affect the transport properties in real concrete, *i.e.*, drying-induced microcracking, aggregate dilution effect and pore tortuosity effect, which are not taken into account in this work. The presented methodology is DEM-based, so it can be expected to provide more reliable data than obtained by conventional RSA methods.

Permeability of partially saturated cement paste was determined by the computational methodology (particle packing - hydration simulation - porosimetry operation – blocking algorithm – tube network model for permeability estimation). The obtained results are compared to other published data of similar cement pastes and a satisfactory agreement is found. The effects of technological parameters (*i.e.*, hydration time, *w/c*, particle size range) on permeability of cement paste observed in this study follow the expected trend, which supports the application of our methodology in practice. The role of the ITZ in determining permeability of a partially saturated specimen depends on the penetrating agent, since distinct agents (water or gas) result in different results. This is attributed to the fact that the effective pores in the ITZ region for water ingress in fact prevent the gas transport as water saturation degree varies. This work can provide a deeper insight into the effects of the ITZ on the transport through cementitious engineering materials.

Chapter 4 Estimating permeability of cement paste using pore characteristics obtained from DEM-based modelling

This chapter is based on Kai Li et al. (2016c), a paper published in Construction and Building Materials 126: 740-746.

Although an earlier developed numerical methodology for permeability estimation of cement pastes can provide satisfactory results in comparison with experiments, it would be of engineering interest to find a simpler way to perform the same task. This method referred to by "the shorter approach" is presented in this chapter. In the approach, water permeability is only correlated to the water-filled porosity of the specimen. A mathematical model is proposed to approximately calculate the water permeability using the water-filled porosity as the only input parameter. The confidence limit is found to yield an appropriate level of reliability. To better understand the proposed mathematical relationship, pore throat size and connectivity of the capillary pores are separately shown as a function of the water-filled porosity. Their respective and successive impacts on permeability are illustrated in this way.

4.1 Introduction

Concrete's permeability that underlies its transport-based durability properties is predominantly governed by the hardened paste since aggregates can usually be assumed impermeable. Hence, the pore microstructure in the hardened binder is the material studied here. Relationships between permeability and the pore characteristics of concrete have been demonstrated based on experimental results on fully and partially saturated specimens by (Ye, 2005; Lafhaj *et al.*, 2006; Gao and Hu, 2013; Zamani *et al.*, 2014). Over the past decades, several empirical formulas (EI-Dieb and Hooton, 1994; Zamani *et al.*, 2014) have been proposed to predict the permeability of cementitious materials based on material parameters like porosity, pore throat size and capillary pressure. The parameters in these empirical models can be obtained by experimental measurements. Unfortunately, physical experiments are typically time-consuming, laborious, tedious and thus expensive. As an alternative, a series of computer simulation approaches have become popular in concrete technology (Breugel, 1995a, b; Garboczi and Bentz, 2001; Bishnoi and Scrivener, 2009; Le and Stroeven,

2012; Li *et al.*, 2016a). These models are developed for simulating cement hydration and the evolution of microstructure of cementitious materials. In general, random sequential addition (RSA) algorithms for distributing cement grains are implemented in these modelling techniques. Recently, more realistic dynamic discrete element method (DEM) has been developed and used (Le and Stroeven, 2012). The contacts between cement particles are simulated in the DEM systems, which can be considered as an advantage over the RSA systems.

These studies found correlations between permeability and pore characteristics of, in most cases, fully saturated cementitious material. Generally speaking, median pore throat size seemed to be a critical parameter in determining permeability (Yazdchi *et al.*, 2011; Gueven, *et al.*, 2017). Unfortunately, the influence of connectivity of the capillary pores on permeability was not explicitly considered in the earlier mentioned studies, whereas its contribution cannot be ignored especially when the effective porosity for transport is low (Ye, 2005; Li *et al.*, 2016a). The effective porosity herein is defined as the porosity available for fluid transport. Ye (2005) reports in that the water permeability of cement pastes appears to depend on the pore size distribution and connectivity of the capillary pores regardless of water/cement ratio (*w/c*) and curing age. It has also been proven that the permeability of cement paste and mortar can be determined by scientifically defined pore parameters (Ma, 2014). Using a DEM approach, to be discussed herein, Li *et al.* (2016a) also reported that both median pore size and the pore connectivity of cement pastes can be related to the effective porosity. This seems to indicate that the permeability could be directly represented by the effective porosity instead of porosity in combination with median pore size and pore connectivity.

A dynamic DEM-based modelling approach (the so-called Complete Methodology, CM) has been developed by the author's group to estimate the permeability of cement pastes on the basis of their pore structures (Le and Stroeven, 2012; Li *et al.*, 2015; Stroeven *et al.*, 2015). There are five stages in the CM, namely, particle packing simulation, hydration simulation, pore delineation, pore measuring and tube network modelling. These stages are extensively described in the international literature to which the reader is referred for details (Li *et al.*, 2015; Stroeven *et al.*, 2015). Although the CM was initially developed for fully saturated pastes, it has been recently extended to also handle partially saturated samples more realistically reflecting situations closer to reality. The CM is advanced and robust; a complete solution is obtained in terms of hours. Nonetheless, it is still interesting and meaningful to further limit the efforts in the CM by closely analyzing the results, trying to understand the main mechanisms leading to the permeability of virtual pastes, and simplifying all that into a mathematical formula. When the penetrating fluid is water, the effective pores for transport are water-filled ones (Zalzale *et al.*, 2013; Li *et al.*, 2016a). Hence, the water permeability of cement pastes can be simply related to water-filled porosity. Note that cement paste is selected in this study instead of concrete or mortar since the permeability of the aggregates can usually be neglected compared to that of the cement paste. In addition, the interfacial

transition zone (ITZ) existing in mortar and concrete can be treated as a special cement paste, as shown by Ma and Li (2014). However, this is outside the scope of this work. A mathematical permeability model has been developed for normal cement pastes and is presented here. In contrast to other methods (including the CM), this approach requires less time and effort but can still provide satisfactory results.

The objective of this chapter is thus to present a shortcut method for permeability estimation of cement paste. The data used for developing the shortcut method are obtained from the CM that has been thoroughly outlined in (Li *et al.*, 2015; Stroeven *et al.*, 2015). Therefore, only a brief introduction of the CM will be given in Section 4.2. The mathematical model for permeability assessment will be outlined in Section 4.3. The water permeability of cement pastes is represented by a formula with only one input parameter, *i.e.* water-filled porosity. The confidence limit is found to be 0.91, indicating that the proposed model is able to provide reliable results to a satisfactory degree. Obviously, the process involves a water permeability decline at reduced water-filled porosities. The results calculated by the proposed method are compared with those obtained by different approaches revealing a satisfactory agreement. Finally, the CM model provides the various inter-relationships between the median pore throat size, pore connectivity, water-filled porosity and permeability. This information will serve as support for the chosen mathematical approach. It provides a more structural basis to this global phenomenon.

4.2 The complete methodology (CM)

The CM consists of five stages, as represented in Figure 4.1. Although 3D structures are used in our simulation, a 2D illustration is presented for simplicity reasons. Interested readers can find all relevant details in (Li *et al.*, 2015; Stroeven *et al.*, 2015).

In stage 1, cement grains (the red circles in Figure 4.1) are dynamically mixed in a cube container (100 µm in size) to obtain a certain packing density (that is, the required *w/c*). The *w/c* is set to 0.4, 0.45 and 0.5 in this work which are normal values for ordinary cement paste. The Rosin-Rammler function was chosen to represent the particle size distribution. The minimum particle size was set to 1 µm, while the maximum size increases from 30 µm via 40 µm to 45 µm. Six periodic boundaries were used to properly represent bulk paste. In contrast to the RSA algorithms, a DEM approach is used for simulating particle packing (Stroeven, 1999; Stroeven and Stroeven, 1999; Stroeven *et al.*, 2009). This is because DEM has shown to be more appropriate for studying structure-sensitive parameters that govern fluid transport, *i.e.* pore size and connectivity of the capillary pores, which are important for the evaluation of permeability.

In stage 2, cement hydration is simulated by XIPKM (Extended Integrated Particle Kinetics Model) (Le *et al.*, 2013). The reaction between cement grains and water results in the

formation of calcium silicate hydrate (C-S-H) and calcium hydroxide (CH). Because of the porous nature of C-S-H, the total volume is bigger than that of the reacted cement. Precipitating C-S-H onto the unhydrated cement results in gradually growing grains. Although C-S-H has been proven porous and weakly-permeable (Feldman and Sereda, 1970; Jennings, 2000, 2008; Ma and Li, 2013; Ma *et al.*, 2014a; Ma *et al.*, 2014b; Ma *et al.*, 2014c), its contribution is only of importance for the total permeability at very low water-filled porosity when all the larger pores are empty and become impermeable to water permeation. This is also in accordance with the studies reported by Ma *et al.* (2015). Therefore, the C-S-H permeability is neglected in this study. The four major compounds of the Portland cement, tricalcium silicate (C_3S), dicalcium silicate (C_2S), tricalcium aluminate (C_3A) and tetracalcium aluminoferrite (C_4AF) have been taken into account in the hydration simulation. The ratio of the successive compounds in the clinker were 61%, 20%, 8%, 11% by volume, respectively. Specimens hydrated for 3 days, 7 days and 28 days were selected for permeability and porosity analysis in this study.

In stage 3, the Double Random Multiple Tree Structuring (DRaMuTS) method is used to assess the topology and relevant pore fractions of the produced virtual matured material. Relevant details can be found in (Stroeven *et al.*, 2012). In brief, random points are distributed inside the specimen of which only those located in pore space are used for porosimetry. The number of points is set as 1×10^5 to ensure the accuracy of the results while the calculation time is still reasonable. Porosity is obtained by dividing the number of points in pore space by the total number of points. Then, points are connected to each other by non-obstructive lines in order to find possible paths through the sample. The isolated and branching dead-end paths are ignored since fluid transport only takes place in continuous pore channels.

In stage 4, the star volume method (SVM) is applied to each point to assess the local pore volume that is used for constructing the tube network for modelling flow transport. Local volume is transformed into local size by means of a representative sphere. To gain realism, the smallest pore sections (denoted as pore throats) are chosen in this study to determine the fluid flow through the transport channels. This structural information is obtained by calculating the smallest pore area on a plane over a large number of randomly oriented planes. In stage 5, a network structure consisting of cylindrical tubes is constructed for fluid transport simulation using the locations and sizes of the pore-points. Effect of actual pore shape (in terms of the Mason and Morrow's shape factor) is accounted for by appropriately reducing local conductance; details can be found in (Le, 2015). The water flow traverses the specimen by applying a pressure gradient between inlet and outlet nodes located at the top and bottom surfaces. The flow inside a tube is assumed to be slow, incompressible, laminar and saturated, such that the total permeability over the specimen can be calculated by Darcy's equation (Le, 2015). Note that applying Darcy's law requires the samples to be fully saturated, which is always the case in simulations. Unfortunately, this assumption is not true in practice. The humidity condition inside the specimen varies significantly resulting in pastes with variable water content (Muller *et al.*, 2013). The major influence of water saturation degree on

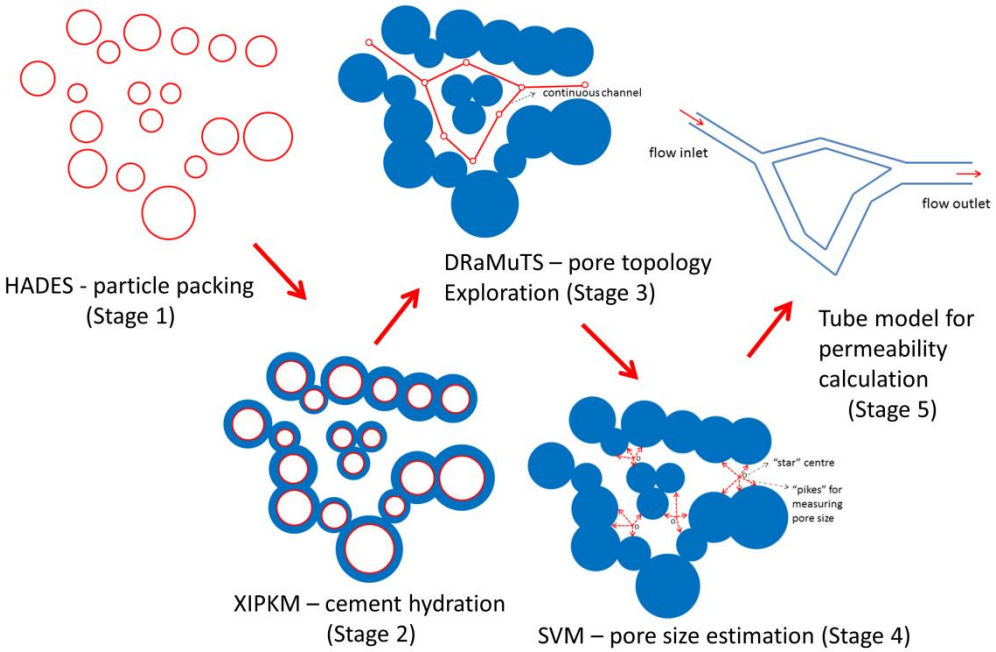

Figure 4.1 2D schematic diagram of the CM for water permeability estimation.

permeability of cement paste has been studied by Zalzale *et al.* (2013), Kameche *et al.* (2014), Zamani *et al.* (2014) and Li *et al.* (2016a). According to the Kelvin-Laplace equation, larger pores are easier to loose water than smaller ones and these empty pores block the paths for water transport. This phenomenon is mimicked by positioning impermeable solid objects in the presumed empty pores. The procedure starts from the largest pores in accordance with the Kelvin-Laplace law. To that end, all pores are sorted by size and stored. Once positions of pores are determined, solid spheres are put at the calculated centres of the largest pores to block the channels for water permeation, representing the partially saturated condition. Details can be found in (Li *et al.*, 2016a). For each stage of the CM, the computation costs around one hour.

4.3 Results

4.3.1 Relationship between permeability and water-filled porosity of cement pastes

In this section, the simulation results on the water permeability and the water-filled porosity of cement pastes with variable water/cement ratio, curing age and particle size range will be discussed and a mathematical model will be proposed for permeability estimation. For each set of experiments, only one technological parameter of the samples is varied and the other two are kept constant. For instance, curing age and particle size range are respectively maintained at 28 days and 1 μm - 30 μm, while the *w/c* is varied from 0.4 via 0.45 to 0.5. The influence of these technological parameters on permeability of partially saturated pastes has

been systematically studied in (Li *et al.*, 2016b). All samples are initially fully saturated, whereupon water evaporation starts from the largest pores. When pores are considered empty, they are replaced by solid spheres, thereby prohibiting any fluid transport. The remaining pore space is still assumed to be fully saturated such that Darcy's equation can still be used for permeability calculation.

The water permeability and the water-filled porosity results of the different cement pastes obtained from our simulations are presented in Figures 4.2-4.4. As a first observation, water permeability declines in all cases with decreasing water-filled porosity. This is because the available pore volume and connected channels for water transport are reduced as the water is gradually removed from the specimen, resulting in a declining permeability. The influence of these two factors on permeability assessment will be discussed later. Moreover, the data shown in Figures 4.2-4.4 (as combined in Figure 4.5) seem to converge to a single curve regardless of water/cement ratio, curing age or particle size range. This seems to indicate that the water permeability is only determined by water-filled porosity and is independent of the material parameters of the specimen. Although a different method is applied, a similar observation is made by Pignat *et al.* (2005) and Zhang *et al.* (2013).

To assess the relationship between water permeability and water-filled porosity of cement pastes, all data shown in Figures 4.2-4.4 are jointly plotted in Figure 4.5. Note that the water permeability in Figure 4.5 is plotted in a logarithmic way versus the water-filled porosity. The

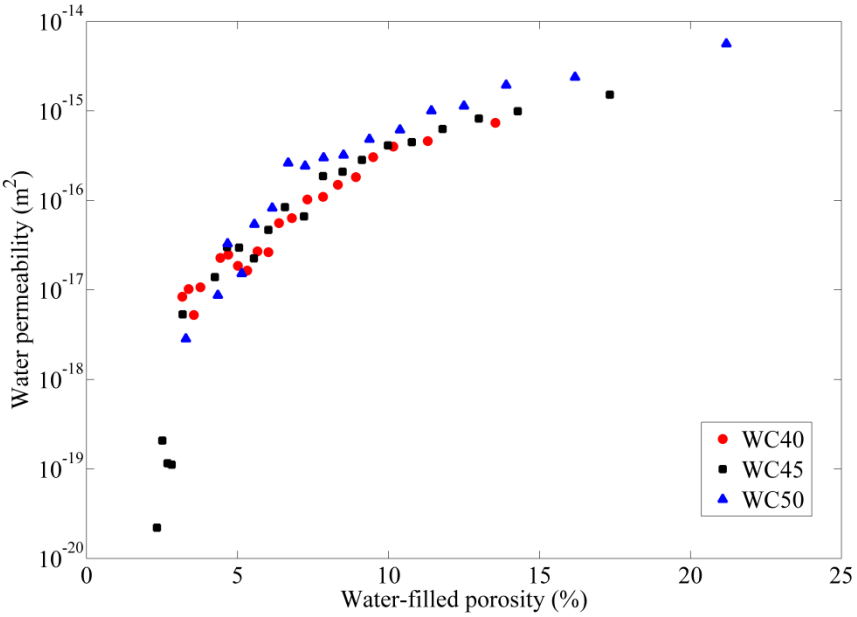

Figure 4.2 Water permeability versus water-filled porosity of cement pastes with variable water/cement ratio. WC40: water/cement ratio = 0.4; WC45: water/cement ratio = 0.45; WC50: water/cement ratio = 0.5. Curing age: 28 days. Particle size range [1 μm, 30 μm].

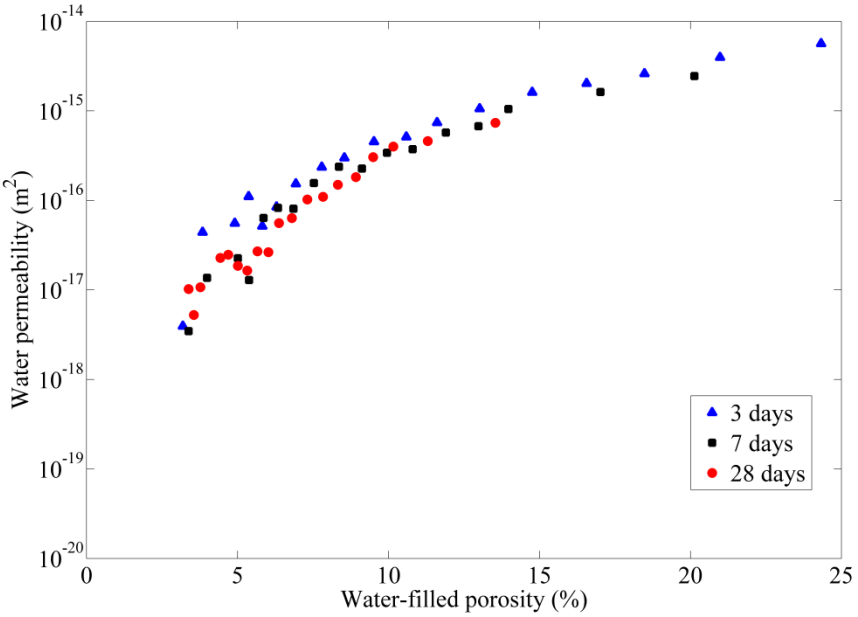

Figure 4.3 Water permeability versus water-filled porosity of cement pastes with variable curing age (3 days, 7 days and 28 days). Water/cement ratio: 0.4. Particle size range [1 μm, 30 μm].

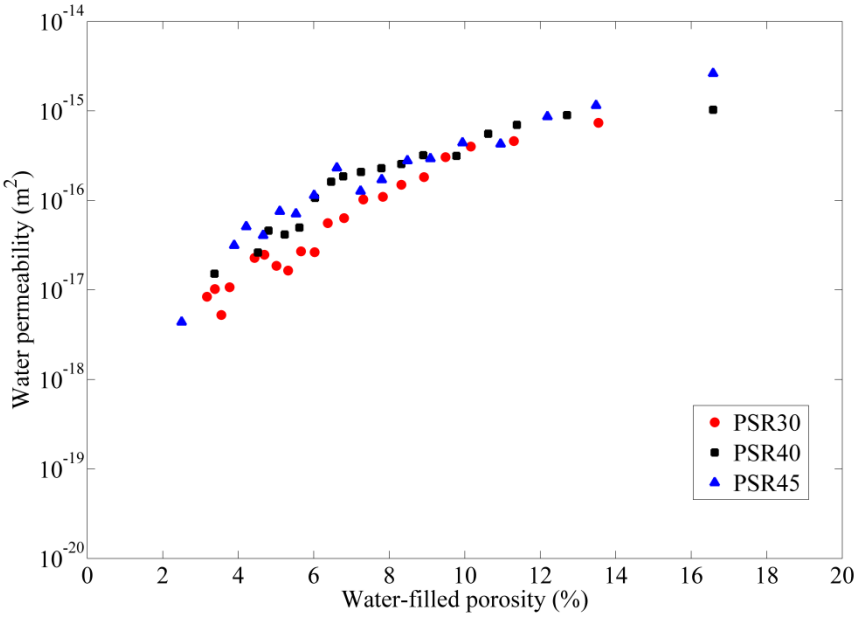

Figure 4.4 Water permeability versus water-filled porosity of cement pastes with variable particle size range. PSR30: particle size range [1 μm, 30μm]; PSR40: particle size range [1 μm, 40 μm]; PSR45: particle size range [1 μm, 45 μm]. Water/cement ratio: 0.4. Curing age: 28 days.

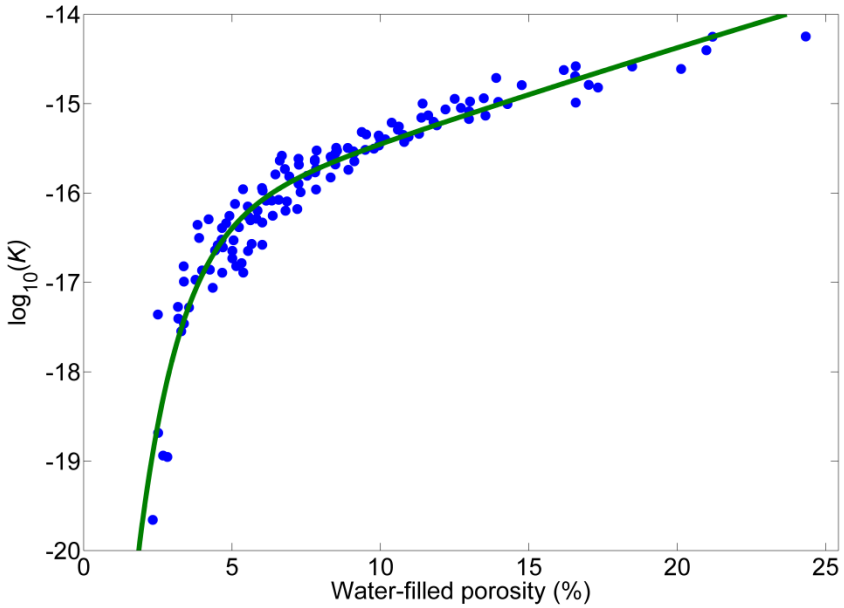

Figure 4.5 Log_{10} (K) versus water-filled porosity P of all samples; K: water permeability. The data obtained from the CM are plotted in blue points, while the green curve represents the results by linear regression.

following equation is thereupon derived from the data using linear regression analysis:

$$\log_{10}(K) = -13.58\exp(-0.71P) - 16.59\exp(-0.007163P) \tag{4.1}$$

In Eq. (4.1), K and P represent the water permeability and the water-filled porosity of the cement pastes, respectively. The curve is shown in Figure 4.5 as a green line. In contrast to the computational efforts required by the CM, water permeability of cement pastes can be quickly estimated by the proposed mathematical formula once the water-filled porosity is known. In this study, the water-filled porosity is obtained by the points counting technique and this just costs a fraction of the time of a full CM computational approach. In general, points are randomly distributed inside the specimen of which those located in the water-filled pore space are counted. The water-filled porosity is therefore obtained by dividing the number of points in water-filled pores to that in the whole specimen. In practical situations, where the permeability of an existing sample needs to be estimated, the water-filled porosity can be experimentally assessed by an oven drying technique (Lafhaj *et al.*, 2006; Kameche *et al.*, 2014) or by the NMR (nuclear magnetic resonance) method discussed in (Muller *et al.*, 2013; Zamani *et al.*, 2014). The confidence limit of the proposed model is 0.91. So, indeed a relationship exists between water permeability and water-filled porosity that can provide reliable results for the chosen normal cement pastes.

Compared to the empirical models for permeability estimation (Lafhaj *et al.*, 2006; Gao and Hu, 2013; Zamani *et al.*, 2014), only one variable parameter (water-filled porosity) is involved in the proposed method that can be measured in experiments. Moreover, the

abovementioned empirical models are mostly used to calculate the relative permeability instead of the absolute permeability.

4.3.2 Validation

In this section, the data obtained from the proposed model will be compared with those from other numerical methods. This is to verify the presented approach in this chapter.

Pignat *et al.* (2005) calculated the permeability of cements (with a *w/c* = 0.42) during hydration for six particle size distributions on the basis of the vector approch. Unfortunately, the samples in (Pignat *et al.* 2005) are fully saturated, which mainly addresses the situation of high water-filled porosity (larger than 10%). Zalzale *et al.* (2013) applied the lattice Boltzmann method to calculate the permeability of partially saturated cement pastes (with a *w/c* = 0.4). In this case, the water-filled porosity ranges from 9.5% to zero. Hence, the simulation data reported in (Pignat *et al.*, 2005; Zalzale *et al.*, 2013) were used to validate the proposed model, as illustrated in Figure 4.6. It is found that a sastifactory agreement exists between the results calculated by our model and those from (Pignat *et al.*, 2005; Zalzale *et al.*, 2013) at high water-filled porosity (above 7%). However, the difference with the model of Zalzale becomes obvious when the water-filled porosity is below 7%. This may be attributed to the fact that the model used in (Zalzale *et al.*, 2013) is a voxel-based system while a network model is chosen in this work. The resolution limit existing in the voxel-based model results in a higher depercolation threshold in contrast to that in the network model (Ye, 2005). Pores smaller than the resolution limit are ignored in (Zalzale *et al.*, 2013), but these pores may still contribute to the water transport through the specimen as properly accomplished in

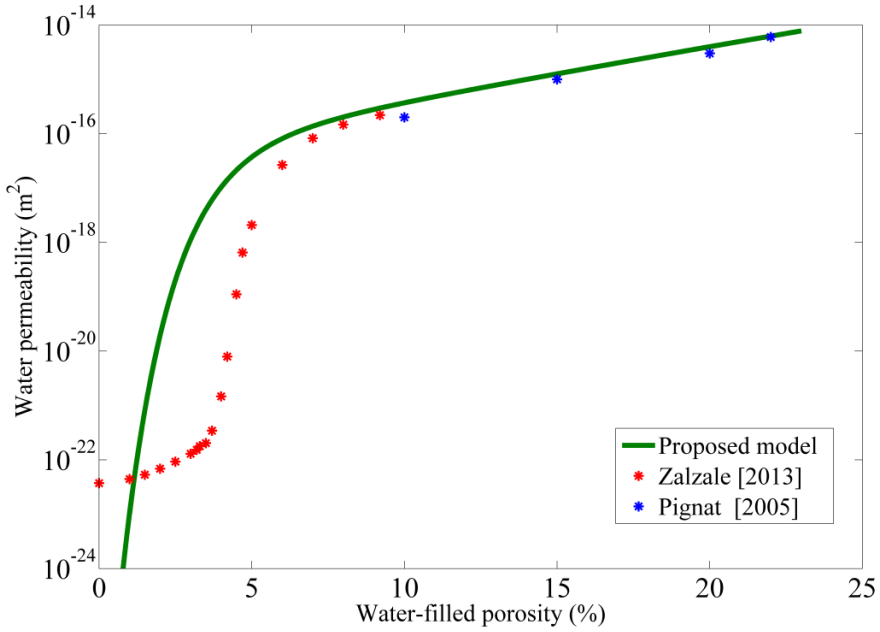

Figure 4.6 Comparison between the proposed model and other simulation data.

the network model. Hence, a higher water permeability is obtained by the proposed model at low water-filled porosity. Moreover, a strong influence of pore connectivity on permeability at low water-filled porosity (below 5%) is observed in this study, as will be discussed later. Another difference, namely the levelling of the permeability value as reported in (Zalzale *et al.*, 2013) compared to the sharp drop in our proposed model, is observed at very low values of the water-filled porosity (below about 3.5%). This is attributed to the fact that C-S-H is treated as an impermeable medium in this work, while its low permeability characteristic is taken into consideration in (Zalzale *et al.*, 2013). According to Ma *et al.* (2014a), the water permeability of C-S-H gel is at the scale of 10^{-23} m^2. However, its contribution to water permeability only becomes significant at very low water-filled porosity, which is not the case in practice. In addition, the structure and formation mechanism of C-S-H are still uncertain and controversial, so C-S-H is just considered as an impermeable medium in this work.

Unfortunately, there exist limited experimental data regarding water permeability because the measurements require a lot of time and seem to produce inconsistent results, as discussed in (Zalzale *et al.*, 2013; Kameche *et al.*, 2014). We therefore do not use experimental data for validation purposes. Specifically, the fully saturated state as required in laboratory testing on water permeability is difficult (if not impossible) to establish and maintain. Hence, data on the water-filled porosity obtained in experiments should be treated with care. Moreover, the self-sealing effect (*i.e.* continuing hydration during water permeability test) (Hearn and Morley, 1997) usually leads to densified structures and high errors in the measured results. This is not taken into account in simulations. All those effects lead to a much lower measured water permeability.

4.3.3 Pore characteristics of cement pastes at various water-filled porosities

Although an easy method is presented in this chapter to determine the water permeability of cement pastes once the water-filled porosity is known, it seems that measurement of the very complex underlying pore network structure (*i.e.* pore throat size and connectivity of the capillary pores) can provide a better understanding of the mechanisms behind the permeability-porosity curve, as illustrated in Figure 4.5. In general, water permeability gradually declines with decreasing water-filled porosity (larger than 5%). Once the water-filled porosity goes down to 5% and below, a sharp drop is observed. To understand why this occurs, both pore throat size and connectivity of the capillary pores of the chosen cement pastes at different water-filled porosities are studied and their influence on permeability will be discussed in what follows.

The same samples as described in Section 4.3.2 are used to investigate the relationship between median pore throat size and water-filled porosity; the results of all the samples are jointly plotted in Figure 4.7. An almost linear decline of median pore throat size is observed for the various mixtures leading to a relatively narrow band of data around the green “average” curve. In Figure 4.5, the impact of this scatter on permeability (in logarithmic form) is not

dramatic, so that a confidence limit of 0.91 could be obtained for the linear regression curve. Nevertheless, the sharp decline in water permeability at low water-filled porosity (below 5%), as shown in Figure 4.5, cannot be explained by the linear decrease in median pore throat size. It is obvious that another factor (pore connectivity) should be taken into account to understand the changes in water permeability at low water-filled porosity.

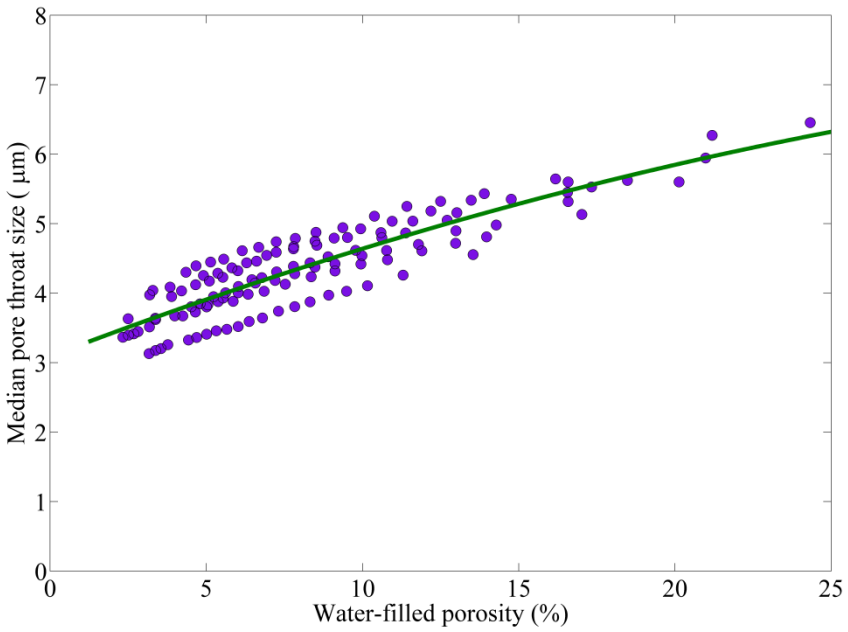

Figure 4.7 Median pore throat size versus water-filled porosity of all the samples.

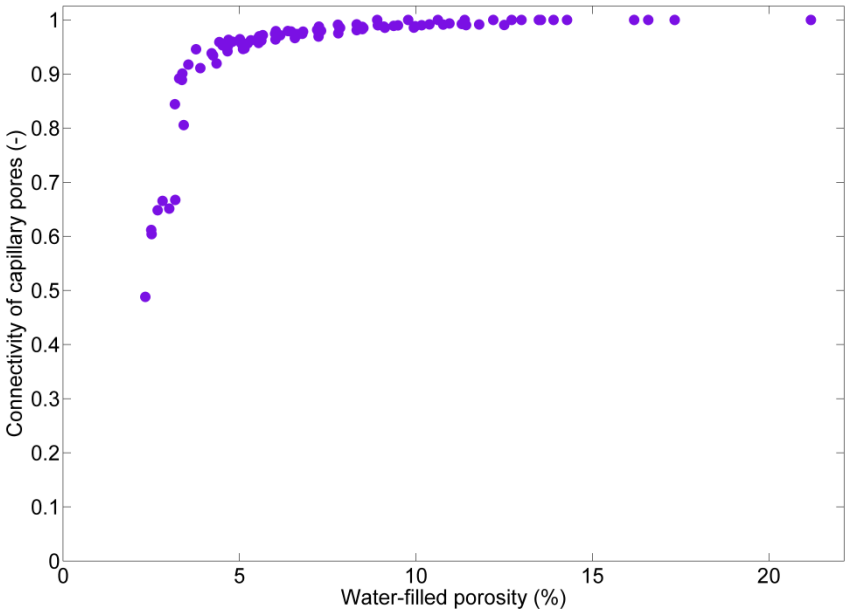

Figure 4.8 Pore connectivity versus water-filled porosity of all the samples.

Connectivity of the capillary pores is defined as the volume ratio of the percolated pores to the total pores. It is an important factor since water transport can only take place in the continuous channels. Figure 4.8 contains results of all mixtures leading to slightly declining values above 5% water-filled porosity. At the lower end, a steep drop is observed. The values representing the various mixtures are very close to an average curve (not shown for clearity reasons). This is the so-called depercolation phenomenon of capillary pores, as already reported by Garboczi and Bentz (2001), Ye (2005) and Chen *et al.* (2006). Interestingly, a turning point in Figure 4.5 is also observed around the water-filled porosity 5%.

Hence, the changes in water permeability of cement pastes at variable water-filled porosities can be understood as follows. When the water-filled porosity is large, capillary pores available for water transport are highly connected, so the reduction in the water permeability is predominantly attributed to the decline in the pore throat size. Once the water-filled porosity is reduced to the depercolation threshold of the capillary pores, pore connectivity starts to play a dominant role in determining permeability compared to the contributions by the abovementioned factor. Specifically, the amount of connected pores for water transport decreases dramatically and the pore structure tends to be depercolated, resulting in a very low permeability. After the structure becomes completely depercolated, there are no paths left for water permeation anymore and the water permeability approaches to zero.

4.4 Discussion

Permeability is an important indicator of the durability of cementitious materials, it is defined as the movement of an agent through the porous medium under an applied pressure (Banthia *et al.*, 2005). The permeability of concrete for different agents has been investigated either by physical experiments or by computational techniques. Although the computational approaches (such as the CM) are less time-consuming and laborious in contrast to the laboratory tests, a few hours are still required to finish successive stages (particle packing simulation - hydration simulation - pore delineation - pore measuring - tube network modelling) in the CM.

Effective porosity, pore throat size and connectivity of the capillary pores are the three most important parameters determining the water permeability of cementitious materials. The first factor represents the available pore space for water permeation, while the other two reflect topology and local geometry of the pore network system. Studies have demonstrated that the water permeability of cement-based materials is related to the abovementioned parameters (Ye, 2005; Lafhaj *et al.*, 2006; Gao and Hu, 2013). Median pore throat size and pore connectivity are found to be related to the water-filled porosity in (Li *et al.*, 2016a). This indicates that the water permeability can be directly related to the water-filled porosity. Ordinary cement pastes under various conditions (*i.e.* water/cement ratio, curing age, particle size range and water saturation degree) are tested using the CM for their permeabilities. At the same time, the water-filled porosity is determined and related to the numerically computed permeability. It is found that the water permeability of the chosen cement pastes can be

represented by the water-filled porosity regardless of water/cement ratio, curing age, particle size range and water saturation degree. A mathematical expression is therefore proposed for permeability estimation based on the water-filled porosity. The confidence limit of the presented model is 0.91, which is satisfactory for engineering purposes. The results calculated by the proposed model are compared with the data from other numerical methods in (Pignat *et al.*, 2005; Zalzale *et al.*, 2013), and a satisfactory agreement is found. In practice, the water-filled porosity can be measured by NMR techniques (Muller *et al.*, 2013; Zamani *et al.*, 2014). In contrast to the traditional oven drying approach, the samples in NMR tests are not heated, so that imposed damage to their pore structure can be avoided. Hence, the water permeability of real cement pastes can be quickly estimated using our proposed model once the water-filled porosity is experimentally determined.

Although the permeability of cement paste can be directly represented by the water-filled porosity, the phenomenon driving the permeability in structural terms is still unknown. To better understand the underlying mechanisms, median pore throat size and connectivity of the capillary pores of cement pastes with different water-filled porosity are therefore studied as well. It is found that median pore throat size almost linearly declines at a decreasing water-filled porosity, as observed in (Gueven, *et al.*, 2017). While pore connectivity slightly goes down first, it then dramatically drops after passing the critical value of de-percolation of effective porosity. Hence, when the water-filled porosity is high, capillary pores are highly connected and the decline in water permeability is attributed to the drop in median pore throat size. Once the water-filled porosity approaches the point where the capillary pores become de-percolated, the amount of connected pores for water permeation is dramatically reduced, which plays a dominant role in governing water permeability as compared to also declining values of median pore throat size.

4.5 Conclusions

Durability of normal concretes is determined by permeability of the relevant cement paste, which is governed by pore characteristics. This leads to an empirical fitting function presented herein. This shorter but still reliable method for permeability estimation makes use of the basics of the CM. Only a few minutes are required for the presented approach, which is a significant improvement as compared to the time investment in the network analysis by the CM. At structural level, a gradual decline in the water-filled porosity is observed leading to an approximately linear reduction in median pore throat size. After passing the de-percolation limit, the effect of this factor on permeability is by far exceeded by the exponential decline in pore connectivity.

Chapter 5 A numerical investigation into the influence of the interfacial transition zone on the permeability of partially saturated cement paste between aggregate surfaces

This chapter shows the influence of the interfacial transition zone on the permeability of partially saturated concrete. It is based on Kai Li et al. (2017), a paper submitted for publication in Cement and Concrete Research.

The interfacial transition zones (ITZs) are supposed to promote fluid transport through concrete. As a consequence, one would expect an increase in permeability with an increasing aggregate fraction. This is verified by experiments, however, the opposite effect is observed as well. The permeability ratio of ITZ to matrix seems to be a key parameter in interpreting this controversial phenomenon. A higher ratio favors the flow of water through the interface zone. This work aims at studying this ratio at various conditions (*i.e.*, hydration degree, water/cement ratio, particle size range and water saturation degree) using a numerical model, so that the influence of the ITZ on the permeability of cementitious composites can be better understood. The findings presented in this chapter can provide a new perspective on controversial experimental results as to the effect of the ITZ on transport capacity.

5.1 Introduction

Concrete on meso-level is generally considered a three-phase material. Major components are the cement matrix and aggregate particles. However, modifications of the cement structure around aggregate surfaces referred to by the interface zone can be viewed as the third phase. The ITZ reveals significant compositional differences as compared to the bulk paste. These differences are most significant very close to the aggregate surface and gradually diminish away from the aggregate grain surface to become insignificant at a certain distance (15-50 μm) (Scrivener *et al.*, 2004). The ITZ differs from bulk paste in porosity, pore size and also in the complementary anhydrous cement and CSH (calcium silicate hydrate) contents. In general, the ITZ contains less anhydrous cement grains, larger pores and higher porosity, resulting in a higher permeability in contrast to that of bulk paste. The ITZ fraction goes up at increased aggregate content, additionally leading to a larger degree of ITZ overlap. According to the

ITZ percolation theory (Scrivener and Nemati, 1996), the ITZs will mutually connect and thus fast-conduction pathways will be formed through the material once the aggregate content reaches a threshold value. In theory, the permeability of concrete should rise at the increased aggregate content and a sudden increase can be expected at the percolation threshold (Winslow *et al.*, 1994). This is confirmed by Halamickova's work (Halamickova *et al.*, 1995). Unfortunately, it is not always the case in practice. Contradictory results are also experimentally obtained in permeability tests. As an example, the permeability of concrete is observed to go down at an increased aggregate fraction in (Wong *et al.*, 2009). A similar controversy exists regarding the influence of the ITZ on chloride diffusivity (Garboczi *et al.*, 1995; Schwartz *et al.*, 1995; Delagrave *et al.*, 1997).

Although earlier studies (Zheng *et al.*, 2009; Zhang *et al.*, 2014; Wu *et al.*, 2015) have been performed to better understand why such contradictory observations exist, the ITZ structures were in general simply treated as homogenous layers of a certain permeability covering the surface of hydrating cement grains. The objective of this chapter is to study the influence of technological parameters (*i.e.*, hydration degree, water/cement ratio, particle size range and water saturation degree) on the permeability of the ITZ and bulk paste. For that purpose, the ITZ is numerically constructed using a DEM-based (Discrete Element Modelling) numerical approach, as will be described in Section 5.2.1. It is expected that the presented work can provide a new perspective on this controversial experimental phenomenon.

In general, there exists a set of competing effects when adding aggregates to the cement matrix (Shah, 2000). On the one hand, porous matrix is replaced by impermeable aggregate, resulting in a decline in the total porosity and thus permeability. This is denoted as the dilution effect. The enlarged amount of aggregates also leads to an increase in the tortuosity of transport paths (Stroeven, 2000). These two effects mainly result in reduced transport properties. This is counteracted by the enlarged area of the more porous ITZ, facilitating the ingress of fluid and thus promotes the transport properties. As a consequence, the effects of aggregates on concrete's transport properties depend on which factor will dominate the scene. According to Garboczi and Bentz (1996), the conductivity ratio of ITZ to matrix paste ($\sigma_{ITZ}/\sigma_{matrix}$) is an important parameter in determining the relationship between mortar conductivity and the sand volume fraction. It is found that a value of the $\sigma_{ITZ}/\sigma_{matrix}$ of about at least 10 to 20 is required to compensate for detrimental effects so that the conductivity of mortar can be enhanced at increased sand content. Later, Shane *et al.* (2000) further pointed out that $\sigma_{ITZ}/\sigma_{matrix}$ varies with the hydration time and is actually a function of the degree of hydration. The peak with a value of approximately 7 only occurs when the degree of hydration is around 0.7. This value is below 10, so it is not likely that the ITZ will significantly enhance the conductivity of mortar (Shane *et al.*, 2000). From permeability studies it is already known that permeability is much more sensitive to pore size than conductivity is (Halamickova *et al.*, 1995). Due to the large pores in the ITZ region, the permeability ratio between ITZ and matrix paste ($\kappa_{ITZ}/\kappa_{matrix}$) is expected to be much larger than the conductivity ratio $\sigma_{ITZ}/\sigma_{matrix}$. Nevertheless, a threshold value for $\sigma_{ITZ}/\sigma_{matrix}$ and

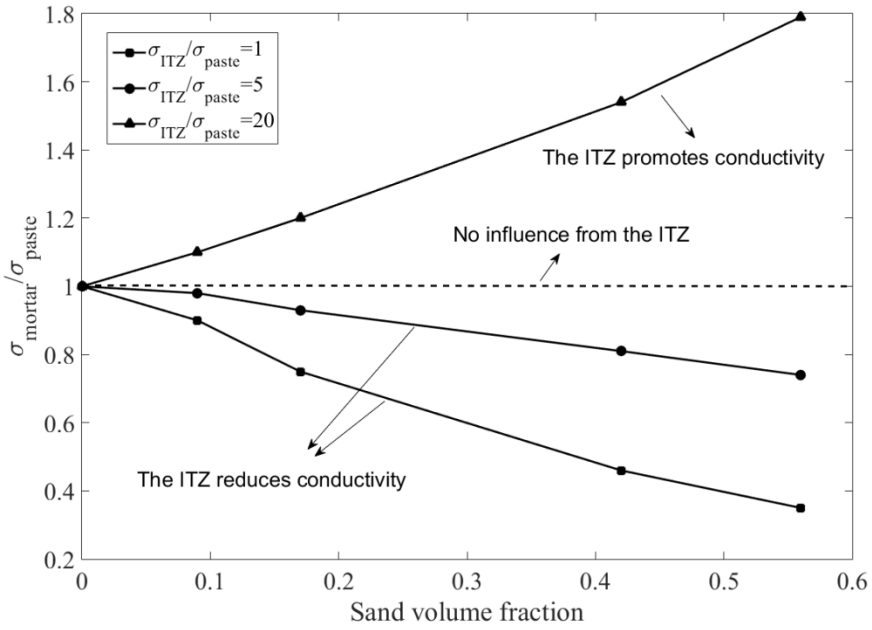

Figure 5.1 Conductivity ratio between mortar and cement paste (σ_m/σ_p) is shown as a function of sand concentration for several values of the interfacial zone conductivity to bulk matrix ($\sigma_{ITZ}/\sigma_{matrix}$). Dash line indicates no difference in conductivity between mortar and cement paste at a certain threshold of $\sigma_{ITZ}/\sigma_{matrix}$. The data shown in this figure are obtained from (Garboczi *et al.*, 1995).

$\kappa_{ITZ}/\kappa_{matrix}$ that is used to evaluate the influence of the ITZ on transport properties of cementitious material is supposed to be similar. When $\kappa_{ITZ}/\kappa_{matrix}$ is exceeding the threshold value, the ITZ effect will outweigh the other effects of the aggregate, so that the ITZ is supposed to enhance the permeability of concrete. Otherwise, the dilution and tortuosity effects become dominant, which leads to a reduced permeability at an increased aggregate content. Figure 5.1 shows the different effects of the ITZ on the conductivity of mortar at increasing sand volume fraction. It seems that the conductivity ratio between the ITZ and the bulk matrix should exceed a threshold so that the ITZ would promote the conductivity of mortar. However, relatively little is known about the quantitative differences between the permeability of the ITZ and the bulk paste.

Additionally, cementitious materials in service are seldom fully saturated due to water evaporation. Yet, the saturation degree of specimens has been proven an important factor governing permeability (Zalzale *et al.*, 2013; Kameche *et al.*, 2014; Li *et al.*, 2015; Li *et al.*, 2016a). It should likewise affect the value of $\kappa_{ITZ}/\kappa_{matrix}$. Unfortunately, experimental research on the $\kappa_{ITZ}/\kappa_{matrix}$ relationship to the permeability of concrete has not been conducted yet. It will constitute therefore the main content of the presented work. Since experimental measurements on permeability of cementitious materials usually require specialized equipment and long periods of time to complete, a modelling approach is employed in the present case due to its economic characteristics. Drying-induced micro-cracking is another

crucial factor affecting the transport properties of concrete and thus the permeability ratio ($\kappa_{ITZ}/\kappa_{matrix}$), as shown by recent experimental and 3D modelling studies (Lee *et al.*, 2016; Liu *et al.*, 2016; Fahy *et al.*, 2017; Plague *et al.*, 2017). Due to the nature of ITZ, cracks in practice tend to initiate in this zone. Once these cracks coalesce, the water ingress process could be promoted, resulting in a higher $\kappa_{ITZ}/\kappa_{matrix}$. This may be the reason why the measured permeability in (Halamickova *et al.*, 1995) goes up with the increasing aggregate content. However, the influence of micro-cracks on water transport of cementitious materials is not within the scope of this study.

In this chapter, a systematical study is performed to evaluate the influence of several parameters (*i.e.*, degree of hydration, water/cement ratio, particle size range and saturation degree) on the value of $\kappa_{ITZ}/\kappa_{matrix}$. A brief introduction on the developed numerical approach will be given in Section 5.2. Since the full methodology has been presented in detail earlier, the interested readers are referred to the relevant publications for more information (Stroeven *et al.*, 2015; Li *et al.*, 2016a). The respective effects of degree of hydration, water/cement ratio, particle size range and saturation degree on the permeability ratio of ITZ to matrix paste will be presented in Section 5.3. The value of $\kappa_{ITZ}/\kappa_{matrix}$ is found to strongly depend on the sample's conditions (degree of hydration, water/cement ratio, particle size range and saturation degree). The findings presented in this work are verified by the results from (Shane *et al.*, 2000).

5.2 Numerical approach

Since the developed modelling techniques have been presented in full detail in (Stroeven *et al.*, 2015; Li *et al.*, 2016a), only a brief introduction is given here. Nevertheless, enough information will be provided in this section to enable the readers to understand how the modelling operation is performed.

5.2.1 Generation of the bulk material and ITZ

It is well known that the origin of the ITZ derives from the cement particles packing against the aggregate surface (Scrivener *et al.*, 2004). Since the aggregate size is in general much larger than that of the cement grains, the aggregate surface can actually be considered flat that prohibit a dense packing of the cement particles close to the surface. When the cement particles approach the flat surface of the aggregate, the packing constraints lead to a gradient structure (Zheng and Li, 2002). The differences in structure gradually diminish away from the aggregate surface to eventually become insignificant at a certain distance from the aggregate surface, as illustrated in Figure 5.2.

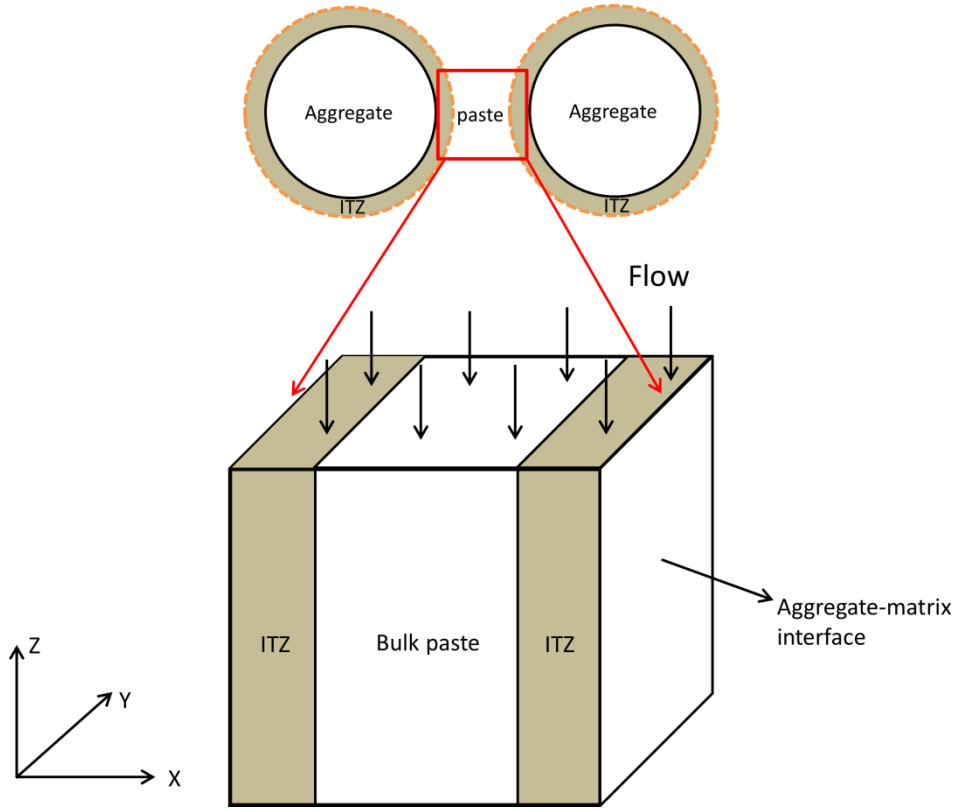

Figure 5.2 Schematic illustration of the ITZ structure in our modelling techniques.

To numerically construct the ITZ structure, the following assumptions are made in this work. (1) Since the size of aggregate is much larger than that of cement grain, the aggregate's surface is assumed to be planar while cement particles are still treated as spheres; (2) Aggregate size and volume fraction do not affect the ITZ characteristics; (3) Aggregates are separated far enough so that they do not interfere with each other. So, to start with, two parallel planes were fixed in the X-direction to represent the surfaces of neighboring aggregate grains. Limitations in Y- and Z-direction of specimens were achieved by periodic boundaries. Fresh cement grains were modelled as spheres for simplification purposes. All particles were initially generated in a larger cuboidal container with two rigid walls in X direction and four periodic ones in the other Cartesian coordinate directions. During the packing simulation, the size of the container was gradually diminished until the container reached its desired size. Various interactions (particle-particle, particle-rigid wall) were taken into account to simulate the mixing process. Herein, the ultimate specimen size was set as 100 μm, commonly considered as a representative size of virtual cementitious material in the used size range. The number of particles depends on the pre-set water/cement ratio (that is, packing density) and particle size distribution. In this case, the water/cement ratio was set to 0.4 and the Rosin Rammler function was chosen to represent the particle size distribution, ranging from 1 to 30 μm (the number of particles were of the order of 2×10^5). Note that the water/cement ratio and the particle size range will be varied later to investigate the effects of the changes in these two parameters on the $\kappa_{ITZ}/\kappa_{matrix}$ function, as will be described in Section 5.3.2 and Section 5.3.3.

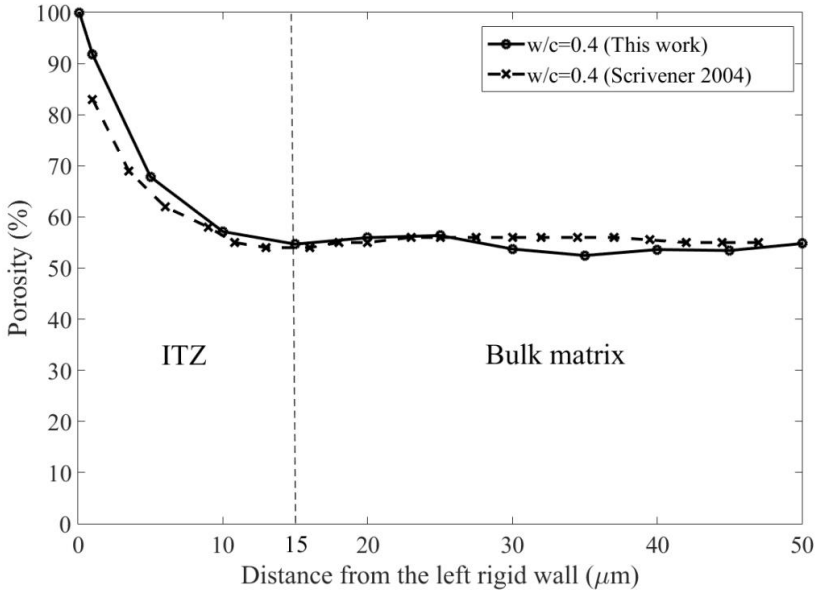

Figure 5.3 Porosity gradient existing in the ITZ of fresh specimen. Solid line represents the simulation results from this study, while the dash line is obtained from experimental data in (Scrivener *et al.*, 2004).

A serial sectioning operation was conducted along the X axis to measure the porosity as a function of the distance to the aggregate surface. Due to symmetry reasons, only the results of the 50 μm thick region neighboring the left rigid wall are plotted and compared to the data obtained by experimental measurements (Scrivener *et al.*, 2004), as given in Figure 5.3. The gradient porosity curve obtained in this way is found to be in satisfactory agreement with experimental data, validating the modelled ITZ and bulk paste structure. This leaves the inner boundary of the ITZ to be assessed in an objective way, so that the respective contributions to the permeability of concrete by ITZ and bulk matrix can be determined. In this work, the border of the ITZ is associated with the point where the porosity will start exceeding the bulk value by a threshold of 2%. A thickness of 15 μm was found as the ITZ thickness in this case, leaving a region of 70 (=100-2×15) μm of bulk zone. Note that no clear border exists in practice between the ITZ and the matrix due to pores in the ITZ connecting with pores in the bulk zone (Wong and Buenfeld, 2006). This complex phenomenon is not within the scope of the presented numerical study. Although the hydration time, water/cement ratio and particle size range have been proven to affect the ITZ thickness, a constant value of 15 μm has been consistently used in this work to keep it in accordance with the setup in (Shane *et al.*, 2000).

5.2.2 Three-dimensional matured microstructures

In the next stage, the densified structure retrieved from the particle packing modelling is used as input for the hydration simulation discussed in this section. Similar to a real experimental setup, the fresh specimen needs to react with water to produce matured samples. The vector-based XIPKM (Extended Integrated Particle Kinetics Model) was used to simulate the

hydration process (Le *et al.*, 2013). The major cement compounds, *i.e.*, tricalcium silicate (C_3S), dicalcium silicate (C_2S), tricalcium aluminate (C_3A) and tetracalcium aluminoferrite (C_4AF), are taken into account. The volume fraction of these four phases of the cement clinker were 61%, 20%, 8% and 11%, respectively. The interested readers are referred to (Le *et al.*, 2013) for more details on XIPKM. The DEM packed particulate microstructure serves as an input for XIPKM. The main hydration product, calcium silicate hydrate (C-S-H), is treated as a homogenous and impermeable material surrounding the hydrating cement grains. Although C-S-H has been proven to be a porous medium, its structure and formation mechanism are still not clear (Jennings, 2000; Jennings, 2008). So, no more details on the internal structure of C-S-H are taken into account. Due to the hydration reactions, cement particles grow concentrically to fill the free space, resulting in a spatial pore network structure with complex geometric and topological properties. The simulation stops when all available water has been consumed. Microstructures at various hydration ages were chosen for further study.

5.2.3 Pore delineation and measuring in hardened microstructures

To measure the permeability of a hydrated structure, the Double Random Multiple Tree Structuring (DRaMuTS) method was used to assess the topology of the pore structure of the abovementioned virtual matured material. DRaMuTS is a robotics-inspired technique, and has been shown able to perform the porosimetry operation and provide reliable results in (Stroeven *et al.*, 2012). It starts by distributing random points throughout the virtual structure of which only the points situated in pore space are used for further analysis. 10^5 points have been shown able to provide reasonable statistics at normal computational efforts in (Li *et al.*, 2016a). The points or nodes dispersed inside the pores are connected by unobstructed straight line segments. The result is a tree-like structure inside the capillary pore network structure of the specimen. It becomes possible to characterize its topological properties using the tree-like structure. Isolated pores and dead-end pores branching off the continuous main channels can be distinguished and taken out from the flow simulation operation at a later stage to optimize performance.

In the next step, local pore volume needs to be assessed to determine the local pore size. A star volume measuring (SVM) approach is applied for that purpose. Each point is the nucleus of a star of which a large number of its random rays is used to estimate the size of the representative sphere. More relevant details can be found in (Le, 2015). The pore information obtained in this way, along with the pore connectivity and pore size, will be used as input parameters for permeability calculations in the next section.

5.2.4 Permeability calculation of microstructures at various water saturation degrees

A tube network model was employed in this work to simulate the fluid flow through the pore network system of the virtual hydrated specimens. Compared to another popular modelling approach, *i.e.*, the Lattice Boltzmann method (Zalzale *et al.*, 2013), the tube model can be directly applied to the virtual materials. It does not require the structure to be discretized into small voxels. The discretization process required by the Lattice Boltzmann method inevitably results in the resolution issue and the accuracy of this approach therefore strongly depends on the resolution limit. The lower minimum resolution leads to more accurate result, but also requires more computational effort especially when there is a large difference between the smallest and largest pores in the system. In the tube model, a structure consisting of cylindrical tubes was constructed to represent the pore channels using the locations and sizes of the pores (pore information is from porosimetry operation as described in Section 5.2.3). The influence of actual pore shape on permeability estimation is also accounted for, as described in detail in (Li *et al.*, 2016a). Only the main channels or trunks are considered and extracted from the system for permeability calculations, while the isolated and dead-end pores are neglected in this study. The main trunk is defined as the direct path through pore space from the bottom to the top of the specimen. The water flow through the specimen is activated by an applied pressure gradient between inlet and outlet nodes located at the top and bottom surfaces. Similar to a real permeability test, Darcy's law is also used in the numerical simulation to calculate permeability. However, applying Darcy's equation requires the specimen to be fully saturated. Consequently, the pore space is always assumed to be saturated with water in simulations. Later how to simulate partially saturated cement paste without violating the condition imposed on using Darcy's law will be illustrated. The ITZ and bulk paste were simply treated as independent phases. This treatment is strictly speaking not true since some pores in the ITZ and cement matrix actually interconnect. This effect is not taken into account in this work.

As stated earlier, full saturation is assumed for the specimens. Unfortunately, this is not always the case in practice. Although the specimens in experiments are immersed into water for long periods of time to ensure their fully saturated states, it is quite difficult (if not impossible) to reach and maintain this state (Muller *et al.*, 2013). In fact, water evaporation inevitably occurs due to humidity changes inside the materials and this results in samples with variable water content (Zalzale, 2014). The major influence of the water saturation degree on permeability of cement paste has been studied in (Zalzale *et al.*, 2013; Kameche *et al.*, 2014; Li *et al.*, 2016a). It is found that water permeability significantly decreases with a reduced degree of water saturation. In fact, the empty pores (filled by air) block the paths for water transport with an identical result as solid grains would have. A blocking algorithm is therefore developed by the author to generate the samples at various water saturation degrees, as described in detail in (Li *et al.*, 2016a). Impermeable solid spheres are put at the positions where water is assumed to have evaporated to block the transport paths. This occurs sequentially starting from the largest pores in accordance with the Kelvin-Laplace law that

tells that air will occupy the largest pores first. This procedure can be easily carried out since all pores are already sorted by size and stored in the abovementioned porosimetry operation. In this way, the samples at different saturation degrees can be well represented. The permeabilities of such partially saturated specimens calculated from the tube model show a satisfactory agreement with other published data, validating our numerical approach (Li *et al.*, 2016a). The blocking algorithm is used in this work to obtain the specimens at various saturation degrees. Since large pores predominantly exists in the ITZ, it can be expected that water evaporation in the ITZ differs from that in the bulk phase. This inevitably affects the permeability of the ITZ and cement matrix and thus the permeability ratio. The influence of water saturation degree on the $\kappa_{ITZ}/\kappa_{matrix}$ function will be described in Section 5.3.4.

5.3 Results

The methodology described in Section 5.2 has been applied to calculate the permeability ratio of the ITZ and the bulk cement matrix ($\kappa_{ITZ}/\kappa_{matrix}$) at various conditions (*i.e.*, degree of hydration, water/cement ratio, particle size range and water saturation degree), while the reference case is a fully saturated specimen with water/cement ratio 0.4 and particle size range [1 μm, 30 μm]. The results are presented in this section. Partially saturated specimens will be considered in Section 5.3.4 while the samples in other cases are always in the fully saturated state.

5.3.1 Influence of the degree of hydration

The permeability of ITZ and matrix paste at different degrees of hydration are respectively plotted in Figure 5.4. Degree of hydration (DOH) is defined as the amount of reacted cement at a certain hydration time divided by the total amount of cement at the initial stage. As a first observation, the permeability of ITZ and bulk region show a downward trend as hydration proceeds. This is attributed to the fact that the structure gradually densifies at prolonged hydration periods. Moreover, the two curves in Figure 5.4 show a similar (almost log-linear) pattern until a sharp drop in permeability is found to occur earlier in the bulk matrix than in the ITZ.

In general, they both slightly decrease at first and then sharply drop after a certain point, which agrees well with the findings as reported in (Li *et al.*, 2016c). The reason why such distinct trend is observed can be explained as follows. At the early stages of hydration, the pore system is highly connected. In such a highly connected pore system, pore size predominantly governs the permeability. The gradual decline in pore size results therefore in a similar smooth decline in permeability. Once the pore system starts to de-percolate, pore connectivity becomes the dominant parameter. As a result, a distinct reduction in pore connectivity during prolonged hydration leads to the sharp drop in permeability. The ITZ contains larger pores and higher porosity, resulting in a higher permeability level at equal

DOH than bulk cement paste. When the system reaches its ultimate degree of hydration, the difference (in terms of porosity) between the ITZ and bulk phase still exists, resulting in different permeability values.

In Figure 5.5, $\kappa_{ITZ}/\kappa_{matrix}$ is plotted as a function of DOH. Since the permeability in ITZ and bulk paste are almost proportionally declining with hydration degree early in the hydration process, the ratio of both remains almost constant, with a value of about 5. At a higher DOH, the pore de-percolation starts leading to a sharp decline in permeability in both cases. Yet, the

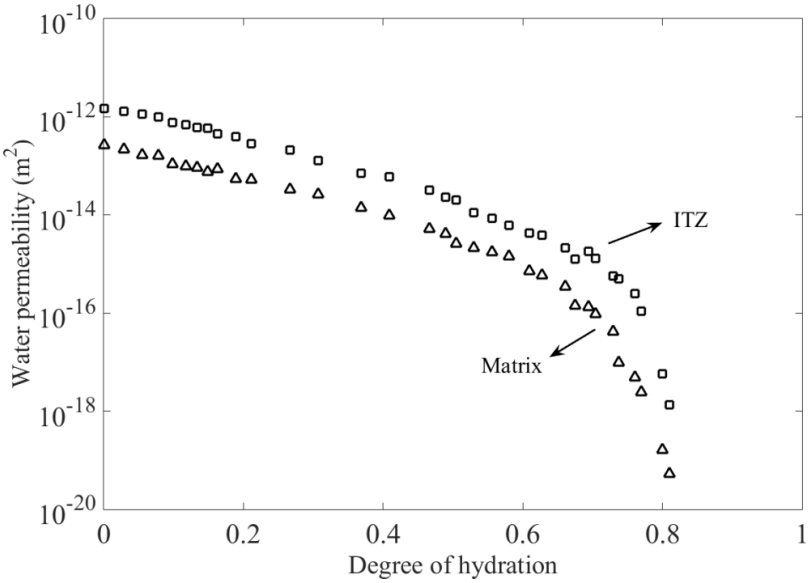

Figure 5.4 Permeability of the ITZ and cement matrix at various hydration degrees.

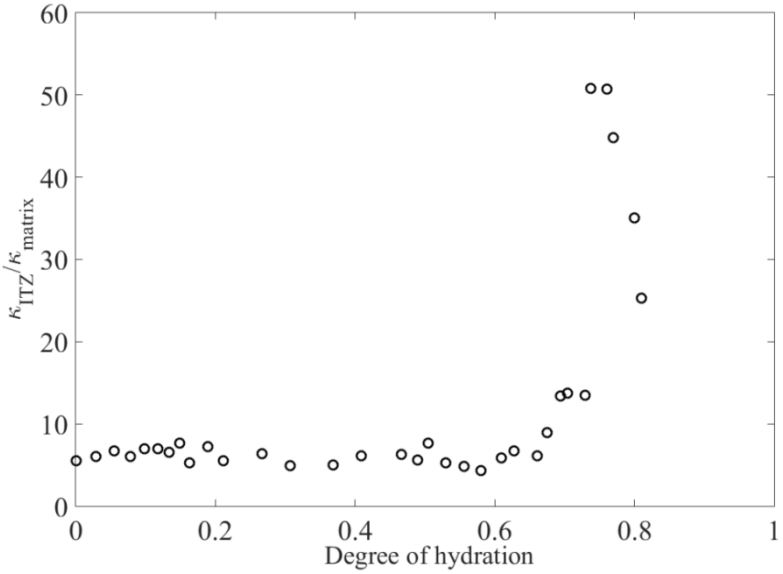

Figure 5.5 The permeability ratio of the ITZ and cement matrix ($\kappa_{ITZ}/\kappa_{matrix}$) at various hydration degrees.

pore de-percolation effect can be expected to start earlier in bulk because of the finer pore network structure. The difference in the pore de-percolation processes of bulk and ITZ will therefore reveal a distinct peak (of about 52) in $\kappa_{ITZ}/\kappa_{matrix}$ at DOH of about 0.76. After this peak value, this ratio will decline at prolonged DOH until hydration ends at the ultimate degree of hydration due to the sharp drop in the permeability of both ITZ and bulk. According to Shane *et al.* (2000), the permeability ratio of the ITZ and the cement matrix should be in the order of 10-20 to overcome the detrimental effects of the aggregate particles, so that the ITZ would promote the transport-based properties. In this study, except for a narrow region (DOH between 0.7 and 0.8), the $\kappa_{ITZ}/\kappa_{matrix}$ is in general below 10. This indicates that it is not likely that the addition of aggregates to cement paste will enhance the permeability of concrete.

To the author' knowledge, there does not exist direct available data about $\kappa_{ITZ}/\kappa_{matrix}$ versus DOH in the literature. As an alternative, the numerical data (already verified by experimental results) about the conductivity ratio of ITZ to matrix paste ($\sigma_{ITZ}/\sigma_{matrix}$) from (Shane *et al.*, 2000) was used to qualitatively validate the observed relationship in Figure 5.5. Permeability and conductivity both belong to transport-based properties, so the general features of the $\kappa_{ITZ}/\kappa_{matrix}$ and $\sigma_{ITZ}/\sigma_{matrix}$ graphs should be similar, making the comparison in the present case acceptable. The outcome is presented in Figure 5.6. The two curves in Figure 5.6 show a similar tendency and a peak is observed at approximately similar DOH in both cases. However, the maximum value of $\kappa_{ITZ}/\kappa_{matrix}$ (about 52) is much larger than that of $\sigma_{ITZ}/\sigma_{matrix}$ (around 7). A distinct difference like that can be explained by the Katz-Thompson equation (Nokken and Hooton, 2008; Ma, 2014), as presented in Eq. (5.1). In this equation, $d_{c,\,ITZ}$ and $d_{c,\,matrix}$ represent the critical pore diameter of ITZ and cement matrix, respectively. As the

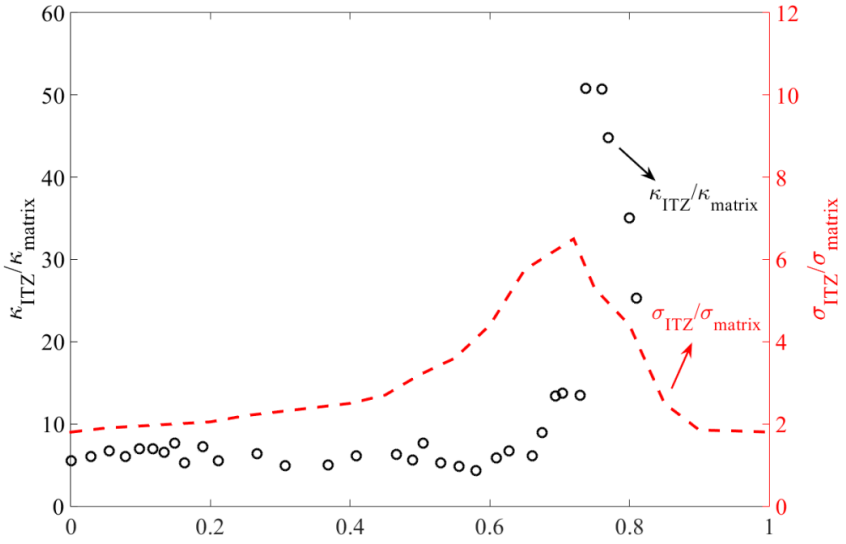

Figure 5.6 The $\kappa_{ITZ}/\kappa_{matrix}$ curve at various hydration degrees obtained in this study and from (Shane *et al.*, 2000).

ITZ contains larger pores than the paste, $d_{c,\,ITZ}$ should be larger than $d_{c,matrix}$. This causes the permeability ratio in general to exceed the conductivity ratio. Also, the peak value of 52 observed in this study is well within the range (10-100) estimated in (Shane *et al.*, 2000), and quite close to the calculated value of 35 in (Garboczi *et al.*, 1995).

$$\frac{\kappa_{ITZ}}{\kappa_{matrix}} = \frac{\sigma_{ITZ}}{\sigma_{matrix}} \frac{d_{c,ITZ}^2}{d_{c,matrix}^2} \tag{5.1}$$

5.3.2 Influence of water/cement ratio

The influence of water/cement ratio (*w/c*) on the $\kappa_{ITZ}/\kappa_{matrix}$ versus DOH graph will be discussed in this section. The results are presented in Figures 5.7-5.8. Note that water/cement ratio is the only parameter in this part of the study that is varied. The other parameters are kept constant. In general, a similar relationship between permeability and DOH is found in all cases while the sample with higher *w/c* has larger permeability. An increase in *w/c* also results in a later de-percolation phenomenon. This is the reason why the peak value of $\kappa_{ITZ}/\kappa_{matrix}$ shifts to the right with increasing values of *w/c*, as revealed by Figure 5.8. The peak values of $\kappa_{ITZ}/\kappa_{matrix}$ in all samples are larger than 20, indicating that adding aggregates to cement paste may lead to an increased permeability of concrete. For the specimens that have a smaller $\kappa_{ITZ}/\kappa_{matrix}$, adding aggregates to cement may have a negative effect on the permeability of concrete due to dilution and tortuosity effects. Additionally, Figure 5.7 shows that the hydration stops at a DOH equal to 0.63, 0.81 and 0.89 in the specimens with *w/c* of 0.3, 0.4 and 0.5, respectively. This is attributed to the different amounts of water available for cement hydration in the abovementioned structures, whereby a larger water content results in a larger value of the DOH. Fig. 5.7a shows that the hydration process of a specimen with *w/c*=0.3 stops at DOH=0.63 (before the de-percolation) since no water is available for further hydration. This is why the permeability of the specimen with *w/c*=0.3 ends at a higher value than that of the sample with *w/c*=0.4 and different permeability values for the ITZ and matrix are still observed at ultimate DOH. In the case of *w/c*=0.4, for the ITZ and cement matrix a similar permeability is found because the difference in pore structure (*i.e.*, porosity and pore size) between the ITZ and matrix is diminished at ultimate DOH (after the de-percolation). Although the specimen with *w/c*=0.5 reaches the highest DOH, the structure still does not de-percolate due to its greatest inherent porosity. As a consequence, no significant reduction in permeability is observed in the cases of *w/c*=0.5.

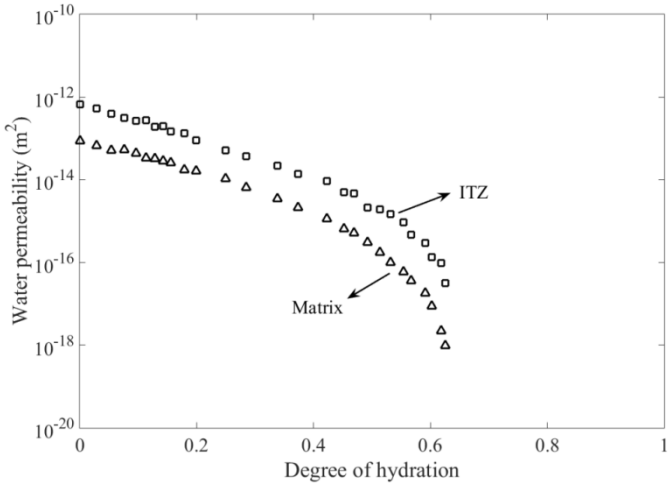

(a) *w/c* = 0.3

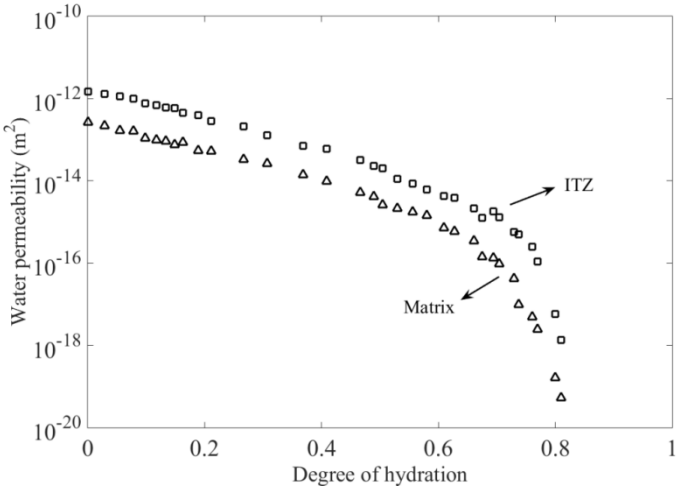

(b) *w/c* = 0.4

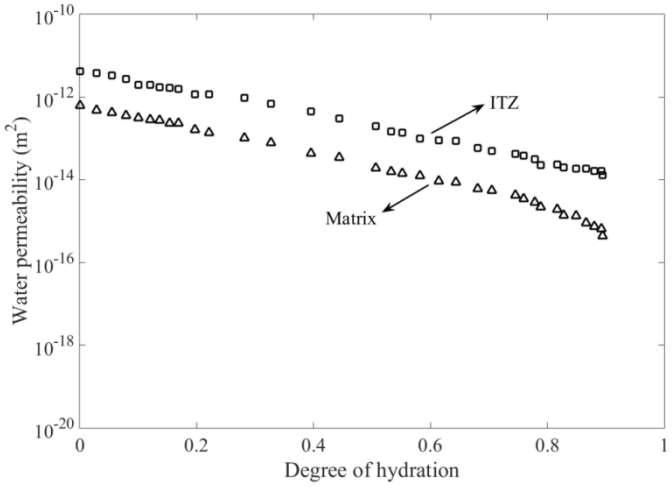

(c) *w/c* = 0.5

Figure 5.7 Permeability of ITZ and matrix versus degree of hydration at different *w/c*.

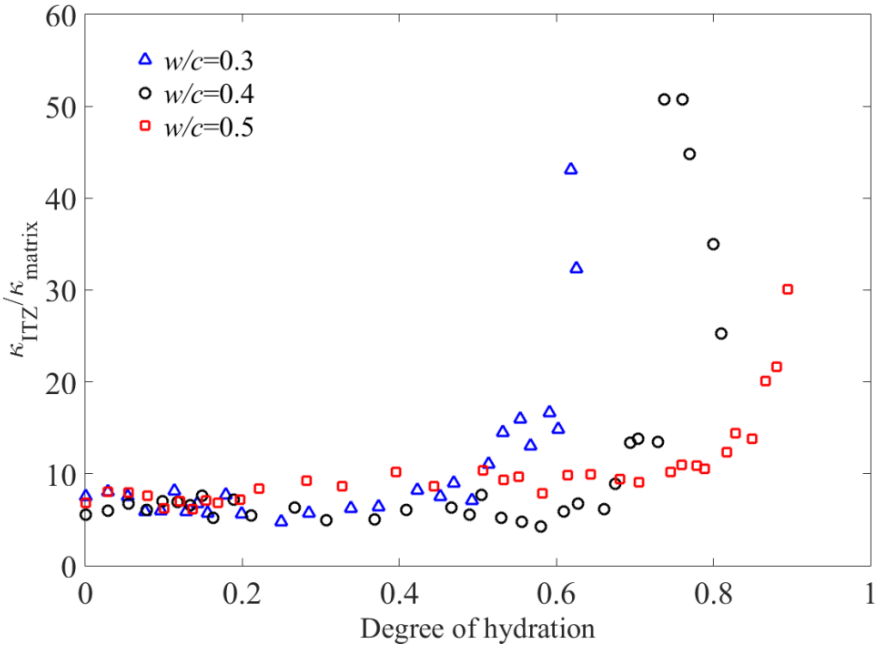

Figure 5.8 $\kappa_{ITZ}/\kappa_{matrix}$ versus degree of hydration at different *w/c*.

5.3.3 Influence of particle size range

Since the particle size range has a significant influence on the hydration process and thus the permeability, its effects on the $\kappa_{ITZ}/\kappa_{matrix}$ curve are also investigated and presented in this section. Similar to Section 5.3.2, the relationship between the permeability of the ITZ and bulk paste with respect to the hydration degree at different particle size ranges (PSRs) is first shown in Figure 5.9. The minimum particle size for all specimens was set to 1 µm. The maximum particle size for the PSR15, PSR30 and PSR45 specimens was set to 15 µm, 30 µm and 45 µm, respectively. The *w/c* was kept constant at 0.4 in this case. The general tendency observed in Figure 5.9 is in accordance with the findings presented in the previous sections. Special attention needs to be given to the samples with PSR15 and PSR45 since they end at a higher permeability and the curves in Figs. 5.9a and 5.9c do not overlap at high degree of hydration in contrast to the PSR30 sample. This is attributed to the different compositions in these cases. PSR15 contains a large amount of small particles and PSR45 a small amount of large particles, while PSR30 is an intermediate case. The difference in composition results in a different hydration process and thus a different pore structure. As a consequence, although the hydration process of PSR15 and PSR30 samples stops at similar ultimate DOH, the structure of PSR15 specimen does not de-percolate similarly as that of PSR30. Hence, PSR15 achieves a higher permeability compared to PSR30. Moreover, the curves for PSR15 (Fig. 5.9a) do not overlap at high DOH, resulting in no apparent drop of the $\kappa_{ITZ}/\kappa_{matrix}$ for PSR15 in Fig. 5.10. In the case of PSR45, although there still exists a small amount of water for continuous hydration, the hydration process after DOH=0.73 becomes very slow and the changes in structure are less significant for further consideration. So, the hydration process of PSR45 is assumed to stop at DOH=0.73 (before the de-percolation point). Therefore, a

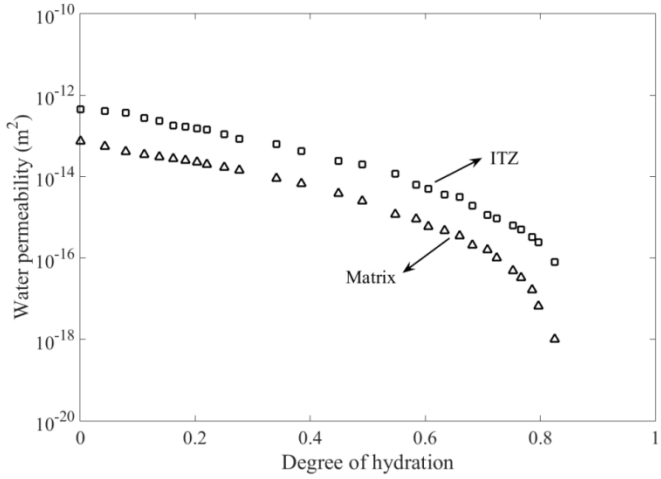

(a) PSR15

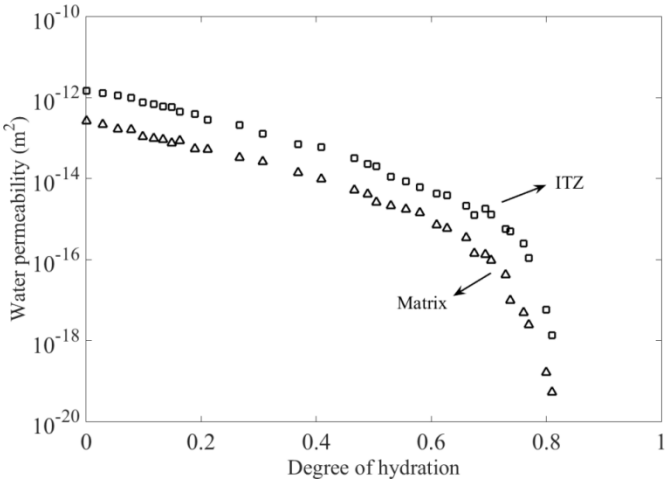

(b) PSR30

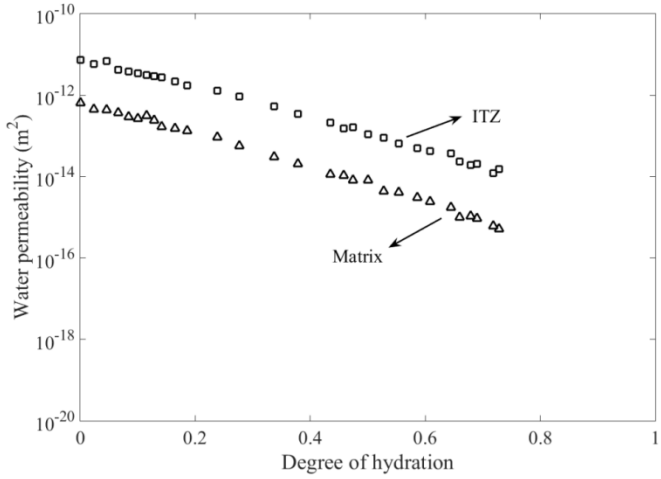

(c) PSR45

Figure 5.9 Permeability of ITZ and matrix versus degree of hydration at different PSR. PSR15, PSR30 and PSR45 represents particle size range [1 μm, 15 μm], [1 μm, 30 μm] and [1 μm, 45 μm], respectively.

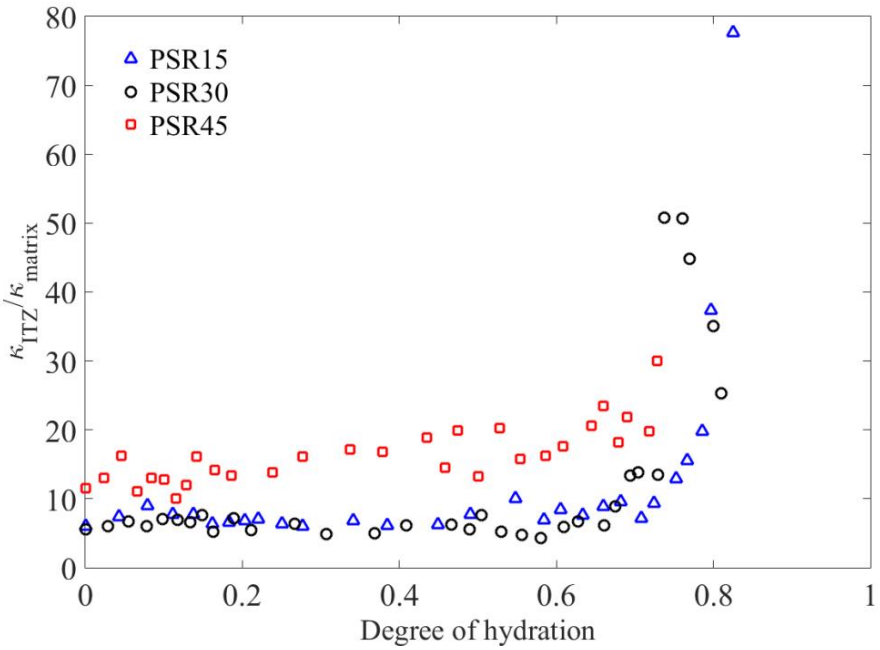

Figure 5.10 $\kappa_{ITZ}/\kappa_{matrix}$ versus degree of hydration at different PSR.

dramatic decrease in permeability values of PSR45 samples do not occur. As a result, similar to PSR15, PSR45 also reaches a higher permeability compared to PSR30 and the curves for PSR45 (Fig. 5.9c) do not overlap at high DOH. Finally, the $\kappa_{ITZ}/\kappa_{matrix}$ level of the PSR45 sample seems to be higher than that of the other two cases. A possible reason may be that the assumption of a constant ITZ thickness in this work is not true. The influence of the particle size range on the ITZ structure has been shown in (Stroeven, 1999). However, this effect is not taken into account in the presented work to maintain consistency with Shane's work (Shane *et al.*, 2000).

5.3.4 Influence of water saturation degree

Until now, all the samples used in this study are presumed at fully saturated state. However, this is not always the case in practice. Due to the humidity changes in the environment, water evaporation inevitably occurs inside samples. The significant effects of the water saturation degree (S) on permeability have been demonstrated in (Zalzale *et al.*, 2013; Kameche *et al.*, 2014; Li *et al.*, 2016a). To simulate the water evaporation in the numerical model, the blocking algorithm as described in Section 5.2.4 was used to obtain samples at various saturation degrees. The data concerning the influence of water saturation degree on $\kappa_{ITZ}/\kappa_{matrix}$ are presented in Figures 5.11-5.12. Large pores are easier to loose water in contrast to the small ones according to the Kelvin-Laplace equation. During the blocking operation for generating the partially saturated specimens, the large pores are first blocked at a decreasing degree of water saturation. Large pores predominantly exist in the ITZ region. This leads to a disproportional amount of blocked pores in the ITZ with respect to the bulk matrix for a given

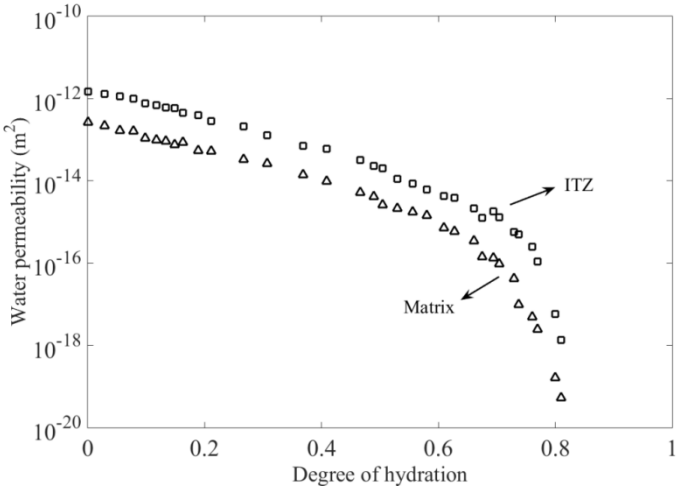

(a) *S*=100%

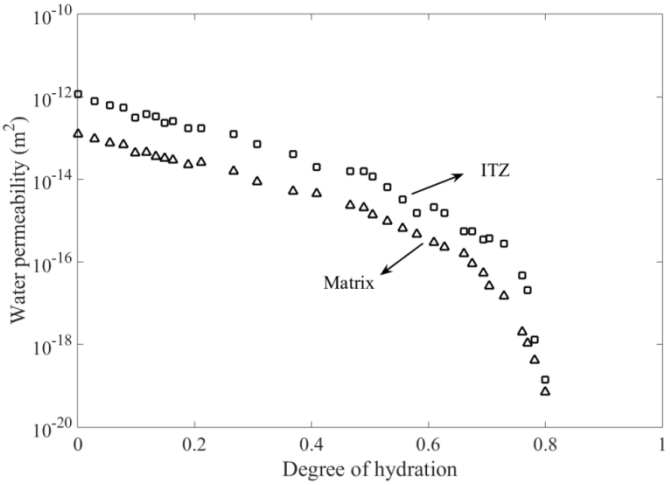

(b) *S*=67%

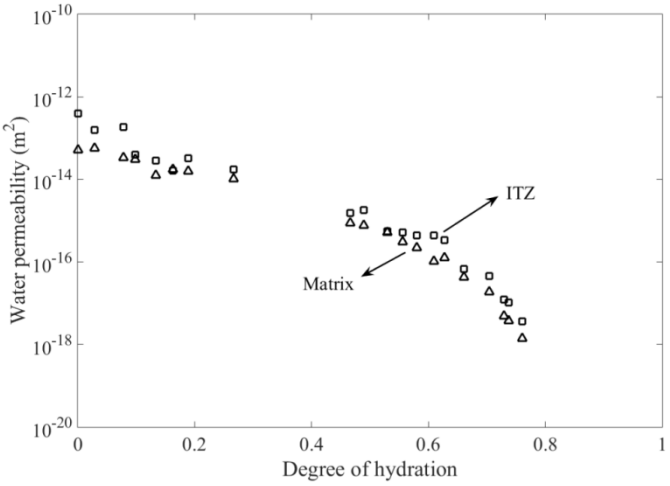

(c) *S*=44%

Figure 5.11 Permeability of ITZ and matrix versus degree of hydration at various saturation degrees.

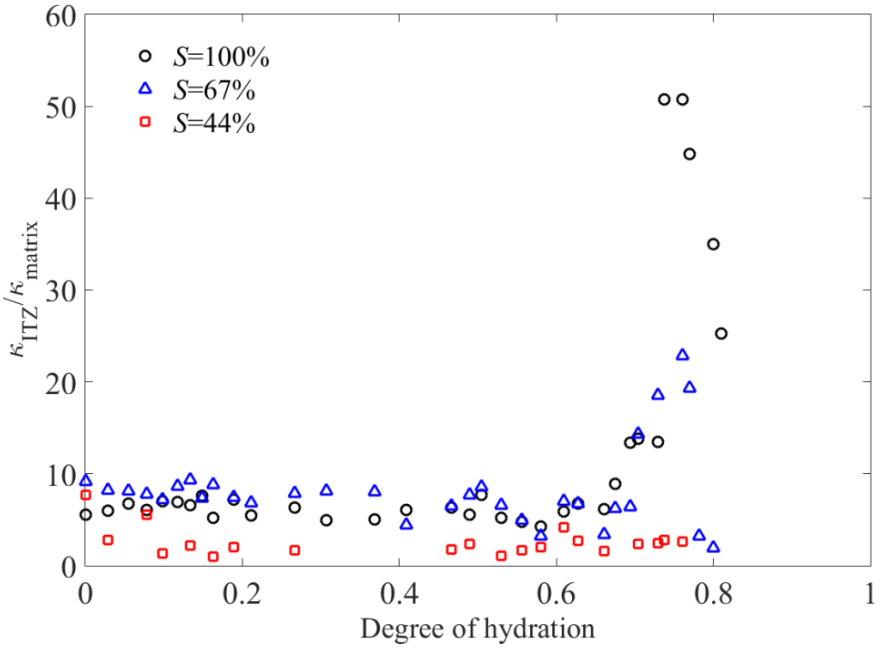

Figure 5.12 $\kappa_{ITZ}/\kappa_{matrix}$ versus degree of hydration at various saturation degrees.

saturation degree. The difference between the ITZ and paste (in terms of pore structure) thus gradually decreases and finally disappears.

Figure 5.11 shows the permeability of the ITZ gradually to approach that of the cement matrix when S is reduced from 100 percent to 67 percent, and the two curves are close at S=44 percent. This indicates that the difference in permeability between the ITZ and cement matrix also gradually decreases and almost vanishes at S=44 percent. Hence, the peak value of $\kappa_{ITZ}/\kappa_{matrix}$ is found to gradually go down to finally completely vanish in Fig. 5.12. When S reaches 44 percent, the permeability of ITZ is close to that of the cement matrix, resulting in an almost constant value (1-2) of $\kappa_{ITZ}/\kappa_{matrix}$. In this case, the dilution and tortuosity effects will cause the ITZ not to contribute to an increase in the overall permeability of concrete, so a reduction in permeability at the increased amount of aggregates can be expected, as experimentally observed in (Wong *et al.*, 2009).

5.4 Discussion

As an important phase in concrete, the ITZ has long been considered as a zone of weakness, in terms of both strength and fluid permeation (Scrivener and Nemati, 1996). Although the ITZ is known to have larger pores and to be more permeable than the cement matrix, its influence on the overall permeability of concrete is still uncertain.

In fact, contradictory experimental results are obtained by different researchers. The ITZ percolation theory predicts that concrete permeability will rise at increasing aggregate content and that a sudden increase in permeability should occur at a critical aggregate fraction when

the more permeable ITZ regions surrounding the aggregates start to interconnect. This is confirmed by Halamickova's work (Halamickova *et al.*, 1995), but an inverse trend is also reported in (Wong *et al.*, 2009), indicating a decreasing permeability with the addition of aggregates into the cement paste. When aggregates are introduced into cement paste to make concrete, except for the ITZ effect, two other competing effects (dilution and tortuosity) should be accounted for. According to Shane *et al.* (2000), the ITZ will govern the ionic transport when the conductivity ratio of the ITZ and cement matrix is of the order of 10-20. Shane's work (Shane *et al.*, 2000) inspired us to study the quantitative difference between the permeability of the ITZ and that of the bulk cement paste, which has not been carried out yet but could provide a new insight into the controversial experimental results. A DEM-based simulation approach is used to achieve these objectives.

For normal concrete (w/c=0.4, particle size range from 1 μm to 30 μm), it is found that the permeability ratio of the ITZ to bulk paste ($\kappa_{ITZ}/\kappa_{matrix}$) is actually a function of the hydration degree. The $\kappa_{ITZ}/\kappa_{matrix}$ curve reaches its peak value (about 52) at a degree of hydration of 0.76, which is larger than the threshold value proposed by Shane. It indicates that the ITZ effect is the dominant factor in this case. The origin of this peak is due to the different starting points of the pore de-percolation process, which can be expected to start earlier in the bulk because of the finer pore network structure. The $\kappa_{ITZ}/\kappa_{matrix}$ curve is in general below 10 in other hydration periods, implying the dilution and tortuosity effects to dominate. This conforms to the observations published in (Shane *et al.*, 2000). Variation in the material parameters (*i.e.*, water/cement ratio and particle size range) leads to similar phenomena, but with a certain shift of the peak value. This is attributed to the fact that the pores in the ITZ and bulk matrix de-percolate at different overall DOH in different samples. Note that for a particle size range of 1 μm to 45 μm, an obvious peak is absent since the hydration process of this specimen becomes very slow and is almost negligible before reaching the de-percolation threshold, so the $\kappa_{ITZ}/\kappa_{matrix}$ curve remains on an almost constant level. Further, the effect of the water saturation degree on the permeability ratio is studied to represent practical conditions. It is found that the peak value of the $\kappa_{ITZ}/\kappa_{matrix}$ curve gradually decreases and finally completely vanishes when the saturation degree is reduced from 100 percent via 67 percent to 44 percent. This indicates that it is not likely that the ITZ would significantly enhance the permeability of concrete that is seldom fully saturated in reality.

The numerical approach used herein is restricted in some respects. In the first place, cracks existing in real 'virgin' concrete are not taken into account in this study. These shrinkage cracks will predominantly develop in the inner side of the ITZ region and interconnect with each other to form only a continuous transport path at high aggregate density, thereby facilitating fluid flow and promoting permeability. This may result in a lifting of the $\kappa_{ITZ}/\kappa_{matrix}$ curve as shown in Fig. 5. However, cracks are not easy to model since their locations and orientations in particularly loaded concrete vary a lot even in similar specimens. The interaction of such cracks and the pore channels make things even more complicated. It is therefore quite reasonable to have limited the number of variables in the present study rather

than making the set up too complicated. In the second place, the thickness of the ITZ is kept constant in our simulations to be able to compare outcomes with those in (Shane *et al.*, 2000). Yet, previous studies have shown that the ITZ thickness depends on the material properties. Then, the sample has to be immersed into water for long periods of time to ensure its fully saturated state before conducting permeability measurements in practice. This surplus of water will inevitably lead to a continuing hydration process. However, this effect is not taken into account in this work and the microstructure obtained after hydration simulation is assumed to be unchanged. Finally, ITZ and bulk paste have to be distinguished to identify their respective contributions to the overall permeability of concrete, as intensively discussed herein. This treatment is somewhat artificial since the pores in the ITZ will actually also connect to the pores in the cement matrix. This is fundamental and therefore not a limitation of the present approach. The first two restrictions could possibly be eliminated in future research. Particularly explicitly considering micro-cracking in combination with porosity could enhance the methodology, although it is expected that the present day restrictions have not significantly affected the conclusions that can be drawn from this study.

5.5 Conclusions

The permeability ratio of the ITZ and the cement matrix is an important parameter that determines the influence of the ITZ on the permeability of concrete. This factor is thoroughly studied by a numerical approach in this chapter for different parameters, *i.e.*, hydration duration, water/cement ratio, particle size range and saturation degree. Although the ITZ contains a higher porosity and thus has a higher local permeability than that of bulk paste, its net effect on the overall permeability of concrete is actually limited. Only in a narrow region of the hydration degree, a peak value is observed in the permeability ratio curve. This undergoes a limited shift for different water/cement ratios and particle size ranges. Specifically, the ITZ dominates the flow transport through the specimen in this narrow range. Otherwise, the insulating and the tortuosity effects will exceed that of the ITZ. Even at a high aggregate fraction, whereby the ITZs would be interconnected or percolated, the relevant predictions by the percolation theory of increasing permeability and finally a dramatic increase can hardly be expected. Concrete in service easily loses water due to the humidity changes in the environment, resulting in a partially saturated specimen. The associated water saturation degree is found to reduce the difference in permeability of the ITZ and the cement matrix. Almost a constant permeability ratio between the ITZ and bulk paste at different hydration stages of 1~2 is observed at a water saturation degree of 44 percent. Therefore, the ITZ and ITZ percolation will not significantly promote the transport properties of concrete in practice. Of course, micro-cracking along the ITZ of real concrete could be an intriguing factor in determining flow transport, particularly when ITZs are percolated. The study of combined porosity and micro-cracking effects would require large computer efforts and is therefore a topic for future research on ‘compucrete (computational concrete)’ as conducted herein.

Chapter 6 Conclusions and future work

6.1 Conclusions

A comprehensive computational methodology was developed in this thesis to predict the permeability of unsaturated cement paste. It consists of the following successive stages:

1. Particle packing simulation representing the fresh cement grains;
2. Hydration simulation;
3. Porosimetry operation to calculate pore characteristics;
4. Blocking algorithm to simulate specimens at various water saturation degrees;
5. Tube network modelling for the permeability assessment.

Each individual stage has been separately verified. Three-dimensional discrete element modelling is used so that the interactions between particles are properly represented. The particle packing simulation stops once the designed packing density is reached. This densified structure is then used as input for hydration simulation, which is realized by the vector-based model XIPKM. In XIPKM, each cement grain is represented by an unhydrated spherical core that becomes gradually covered by concentric shells of hydration products. As hydration proceeds, cement grains gradually expand, calcium hydroxide particles nucleate and grow in the empty region, resulting in a reduced pore space. Next, the DRaMuTS approach and the star volume method are employed to determine porosity, pore size and pore connectivity of the generated virtual matured material. Since specimens in practice are seldom in a fully saturated state, a blocking algorithm was proposed and implemented in this work to generate the samples at various water saturation degrees. According to the Kelvin-Laplace equation, larger pores drain earlier than smaller ones because of the capillary force and are thus the first to get empty. This process is mimicked by positioning solid objects in the presumed empty pores. Starting from a fully saturated specimen, a pre-defined amount of water can be removed from the structure by placing spherical solid objects at the locations of drained pores. In case of water permeability, the empty algorithm starts from the largest pores. The remaining open space is assumed fully filled by water so that Darcy's law can still be applied to calculate the permeability of partially saturated cement paste. From this situation, a tube network can be established of which the tube sizes are derived from the calculated pore sizes to simulate fluid transport. Based on this network, permeability can be calculated by solving the equations of flow.

Using the described procedure, the calculated intrinsic permeability of fully saturated specimen was found to agree well with measurements of gas permeability on dried samples (10^{-16}-10^{-17} m^2). However, those values exceed experimental results for fluid permeability by several orders of magnitude. This is attributed to the different saturation degree of specimens in simulations and in experiments. In this work, as the water saturation degree was decreased using the blocking algorithm, it is found that the calculated water permeability drops several orders of magnitudes (10^{-16}-10^{-20} m^2), spanning the major part of the range of experimentally measured values when the water saturation degree is reduced from 100 percent to 35 percent. Compared to water permeability, an inverse tendency was observed for gas permeability at various water saturation degrees. Thus, air permeability decreased at increasing saturation degree. Air blocks the water transport, while water acts as a barrier in gas flow. The permeabilities obtained from this research work agree well with those found in other available sources (Zalzale *et al.*, 2013; Kameche *et al.*, 2014), validating the presented computational methodology (Li *et al.*, 2016a). In accordance with a real experimental setup, the effects of several technological parameters (*i.e.*, hydration time, water/cement ratio, particle size range) on permeability of cement paste were studied using the proposed numerical models (Li *et al.*, 2016b). The obtained results follow the expected influence of abovementioned factors on permeability of cementitious materials.

On the basis of the parameter study (Li *et al.*, 2016b), permeability of cement paste was found to be predominantly determined by its effective porosity and to be independent of the conditions of the specimens. The effective porosity herein is defined as the porosity available for fluid transport. In the case of water permeability, the effective porosity indicates the porosity filled with water. A simple mathematical function was proposed to quickly estimate the permeability of cement paste using water-filled porosity as the only input parameter, which can be experimentally assessed by an oven drying technique or by the nuclear magnetic resonance method. The calculated permeability using the proposed formula showed a reasonable agreement with the other numerical data (Pignat *et al.*, 2005; Zalzale *et al.*, 2013).

To apply the developed methodology to concrete, the ITZ has to be taken into account in numerical models. Hence, the influence of the ITZ on the permeability of concrete has been studied in the end. The ITZ between aggregates and cement matrix is an important region to be taken into account for durability assessment of concrete. Although this phase is more porous and permeable than the cement matrix, its effects on the overall permeability of concrete are still controversial. Although the permeability of concrete is found to increase with an increasing aggregate fraction, the opposite effect is observed as well. The outcome from this work revealed that it is likely that the ITZ would not promote permeability of normal concrete. So in normal situations, adding aggregates will not lead to an increased permeability of concrete.

6.2 Recommendations for future work

In this thesis, an efficient numerical approach for determining the permeability of unsaturated cementitious materials based on their microstructures is presented. Hopefully, this work can be utilized by engineers or researchers and will serve as a starting point for further studies. In the next paragraphs, a few possible research directions are highlighted.

First of all, the major component among the hydration products, calcium silicate hydrate (C-S-H) is simply treated as an impermeable phase and its contribution to permeability is ignored in this work. Obviously, this is not the real situation. The C-S-H has been proven to be a porous medium with low permeability (Jennings, 2000, 2008; Muller *et al.*, 2013). The gel pores at the nano-scale inside the C-S-H contribute to fluid transport when the capillary pores become de-percolated (Zalzale *et al.*, 2013). To date, however, the structure of C-S-H still remains uncertain and controversial which makes it difficult to numerically determine the contribution of C-S-H to the permeability of cement paste. More investigations are required to better understand the mechanism of cement hydration and C-S-H phase at nano-level. In addition, a method or model is required to link the nano-scale to the meso-scale and micro-scale where this thesis has focused on.

Another direction may be a more realistic representation of the structure of concrete. Although a case study on concrete has been conducted and presented in Chapter 5, the concrete structure concerned in this work is just a simplified example and does not include micro-cracks. In practice, micro-cracks may be actually interconnected and a fast transport path for a fluid could be formed in the material. In this case, micro-cracks could predominantly facilitate the ingress of a fluid and significantly enhance the permeability of concrete. Unfortunately, there does not exist an effective way to properly characterize dispersed cracks in concrete. Developing an efficient method (*i.e.*, X-ray micro-CT approach) for representing micro-cracks in virtual concrete is thus interesting and attractive (Zhang, 2017). Furthermore, a multi-scale approach is still required linking the structure of cement and concrete at different scales, so that the information about cement paste at micro-level can be used as input for the permeability calculation of concrete at meso-level (Zhang, 2013). Effective media theory as mentioned by Zalzale (2014) could be a possible choice for such study.

And finally, all simulation results have to be validated by experimental data. The limitations on the current experimental techniques of permeability measurement of cement paste have been intensively discussed in this thesis. Precisely controlling the saturation degree of experimental specimens and directly measuring their permeabilities without destroying the material (*i.e.*, oven heating usually used in experiments) are difficult and challenging. This makes a straightforward comparison between the simulation results and experimental data impossible since the specimens are not subjected to the same conditions. A well-designed experiment would be necessary to accurately determine the saturation degree and the

correlated permeability of the specimen for validation purposes. Recent developments in nuclear magnetic resonance techniques (Muller *et al.*, 2013) and the beam bending method (Vichit-Vadakan and Scherer, 2002; Amriou and Bencheikh, 2017) are one of promising ways to overcome the abovementioned experimental limitations.

References

Abbas, A., Carcasses, M., Ollivier, J.P., Gas permeability of concrete in relation to its degree of saturation. *Materials and Structures* **32**(1), 3-8 (1999).

Ai, H., Young, J.F., Scherer, G.W., Thermal expansion kinetics: method to measure permeability of cementitious materials: II. Application to hardened cement pastes. *Journal of the American Ceramic Society* **84**(2), 385-391 (2001).

Amriou, A., Bencheikh, M., New experimental method for evaluating the water permeability of concrete by a lateral flow procedure on a hollow cylindrical test piece. *Construction and Building Materials* **151**, 642-649 (2017).

Banthia, N., Mindess, S., Water permeability of cement paste. *Cement and Concrete Research* **19**(5), 727-736 (1989).

Banthia, N., Biparva, A., Mindess, S., Permeability of concrete under stress. *Cement and Concrete Research* **35**(9), 1651-1655 (2005).

Baroghel-Bouny, V., Characterization of cement pastes and concretes: Methods, analysis, interpretations. *Bulletin Edition LCPC*, Paris, 1994.

Baroghel-Bouny, V., Water vapor sorption experiments on hardened cementitious materials. Part II: Essential tool for assessment of transport properties and for durability prediction. *Cement and Concrete Research* **37**(3), 438-454 (2007).

Baroghel-Bouny, V., Development of a global approach, performance-based and predictive of the durability of (reinforced) concrete structures on the basis of durability indicator, Billan and perspectives. *LCPC Editions*, Paris, 2008.

Baroghel-Bouny, V., Thiery, M., Wang, X., Modelling of isothermal coupled moisture-ion transport in cementitious materials. *Cement and Concrete Research* **41**(8), 828-841 (2011).

Bishnoi, S., Scrivener, K.L., μic: A new platform for modelling the hydration of cements. *Cement and Concrete Research* **39**(4), 266-274 (2009).

Breugel, K. van, Numerical simulation of hydration and microstructural development in hardening cement-based materials (I) theory. *Cement and Concrete Research* **25**(2), 319-331 (1995a).

Breugel, K. van, Numerical simulation of hydration and microstructural development in hardening cement-based materials (II) applications. *Cement and Concrete Research* **25**(3), 522-530 (1995b).

Chatterji, S., An explanation for the unsaturated state of water stored concrete. *Cement and Concrete Composites* **26**(1), 75-79 (2004).

Chen, H.S., Stroeven, P., Ye, G., Stroeven, M., Influence of boundary conditions on pore percolation in model cement paste. *Key Engineering Materials* **302-303**, 486-492 (2006).

Chen, H.S., L.J. Sluys, Stroeven, P, Sun, W., Theoretical prediction on thickness distribution of cement paste among neighboring aggregates in concrete. *Computers and Concrete* **8**(2),

163-176 (2011).

Coussy, O., Eymard, R., Lassabatere, T., Constitutive unsaturated modeling of drying deformable materials. *Journal of Engineering Mechanics* **124**(6), 658-667 (1998).

Darcy, H., Les Fontaines Publiques de la Ville de Dijon. *Dalmont*, Paris, 1856 [in French].

Delagrave, A., Bigas, J.P., Ollivier, J.P., Marchand, J., Pigeon, M., Influence of the interfacial zone on the chloride diffusivity of mortars. *Advanced Cement Based Materials* 5(3-4), 86-92 (1997).

EI-Dieb, A.S., Hooton, R.D., Evaluation of the Katz-Thompson model for estimating the water permeability of cement-based materials from mercury intrusion porosimetry data. *Cement and Concrete Research* **24**(3), 443-455 (1994).

Fahy, C., Wheeler, S.J., Gallipoli, D., Grassl, P., Corrosion induced cracking modelled by a coupled transport-structureal approach. *Cement and Concrete Research* **94**, 24-35 (2017).

Feldman, R., Sereda, P., A new model for hydrated Portland cement and its practical implications. *Engineering Journal* **53**(8-9), 53-59 (1970).

Gao, Z.Y., Hu, Q.H., Estimating permeability using median pore-throat radius obtained from mercury intrusion porosimetry. *Journal of Geophysics and Engineering* **10**(2), 025014 (2013).

Garboczi, E.J., Bentz, D.P., Computer simulation of the diffusivity of cement-based materials. *Journal of Materials Science*, **27**(8), 2083-2092 (1992).

Garboczi, E.J., Bentz, D.P., Modelling of the microstructure and transport properties of concrete. *Construction and Building Materials* **10**(5), 293-300 (1996).

Garboczi, E.J., Bentz, D.P., The effect of statistical fluctuation, finite size error, and digital resolution on the phase percolation and transport properties of the NIST cement hydration model. *Cement and Concrete Research* **31**(10), 1501-1514 (2001).

Garboczi, E.J., Schwartz, L.M., Bentz, D.P., Modeling the influence of the interfacial zone on the DC electrical conductivity of mortar. Advanced Cement Based Materials **2**(5), 169-181 (1995).

Gartner, E.M., Kurtis, K.E., Monteiro, P.J.M., Proposed mechanism of C-S-H growth tested by soft X-ray microscopy. Cement and Concrete Research **30**(5), 817–822 (2000).

Genuchten, M.T. Van, A closed form equation for predicting the unsaturated hydraulic conductivity of soils. *Soil Science Society of America Journal* **44**(5), 892-898 (1980).

Glasser, F.P., Zhang, L., High-performance cement matrices based on calcium sulfoaluminate-belite composition. *Cement and Concrete Research* **31**(12), 1881-1886 (2001).

Grasley, Z.C., Scherer, G.W., Lange, D.A., Valenza, J.J., Dynamic pressurization method for measuring permeability and modulus: II. Cementitious materials. *Materials and Structures* **40**(7), 711-721 (2007).

Gueven, I., Frijters, S., Harting, J., Luding, S., Steeb, H., Hydraulic properties of porous sintered glass bead systems. *Granular Matter* **19**, 28 (2017).

Halamickova, P., Detwiler, R.J., Bentz, D.P., Garboczi, E.J., Water permeability and chloride ion diffusion in Portland cement mortars: Relationship to sand content and critical pore

diameter. *Cement and Concrete Research* **25**(4), 790-802 (1995).

He, H., Computational modelling of particle packing in concrete. Ph.D. Thesis, Delft University of Technology, Delft, The Netherlands, 2010.

Hearn, N., Morley, C.T., Self-sealing property of concrete – Experimental evidence. *Materials and Structures* 30(7), 404-411 (1997).

Hu, J., Chen, H.S., Stroeven, P., Spatial dispersion of aggregate in concrete: A computer simulation study. *Computers and Concrete* 3(5), 301-312 (2006).

Jason, L., Relationship damage permeability for concrete: application to the calculation of structures. Ph.D. Thesis, Central School of Nantes, Nantes, France, 2004.

Jennings, H.M., A model for the microstructure of calcium silicate hydrate in cement paste. *Cement and Concrete Research* **30**(1), 101-116 (2000).

Jennings, H.M., Refinements to colloid model of C-S-H in cement: CM-II. *Cement and Concrete Research* **38**(3), 275-289 (2008).

Kameche, Z.A., Ghomari, F., Choinska, M., Khelidj, A., Assessment of liquid water and gas permeability of partially saturated ordinary concrete. *Construction and Building Materials* **65**, 551-565 (2014).

Koster, M., Hannawald, J., Brameshuber, W., Simulation of water permeability and water vapour diffusion through hardened cement paste. *Computational Mechanics* **37**(2), 163-172 (2006).

Lafhaj, Z., Goueygou, M., Djerbi, A., Kaczmarek, M., Correlation between porosity, permeability and ultrasonic parameters of mortar with variable water/cement ratio and water content. *Cement and Concrete Research* **36**(4), 625-633 (2006).

Le, L.B.N., Stroeven, P., Strength and durability evaluation by DEM approach of green concrete based on gap-graded cement blending. *Advanced Materials Research* **450-451**, 631-640 (2012).

Le, L.B.N., Stroeven, M., Sluys, L.J., Stroeven, P., A novel numerical multi-component model for simulating hydration of cement. *Computational Materials Science* **78**, 12-21 (2013).

Le, L.B.N., Micro-level porosimetry of virtual cementitious materials – Structural impact on mechanical and durability evolution. Ph.D. Thesis, Delft University of Technology, Delft, The Netherlands, 2015.

Lee, H.X.D., Wong, H.S., Buenfeld, N.R., Self-sealing of cracks in concrete using superabsorbent polymers. *Cement and Concrete Research* **79**, 194-208 (2016).

Li, K., Stroeven, P., Le, L.B.N., Methodology for porosimetry in virtual cementitious composites to economically and reliably estimate permeability. *Image Analysis & Stereology* **34**(2), 73-86 (2015).

Li, K., Stroeven, M., Stroeven, P., Sluys, L.J., Investigation of liquid water and gas permeability of partially saturated cement paste by DEM approach. *Cement and Concrete Research* **83**, 104-113 (2016a).

Li, K., Stroeven, M., Stroeven, P., Sluys, L.J., Effects of technological parameters on permeability estimation of partially saturated cement paste by a DEM approach. *Cement and Concrete Composites*, Under review (2016b).

Li, K., Stroeven, P., Stroeven, M., Sluys, L.J., Estimating permeability of cement paste using pore characteristics obtained from DEM-based modelling. *Construction and Building Materials* **126**, 740-746 (2016c).

Li, K., Stroeven, P., Stroeven, M., Sluys, L.J., A numerical investigation into the influence of the interfacial transition zone on the permeability of partially saturated cement paste between aggregate surfaces. *Cement and Concrete Research*, Under review (2017).

Liu, L., Wang, X.C., Chen, H.S., Wan, C.J., Microstructure-based modelling of drying shrinkage and microcracking of cement paste at high relative humidity. *Construction and Building Materials* **126**, 410-425 (2016).

Loosveldt, H., Lafhaj, Z., Skoczylas, F., Experimental study of gas and liquid permeability of a mortar. *Cement and Concrete Research* **32**(9), 1357-1363 (2002).

Ma, H.Y., Li, Z.J., Realistic pore structure of Portland cement paste: experimental study and numerical simulation. *Computers and Concrete* **11**(4), 317-336 (2013).

Ma, H.Y., Mercury intrusion porosimetry in concrete technology: Tips of measurement, pore structure parameter acquisition and application. *Journal of Porous Materials* **21**(2), 207-215 (2014).

Ma, H.Y., Hou, D.S., Liu, J., Li, Z.J., Estimate the relative electrical conductivity of C-S-H gel from experimental results. *Construction and Building Materials* **71**, 392-396 (2014a).

Ma, H.Y., Hou, D.S., Lu, Y.Y., Li, Z.J., Two-scale modelling of the capillary network in hydrated cement paste. *Construction and Building Materials* **64**, 11-21 (2014b).

Ma, H.Y., Li, Z.J., Multi-aggregate approach for modeling interfacial transition zone in concrete. *ACI Materials Journal*, **111**(2), 189-200 (2014c).

Ma, H.Y., Hou, D.S., Li, Z.J., Two-scale modeling of transport properties of cement paste: Formation factor, electrical conductivity and chloride diffusivity. *Computational Materials Science* **110**, 270-280 (2015).

Maghsoodi, V., Ramezanianpour, A.A., Effects of volumetric aggregate fraction on transport properties of concrete and mortar. *Arabian Journal for Science and Engineering* **34**(2), 327-335 (2009).

Marechal, J.C., Beaudoux, M., Experimental diphasic transfer on a thick concrete wall subjected to rapid assessment of pressure and temperature. Ann ITBTP 506, 73-112 (1992).

Monlouis-Bonnaire, J.P., Verdier, J., Perrin, B., Prediction of the relative permeability to gas flow of cement-based materials. *Cement and Concrete Research* **34**(5), 737-744 (2004).

Mualem, Y., A new model for predicting the unsaturated hydraulic conductivity of porous media. *Water Resources Research* **12**(3), 513-522 (1976).

Muller, A.C.A., Scrivener, K.L., Gajewicz, A.M., McDonnald, P.J., Densification of C-S-H measured by ^{1}H NMR relaxometry. *The Journal of Physical Chemistry C* **117**(1): 403-412 (2013).

Nokken, M.R., Hooton, R.D., Using pore parameters to estimate permeability or conductivity of concrete. *Materials and Structures* **41**, 1-16 (2008).

Nyame, B.K., Illston, J.M., Relationships between permeability and pore structure of hardened cement paste. *Magazine of Concrete Research* **33**(116), 139-146 (1981).

O'Connor, R.M., A distributed discrete element modeling environment – Algorithms, implementations ans applications. Ph.D. Thesis, Massachusetts Institute of Technology, Massachusetts, USA, 1996.

Picandet, V., Khelidj, A., Bastian, G., Effect of axial compressive damage on gas permeability of ordinary and high performance concrete. *Cement and Concrete Research* **31**(11), 1525-1532 (2001).

Pignat, C., Navi, P., Scrivener, K.L., Simulation of cement paste microstructure hydration, pore space characterization and permeability determination. *Materials and Structures* **38** (4), 459-466 (2005).

Pivonka, P., Hellmich, C., Smith, D., Microscopic effects on chloride diffusivity of cement paste - A scale-transition analysis. *Cement and Concrete Research* **34**(12), 2251-2260 (2004).

Plague, T., Desmettre, C., Charron, J.P., Influence of fiber type and fiber orientation on cracking and permeability of reinforced concrete under tensile loading. *Cement and Concrete Research* **94**, 59-70 (2017).

Qin, C.Z., Hassanizadeh, S.M., Van Oosterhout, L.M., Pore-network modeling of water and vapor transport in the micro porous layer and gas diffusion layer of a polymer electrolyte fuel cell. *Computation* **4**(2), 21 (2016).

Savage, B.M., Janssen, D.J., Soil physics principles validated for use in predicting unsaturated moisture movement in Portland cement concrete. *ACI Materials Journal* **94** (1), 63-70 (1997).

Schwartz, L.M., Garboczi, E.J., Bentz, D.P., Interfacial transport in porous media: Application to DC electrical conductivity of mortars. *Journal of Applied Physics* **78** (10), 5898-5908 (1995).

Scrivener, K.L., Crumbie, A.K., Laugesen, P., The interfacial transition zone (ITZ) between cement paste and aggregate in concrete. *Interface Science* **12**(4), 411-421 (2004).

Scrivener, K.L., Nemati, K.M., The percolation of pore space in the cement paste/aggregate interfacial zone of concrete. *Cement and Concrete Research* **26**(1), 35-40 (1996).

Sercombe, J., Vidal, R., Galle, C., Adenot, F., Experimental study of gas diffusion in cement paste. *Cement and Concrete Research* **37**(4), 579-588 (2007).

Shah, S.P., In: C.K.Y. Leung, Z. Li, J.T. Ding (Eds.), High Performance Concrete—Workability, Strength and Durability. The Hong Kong University of Science and Technology, Hong Kong, 2000.

Shane, J.D., Mason, T.O., Jennings, H.M., Garboczi, E.J., Bentz, D.P., Effect of the interfacial transition zone on the conductivity of Portland cement mortars. *Journal of the American Ceramic Society* **83**(5), 1137-1144 (2000).

Stroeven, M., Discrete numerical modelling of composite materials – application to cementitious materials. Ph.D. Thesis, Delft University of Technology, Delft, The Netherlands, 1999.

Stroeven, P., Stroeven, M., Assessment of packing characteristics by computer simulation. *Cement and Concrete Research* **29**(8), 1201-1206 (1999).

Stroeven, P., A stereological approach to roughness of fracture surfaces and tortuosity of

transport paths in concrete. *Cement and Concrete Composites* **22**(5), 331-341 (2000).

Stroeven, P., Hu, J., Stroeven, M., On the usefulness of discrete element computer modeling of particle packing for material characterization in concrete technology. *Computers and Concrete* **6**(2), 133-153 (2009).

Stroeven, P., Hu, J., Koleva, D.A., Concrete porosimetry: Aspects of feasibility, reliability and economy. *Cement and Concrete Composites* **32**(4), 291-299 (2010).

Stroeven, P., Le, L.B.N., Sluys, L.J., He, H., Porosimetry by double random multiple tree structuring. *Image Analysis & Stereology* **31**(1), 55-63 (2012).

Stroeven, P., Li, K., Le, L.B.N., He, H., Stroeven, M., Capabilities for property assessment on different levels of the micro-structure of DEM-simulated cementitious materials. *Construction and Building Materials* **88**, 105-117 (2015).

Udell, K.S., Heat transfer in porous media considering phase change and capillarity – the heat pipe efect. *International Journal of Heat and Mass Transfer* **28**(2), 485-495 (1985).

Vichit-Vadakan, W., Scherer, G.W., Measuring permeability of rigid materials by a beam-bending method: III. Cement paste. *Journal of the American Ceramic Society* **85**(6), 1537-1544 (2002).

Vichit-Vadakan, W., Scherer, G.W., Measuring permeability and stress relaxation of young cement paste by beam bending. *Cement and Concrete Research* **33**(12), 1925-1932 (2003).

Villain, G., Baroghel-Bouny, V., Kounkou, C., Hua, C., Measuring the gas permeability as a function of saturation rate of concretes. *French Journal of Civil Engineering* **5**, 251-268 (2001).

Williams, S.R., Philipse, A.P., Random packings of spheres and spherocylinders simulated by mechanical contraction. *Physical Review E* **67**, 051301/1-9 (2003).

Winslow, D.N., Cohn, M.D., Bentz, D.P., Snyder, K.A., Garboczi, E.J., Percolation and pore structure in mortars and concrete. *Cement and Concrete Research* **24**(1), 25-37 (1994).

Wong, H.S., Buenfeld, N.R., Patch microstructure in cement-based materials: Fact or artefact? *Cement and Concrete Research* **36**(5), 990-997 (2006).

Wong, H.S., Buenfeld, N.R., Hill, J., Harris, A., Mass transport properties of mature wasteform grouts. *Advances in Cement Research* **19**(1), 35-46 (2007).

Wong, H.S., Zobel, M., Buenfeld, N.R., Zimmerman, R.W., Influence of the interfacial transition zone and microcracking on the diffusivity, permeability and sorptivity of cement-based materials after drying. *Magazine of Concrete Research* **61**(8), 571-589 (2009).

Wong, H.S., Zimmerman, R.W., Buenfeld, N.R., Estimating the permeability of cement pastes and mortars using image analysis and effective medium theory. *Cement and Concrete Research* **42**(2), 476-483 (2012).

Wu, K., Xu, L.L., Schutter, G.D., Shi, H.S., Ye, G., Influence of the interfacial transition zone and interconnection on chloride migration of Portland cement mortar. *Journal of Advanced Concrete Technology* **13**(3), 169-177 (2015).

Yazdchi, K., Srivastava, S., Luding, S., Microstructural effects on the permeability of periodic fibrous porous media. *International Journal of Multiphase Flow* **37**(8), 956-966 (2011).

Ye, G., Experimental study and numerical simulation of the development of the micro-

structure and permeability of cementitious materials. Ph.D. Thesis, Delft University of Technology, Delft, The Netherlands, 2003.

Ye, G., Percolation of capillary pores in hardening cement pastes. *Cement and Concrete Research* **35**(1), 167-176 (2005).

Ye, G., Lura, P., Breugel, K. van, Modelling of water permeability in cementitious materials. *Materials and Structures* **39**(9), 877-885 (2006).

Zalzale, M., McDonnald, P.J., Lattice Boltzmann simulations of the permeability and capillary adsorption of cement model microstructures. *Cement and Concrete Research* **42** (12), 1601-1610 (2012).

Zalzale, M., McDonnald, P.J., Scrivener, K.L., A 3D lattice Boltzmann effective media study: understanding the role of C-S-H and water saturation on the permeability of cement paste. *Modelling and Simulation in Materials Science and Engineering* **21**, 085016 (2013).

Zalzale, M., Water dynamics in cement paste: insights from lattice Boltzmann modelling. Ph.D. Thesis, Ecole Polytechnique Federale De Lausanne, Lausanne, Switzerland, 2014.

Zamani, S., Kowalczyk, R.M., McDonald, P.J., The relative humidity dependence of the permeability of cement paste measured using GARField NMR profiling. *Cement and Concrete Research* **57**, 88-94 (2014).

Zhang, M.Z., Multiscale lattice Boltzmann-finite element modelling of transport properties in cement-based materials. Ph.D. Thesis, Delft University of Technology, Delft, The Netherlands, 2013.

Zhang, M.Z., Ye, G., Breugel, K. van, Microstructure-based modeling of permeability of cementitious materials using multiple-relaxation-time lattice Boltzmann method. *Computational Materials Science* **68**, 142-151 (2013).

Zhang, M.Z., Ye, G., Breugel, K. van, Multiscale lattice Boltzmann-finite element modelling of chloride diffusivity in cementitious materials. Part II: Simulation results and validation. *Mechanics Research Communications* **58**, 64-72 (2014).

Zhang, M.Z., Pore-scale modelling of relative permeability of cementitious materials using X-ray computed microtomography images. *Cement and Concrete Research* **95**, 18-29 (2017).

Zhang, Y., Zhang, M.Z., Transport properties in unsaturated cement-based materials – A Review. *Construction and Building Materials* **72**, 367-379 (2014).

Zheng, J.J., Li, C.Q., Three-dimensional aggregate density in concrete with wall effect. *ACI Materials Journal* **99**(6): 568-575 (2002).

Zheng, J.J., Wong, H.S., Buenfeld, N.R., Assessing the influence of ITZ on the steady-state chloride diffusivity of concrete using a numerical model. *Cement and Concrete Research* **39**(9), 805-813 (2009).

Acknowledgements

The research work reported in this dissertation was conducted in the Computational Mechanics group in the Faculty of Civil Engineering and Geosciences of Delft University of Technology, the Netherlands. Financial support from China Scholarship Council (CSC) made it possible realizing this study successfully, so both facilities are herewith acknowledged.

I would like to express my true appreciation to my promotor Prof. L.J. Sluys, who gave me the opportunity to work with him at TU Delft. This work could not have been accomplished without his guidance, support, encouragement and comments throughout my study. I also thank my co-promotor Dr. Martijn Stroeven for many valuable discussions and critical comments on this thesis and our journal papers. His assistance helped me getting familiar with the HADES system. This is greatly appreciated. In addition, I am sincerely grateful to my supervisor Prof. Piet Stroeven for his valuable suggestions, continuous support and great patience. His active involvement in international science events, enthusiastic approach to research and optimistic attitude towards life has impressed me deeply. I am also grateful to Prof. Zhonghe Shui from Wuhan University of Technology for recommending me as a Ph.D. candidate to my supervisors at TU Delft.

Dr. M. Zalzale (EPFL, Switzerland) and Prof. F. Ghomari (University of Tlemcen, Algeria) are sincerely acknowledged for the discussion regarding fluid transport in unsaturated cement paste and for providing their data for comparison reasons used in in Chapter 2. Dr. H.Y. Ma (Missouri University of Science and Technology, USA) provides invaluable help with the work in Chapter 4, which is highly appreciated. Finally, I want to show my appreciation to Dr. H.S. Wong (Imperial College London, UK) and Dr. D.P. Bentz (NIST, USA) are appreciated for the discussion regarding the influence of the interfacial transition zone on transport properties of concrete treated in Chapter 5.

My special thanks go to Frank Everdij and Anneke Meijer for all the help and support. I also thank all my former and present colleagues at the section of Computational Mechanics of TU Delft. I really enjoyed the lunch time, coffee break, CM meetings and EM symposiums with you. L.B.N. Le's assistance helped me getting familiar with XIPKM and DRaMuTS is also greatly appreciated. My special thanks go to Erik Simons and Prashanth Srinivasan for sharing the office and enjoyable time together, *i.e.* BBQ, PSOR, bowling, coffee break. I am also very grateful to my friends in Delft for a lot of joyful activities together, *i.e.* cooking, travelling, funny and relaxing conversations. Unfortunately, I am not able to list all the names herein. Nonetheless, I am deeply grateful in that respect to Jing Hu, Huan He, Kai Zhang, Li Zhu, Jiayi Chen, Wenqing Shi, Tao Lv, Zilong Wei, Yan Zhou, Hao Huang, Mingjuan Zhao, Yang Qu, Xiaowei Ouyang, Cui Wei, Zhanxiong Liu, Min Qu, Yu Xin, Yaolu Liu, Liting Qiu, Yueye Caoyang.

Last, but most important of all, I would like to express my deepest gratitude to my parents and of course my beloved wife (Shulan Shu) and daughter (Zhixi Li). I would never have accomplished this work without their unconditional support and love.

Kai Li
Delft, March 2017

List of relevant publications

Article – letter to the editor

1. Li, K., Stroeven, M., Stroeven, P., Sluys, L.J. (2017). Effects of technological parameters on permeability estimation of partially saturated cement paste by a DEM approach. *Cement and Concrete Composites*, under review.
2. Li, K., Stroeven, P., Stroeven, M., Sluys, L.J. (2017). A numerical investigation into the influence of ITZ on the permeability of partially saturated cement paste between aggregate surfaces. *Cement and Concrete Research*, under review.
3. Stroeven, P., Li, K. (2017). RSA vs DEM in view of particle packing-related properties of cementitious materials. *Computers and Concrete*, under review.
4. Li, K., Stroeven, P. (2017). Systematic research on compucrete can shed light on some controversial issues in concrete technology. *Heron*, 62 (1), 47-59.
5. Stroeven, P., Li, K. (2017). Breakthrough in economizing a modern approach to porosimetry of virtual cementitious materials. *Magazine of Concrete Research*, in press.
6. Li, K., Stroeven, M., Stroeven, P., Sluys, L.J. (2016). Investigation of liquid water and gas permeability of partly saturated cement paste by DEM approach. *Cement and Concrete Research*, 83, 104-113.
7. Li, K., Stroeven, P., Stroeven, M., Sluys, L.J. (2016). Estimating permeability of cement paste using pore characteristics obtained from DEM-based modelling. *Construction and Building Materials*, 126, 740-746.
8. Stroeven, P., Li, K. (2016). Size and shape revisited in the light of 400 years old Cavalieri principle. *Heron*, 61 (1), 57-67.
9. Li, K., Stroeven, P., Le, L.B.N. (2015). Methodology for porosimetry in virtual cementitious composites to economically and reliably estimate permeability. *Image Analysis & Stereology*, 34 (2), 73-86.
10. Stroeven, P., Li, K., Le, L.B.N., He, H., Stroeven, M. (2015). Capabilities for property assessment on different levels of the microstructure of DEM-simulated cementitious materials. *Construction and Building Materials*, 88, 105-117.

Article in volume – proceedings

1. Li, K., Stroeven, P., Stroeven, M., Sluys, L.J. (2016). An engineering approach for permeability assessment of virtual cement-based materials. *Proceedings of 2016 international concrete sustainability conference*, Washington, DC, USA.
2. Li, K., Stroeven, P., Stroeven, M., Sluys, L.J. (2015). Liquid water permeability of partially saturated cement paste assessed by DEM-based methodology. In A.M. Brandt, J. Olek, M.A. Glinicki, C.K.Y. Leung & J. Lis (Eds.), *Proceeding of the 11th international symposium on brittle matrix composites* (pp. 121-130), Warsaw, Poland.
3. Le, L.B.N., Stroeven, P., Li, K., Stroeven, M., Sluys, L.J. (2015). Demonstration and validation by simple examples of a complete analogue porosimetry methodology for virtual cement pastes on micro-level. In A.M. Brandt, J. Olek, M.A. Glinicki, C.K.Y. Leung & J. Lis (Eds.), *Proceeding of the 11th international symposium on brittle matrix composites* (pp. 1-10), Warsaw, Poland.
4. Li, K., Stroeven, P., Stroeven, M. (2014). Strategy for predicting transport-based durability properties of concrete based on DEM approach. IN D. Bjegovic, H. Beushausen & M. Serdar (Eds.). *Proceedings of the RILEM international workshop on performance-based specification and control of concrete durability* (pp. 443-450), Zagreb, Croatia.
5. Stroeven, P., He, H., Le, L.B.N., Li, K. (2014). Modeling possibilities of concrete structure for durability purpose. In N.B., Barabash (Ed.), *Proceeding of the international seminar on modelling and optimization of composites* (pp. 60-63), Odessa, Ukraine.
6. Li, K., Stroeven, M., Stroeven, P., Sluys, L.J. (2013). C-S-H globule clustering on nano-scale simulated by the discrete element method for pore structure exploration. *Proceedings of the TRANSCEND conference water transport in cementitious materials* (pp. 32-35), Guildford, UK.

Curriculum Vitae

Name: Kai Li

Date of Birth: January 1, 1988

Place of birth: Honghu, Hubei Province, China

Email address: likai385888@gmail.com

October 2012 – March 2017 Ph.D. candidate at Structural Mechanics Section, Faculty of Civil Engineering and Geosciences, Delft University of Technology, the Netherlands

September 2009 – September 2012 Graduate study of Construction Materials Science and Engineering at Wuhan University of Technology, China

September 2005 – September 2009 Undergraduate study of Materials Science and Engineering at Wuhan University of Technology, China